SEA TRIALS OF A DUCTED TIP PROPELLER

DESIGNED FOR IMPROVED CAVITATION PERFORMANCE

by

Ivar Hordnes

B.Eng. (Mechanical Engineering)

University of Strathclyde, 1992

A THESIS SUBMITTED IN PARTIAL FULFILLMENT OF

THE REQUIREMENTS FOR THE DEGREE OF

MASTER OF APPLIED SCIENCE

in

THE FACULTY OF GRADUATE STUDIES

DEPARTMENT OF MECHANICAL ENGINEERING

We accept this thesis as conforming

to the required standard

UNIVERSITY OF BRITISH COLUMBIA

July 1996

In presenting this thesis in partial fulfilment of the requirements for an advanced degree at the University of British Columbia, I agree that the Library shall make it freely available for reference and study. I further agree that permission for extensive copying of this thesis for scholarly purposes may be granted by the head of my department or by his or her representatives. It is understood that copying or publication of this thesis for financial gain shall not be allowed without my written permission.

Department of MECHANICAL ENGINEERING

The University of British Columbia
Vancouver, Canada

Date July 19, 1996

Abstract

Tip vortices produced by marine propellers can be suppressed by attaching tip devices to the propeller blades, which will obstruct the roll-up process and reduce the strength of the vortices. This will decrease the induced drag on the blades and delay onset of the cavitation associated with the low pressure near the core of the vortices. However, most of the previously tested tip devices have suffered large drag penalties due to the added parasite drag of the device, which have resulted in a net loss of propeller efficiency.

In this research sea trials of a ducted tip propeller has shown that flow-through ducts installed at the blade tips will suppress the tip vortex roll-up and result in a substantial delay of the onset of tip vortex cavitation, without reducing the efficiency of the propeller. The sea trials consisted of efficiency measurements and cavitation observations of a conventional propeller that was tested and subsequently modified by replacing a radial fraction of the blade tips by flow-through ducts that are aligned with the blades and bent to follow the outer radius of the propeller. Previous research on the ducted tips suggested that an efficiency improvement could be expected when the propeller operates at low advance ratios. The sea trials indicate, however, that the ducted tips caused an increase in the propeller efficiency when it operates at high advance ratios, i.e. close to its peak performance. The success of the ducted tip propeller can mainly be attributed to the effectiveness of the ducts as tip vortex suppressing devices; first of all by obstructing the path of the vortex, and secondly, by diffusing the vortex through mixing of the external and internal flow at the exit of the ducts. However, the low parasite drag of the ducts also play an important role by keeping the drag penalty at a minimum.

The ducted tip propeller was originally thought to be useful for boats with heavily loaded propellers, such as tug boats and trawlers. The current research has shown that the ducted tips may have a potential for application on propellers for a much wider aspect of ships, possibly only limited by the tip speed of the propellers.

Table of Contents

List of Tables

List of Figures

Nomenclature

A_E	=	expanded area of the propeller blades
A_0	=	propeller disc area
C_D	=	drag coefficient
C_L	=	lift coefficient
D	=	propeller diameter
D_S	=	shaft diameter
DAC	=	dissolved air content
J	=	measured advance ratio .....(Equation 4.3)
J_A	=	true advance ratio .....(Equation 4.4)
K_Q	=	torque coefficient .....(Equation 4.5)
K_T	=	thrust coefficient .....(Equation 4.6)
L	=	tow load
L/D	=	lift/drag ratio
N	=	shaft rotation [rpm]
P	=	pitch
P_Q	=	delivered power
P_T	=	propulsive power
Q	=	torque
R	=	propeller radius
Re	=	Reynolds number
S	=	slip ratio = 1 - V_A/Pn
T	=	thrust
U	=	relative blade velocity = $\sqrt{V_A^2 + U_\theta^2}$
U_θ	=	tangential blade velocity = $2\pi nr$
V	=	velocity of the boat relative to the water
V_A	=	speed of advance = $V(1-w)$
b	=	span
c	=	chord

d = duct diameter

d_S = reduced shaft diameter

l = duct length

n = shaft rotation in rps

p_c = pressure near the core of the tip vortex

p_v = vaporization pressure = 900 N/m² (saltwater at 5°C)

p_∞ = freestream pressure = 116688 N/m² at 5 ft. depth (saltwater at 5°C)

r = fraction of propeller radius

t = duct thickness

u = induced velocity

w = Taylor wake fraction

Γ = circulation

α = angle of attack

β = angle of incoming flow

ε = camber

ϕ = pitch angle

η = efficiency .....(Equation 4.1 & 4.2)

ν = kinematic viscosity = $1.56 \cdot 10^{-6}$ m²/s (saltwater at 5°C)

ρ = density of seawater = 1028 kg/m³ (saltwater at 5°C)

σ = cavitation index

σ_i = cavitation inception index .....(Equation 4.8 & 4.9)

σ_d = design stress

σ_y = yield stress

Subscripts:

I	=	induced	i	=	inception
P	=	parasite	o	=	open-water
F	=	flat plate	r	=	relative to the blades at $r = 0.7R$
0	=	zero lift			

Acknowledgments

Many people have made what they believe is a rather insignificant contributions to this project, but for me these contributions have been crucial for the completion of my thesis all the hard work more enjoyable.

Thanks to:

Andre and Susie Bidaud, Cherryl, Allan Ikari, Alfred Burns, Fred Watmough, Joe Dan, Anton, Ed, Lenny, Doug, Dave, Geoff Liggins, Gary Schwartz, Jan, Marje, Christine, Duan, Brent, Hans Bystrøm, B. Haggarty, D. McGreer, Leon Smith and W. Towland.

Special thanks to:

Prof. Sheldon Green - for your support and endless patience.

Andre Bidaud - for your time, advice and encouragement.

Alfred & Gertrude Leslie - for lending me the Pearl Sea
and for your boundless hospitality.

Douglas Leslie - for expanding my horizons.

The following companies supplied parts, or were hired to carry out special tasks:

Truck Tech Corporation - signal conditioners for torque and thrust measurements.

Celtic Shipyards - room and tools for building the propeller.

The departmental machine shop - general machining and welding.

Coles Marine - marine ways for bringing Pearl Sea out of the water.

Watervisions - underwater video equipment and film crew.

Osborne Propellers - attaching the ducted tips to the propeller.

Chapter 1 - INTRODUCTION

Cavitation occurs in a fluid where voids of vapor form because the local pressure is equal to or less than the vapor pressure of the fluid. Low local pressure may, for example, be a result of the dynamics of a fluid as it flows around a lifting surface such as a blade of a marine propeller.

Cavitation on marine propellers is a phenomena that has received wide attention from scientists and engineers since its first recorded occurrence on propellers mounted on steam boats over a century ago. The work described in this report focuses on the cavitation formed in the core of the vortex trailing behind the tip of a propeller blade. This particular chapter is concerned with the nature of a tip vortex and its associated cavitation, its effects, and how these can be controlled.

1.1 Tip vortex cavitation on marine propellers

1.1.1 Tip vortices and tip vortex cavitation

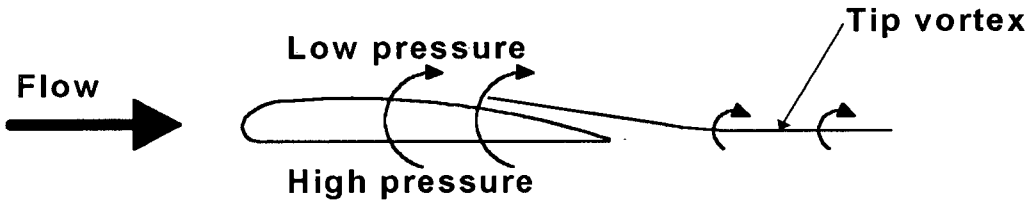

Figure 1.1 Pressure field interpretation of tip vortices.

All lifting surfaces that terminate in a moving fluid create tip vortices. The physics of a tip vortex can best be explained in terms of the pressure fields induced by the lifting surface (e.g. the wing of an aircraft). In order to generate lift, larger static pressure is produced below the wing than above it. The nature of all fluids is to flow in the direction of a negative pressure gradient, and therefore, where the wing ends, at the tip, the air flows around from the pressure side to the suction side, forming a tip vortex that trails behind the wing (Figure 1.1). Other explanations, involving shear layer flows and Helmholtz Vortex Laws are outlined by Green

(1995). A marine propeller consists of a number of blades that are lifting surfaces terminating in the water. Unlike the tip of an aircraft wing, which travels linearly, the motion of the tips of the propeller, and hence its tip vortices, form a helical pattern (Figure 1.2).

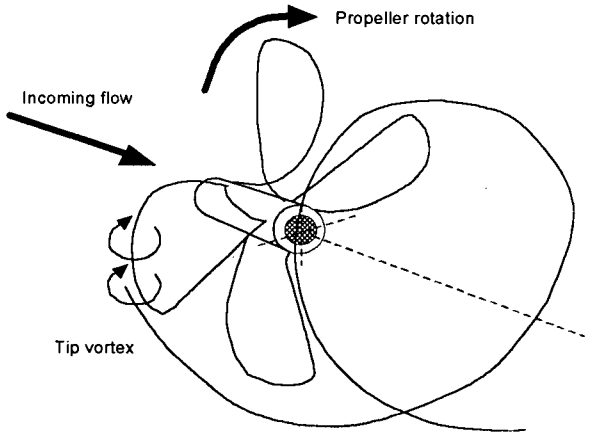

Figure 1.2 The helical pattern of tip vortices trailing behind a marine propeller.

Tip vortices on marine propellers have two undesirable effects:

1. A tip vortex induces a flow component normal to the blade planform, equivalent to the downwash ahead of an airfoil. This reduces the effective angle of attack and creates induced drag, and consequently, reduces the efficiency of the blade as a lifting surface (Figure 1.3).

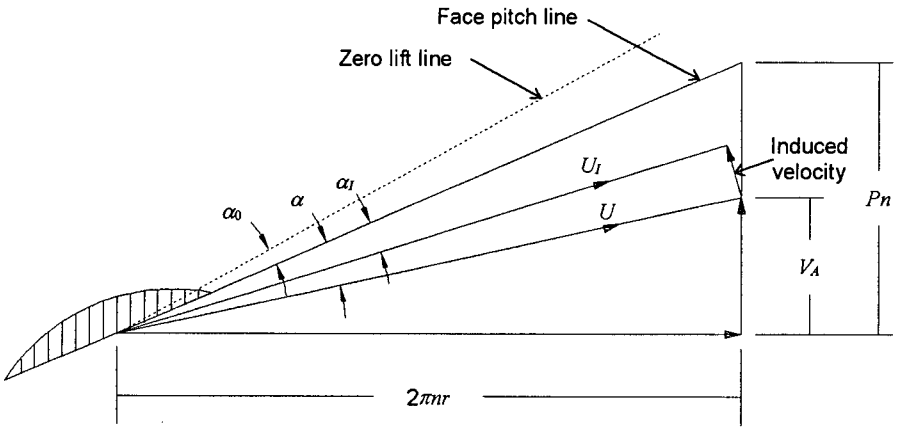

Figure 1.3 Blade velocity diagram showing how the induced velocity reduces the geometric angle of attack from α to α_I.

2. Due to high tangential velocities near the core of the vortex, the local pressure may fall below vapor pressure, causing local cavitation.

1.1.2 The effects of tip vortex cavitation

Cavitation is in general undesirable because of its detrimental effects both on equipment and on the comfort of boat passengers. Cavitation is a major source of corrosion on the propeller and the hull, above and aft, of the propeller. It is a major source of vibration of a ship, which can not only cause damage to the hull, but also to the propeller itself, the rudder, the shaft, the bearings and the engine. The vibration also creates discomfort for anyone that is traveling aboard the ship. Cavitation produces intense noise, associated with the collapse of the cavities, which is a second cause of discomfort onboard the ship. The noise is of particular importance for naval ships, which wish to minimize cavitation in order to avoid detection by enemy observers. Cavitation noise is also of interest for fishing boats. Olsen et al. (1983) and Engås et al. (1995) have observed an avoidance behavior among fish such as herring, polar cod and capelin when approached by boats. While the hearing ability of fish ranges from ultra sound to approximately 1 kHz, the noise frequencies that evoked the strongest avoidance behavior range from 60 - 300 Hz (Engås et al. 1995). A typical frequency range for cavitation noise is 0.1 - 100 kHz, with the highest noise levels recorded below 1 kHz (Sponagle 1989, Sharma et al. 1990). These observations indicate that a cavitating propeller may scare away fish, resulting in a reduced catch. Many fishermen on the Faeroe Islands believe there exists a correlation between cavitation noise and reduced catches, and researchers at The Faeroe Fisheries Laboratories are currently doing a project, involving a fleet of 20 different fishing boats, in which they are trying to determine in detail which types of noise frighten the fish (Smith 1996).

Tip vortex cavitation does not have the same corrosive effect on the blades as sheet cavitation, bubble cavitation and cloud cavitation, which all occur near the surface of the blades, and are referred to as *surface cavitation* in subsequent

chapters. However, tip vortex cavitation will normally appear at an earlier stage than does surface cavitation, i.e. at a higher value for the *cavitation index*,

$$\sigma = \frac{p_\infty - p_v}{\frac{1}{2}\rho U_\infty^2}$$

Green et al. (1988) demonstrated, on a hydrofoil, that cavitation inception occurs first in the tip vortex for a range of angles of attack that covers most of the operating, or loading, range of the hydrofoil. Lodha and Arakeri (1984) also mention, from observations of a model propeller, that tip vortex cavitation was the dominant type of cavitation at inception. From experiments on model propellers in cavitation tunnels, Kuiper (1978) comments that tip vortex cavitation already exists when conditions for leading edge cavitation are approached. Crump (1948) plotted the cavitation inception data from experiments on two model propellers and showed that for both propellers, at operating loads, tip-vortex cavitation had the highest inception index.

Therefore, tip vortex cavitation can cause substantial damage, due to vibration, at a propeller loading that is not sufficient for leading edge cavitation to appear. The extent of the damage that tip vortex cavitation can produce is described in a paper (English et al. 1992), where a combination of tip vortex and propeller-hull vortex (*PHV*) cavitation has been reported to induce severe vibrations in the hull of an offshore support vessel, resulting in cracked plating in the vicinity of the two propellers. (For a detailed description of *PHV*, see English 1992.) The same phenomena was reported (Weitendorf 1993) to be the reason for the unacceptable vibration and noise level in the cabins of the afterbody of the passenger vessel *Queen Elizabeth 2*. Severe vibrations were also experienced on the Norwegian *Bastø Ferry* when one of the thrusters (i.e., propeller and nozzle mounted on a 360° rotating stem), was turned towards the center to push the stern sideways. The engineers at KaMeWa, Sweden, where the thrusters were manufactured, are 90% confident that the problem is caused by tip vortex cavitation. The problem was

solved by slightly bending, or *cupping*, the tips of the propeller blades towards the pressure side (Bystrøm 1996).

1.1.3 Prevention of tip vortex cavitation

In light of the discussion in the previous sub-chapter, it is obvious that designing a cavitation free propeller will involve prevention of tip vortex cavitation. This is a very difficult task due to the complexity of the tip flow, which is further complicated by the wake of the hull in which the propeller operates. Some fairly simple guidelines exist, though. A two dimensional model of an irrotational vortex with a solid body rotation in the core, the *Rankine Vortex*[1], predicts that the difference between the freestream pressure and the pressure near the core of the tip vortex is proportional to the square of the circulation of the lifting surface generating the vortex, and inversely proportional to the square of the size of the solid core:

$$p_\infty - p_c \propto \frac{\Gamma^2}{r_c^2}$$

Thus, the onset of tip vortex cavitation can be prevented, or at least delayed, by either reducing the lift on the propeller blades, or expanding the core of the tip vortices. This has previously been achieved by unloading the blade tips, or surrounding the propeller by an external shroud or nozzle, or by attaching appendages to the blade tips and other types of tip modifications. Unloading is obtained by reducing the pitch of the propeller blades, from a radius of approximately equal to $0.7R$, radially towards the tips. By reducing the pitch, the local angle of attack is reduced and consequently the local loading is reduced. When the loading is reduced near the tip, the core pressure increases, and hence the core of the vortex is less likely to cavitate. However, by reducing the loading, a

[1] For further information on the Rankine Vortex see Green (1995).

higher propeller rotation is required to maintain the same forward velocity of the boat, and therefore the *propeller efficiency*[1] decreases.

Shrouds and nozzles (nozzles are preferred, as they accelerate the flow and are capable of producing thrust from the incoming water) are mounted to the hull, or to a strut, or in the case of a Z-drive, to the drive arm. The axis of the nozzle is aligned with the propeller axis, and the propeller is located midways along the length of the nozzle. The clearance at the tips of the propeller and the inner wall of the nozzle is very small so that tip vortices are not allowed to develop. In many cases, the nozzle replaces the rudder; such nozzles have a larger clearance to the propeller tips in order to give room for rotation of the nozzle about a vertical axis. Nozzles are normally installed because of their thrust augmenting capacity, although some vessels could not operate without them because of the strong tip vortices produced by the propeller. However, nozzles have some negative attributes: the added wetted surface creates extra drag, and there are installation limitations with regards both to the space and the strength of the hull.

Tip appendages and modification of the tip geometry, such as bladelets, bulbs, porous tips and many more, are not used very often, although many of these methods have been proven to reduce the tip vortex cavitation. The reason for their infrequent use is that most of the modifications suffer from either loss of lift due to a reduced lifting surfaces area, an increased drag due to added wetted surface, or a combination of both. Tip devices are, however, still a very attractive solution to the tip vortex cavitation problem because they require no alterations to the shape or structure of the hull. The only installation limit is the clearance between the propeller tips and the rudder and/or the hull. The ideal tip device should preferably be cast as an integral part of the propeller, although, it can readily be retrofit to a conventional propeller. In summary, it is desirable to find a tip device that reduces the tip vortex cavitation, and for which the lift and drag penalties can be controlled so that there is no loss, but rather a gain in the propeller efficiency.

[1] For a definition of propeller efficiency, see Chapter 4.1.

1.2 Literature review

Presently no tip device for marine propellers exists which both satisfies the criteria mentioned above and which has found a universal application. The reason is that scientists and engineers still don't know enough about the three-dimensional fluid flow and cavitation around the tip of lifting surfaces to be able to design the optimum tip shape. Although tip devices for lifting surfaces is an old concept, extensive research in the field was not started before the end of the Second World War and the advent of modern jet planes. Even then, few contributions of importance for marine propellers were made before the early 60's.

1.2.1 Basic research on tip vortex cavitation

The majority of the research into tip vortex cavitation has been focused on expanding our fundamental understanding of the physics of both the single and multi phase flow in tip vortices on marine propellers, in pumps and in turbines. One of the most important contributions to our understanding of the nature of tip vortex cavitation was McCormick's (1962) semi-empirical analysis of the tip vortices produced by a set of rectangular and elliptic hydrofoils. He postulated that the size of the tip-vortex core is determined by the thickness of the boundary layer on the pressure side of the hydrofoil. Hence, by manipulating this boundary layer, the diameter of the vortex core can be altered to increase the core pressure and thereby delay cavitation inception. By combining equations for the thickness of the boundary layer and the spanwise distribution of the circulation of the hydrofoil, and then determining the constants using the experimental data obtained from 20 hydrofoils, he arrived at the following equation for the cavitation *inception index*:

$$\sigma_i = C \cdot Re^{0.35}\, \alpha^m$$

where C is a constant dependent on the geometry and aspect ratio of the foil, and the exponent $m \approx 1.29$ and 1.44 (Falcao de Campos et al. 1989) for elliptical and rectangular planforms, respectively. This equation is still widely accepted as one of

the most accurate models for the prediction of tip vortex cavitation inception. McCormick also commented on the effect of the air content of the water on cavitation inception, in particular that inception is a function of the presence of undissolved air. However, he did not try to account for this dependence in his analysis.

McCormick's work was aimed at suppression of tip vortex cavitation on marine propellers. Model scale experiments were at that time the main guide for the design of propellers, and are still a widely used method for prototype testing and for solving problems on existing full scale propellers. By showing that tip vortex cavitation inception depends strongly on the Reynolds number and the undissolved air content, McCormick opened up a new *can of worms* for engineers trying to design cavitation free propellers; a correct prediction of the inception index could not be scaled from the results from tests on model propellers, based simply on the freestream velocity, ambient and vaporization pressure of the fluid. Nevertheless, he also opened up for the possibilities of delaying inception by manipulating both the boundary layer and the air content of the fluid. It was therefore desirable to study in detail the effect of the Reynolds number to confirm the scaling equation, to determine in which range it is valid, and eventually incorporate the effect of the air content of the water into the equation.

Higuchi et al. (1986) made observations of an elliptical hydrofoil for a limited range of Reynolds numbers and obtained inception data that correlates well with McCormick's results at low dissolved air contents, although there is, at low Reynolds numbers, a strong deviation from the $Re^{0.35}$ relation as the dissolved air content rises. Experiments by Falcao de Campos et al. (1989) show no particular dependency on Re, but show a large drop in the inception index, coinciding with a change from detached to attached inception, that can be connected to the transition from laminar to turbulent flow at the tip of the foil. This paper also suggest a higher exponent, m, for the angle of attack dependence of σ_i then is commonly used. Johnsson and Rutgersson (1991) carried out cavitation tunnel experiments on a hydrofoil that was a full scale copy of the tip (32% of the radius) of a highly skewed

propeller. Their experiments show the same trends as McCormick's; σ_i varies with $Re^{0.35}$. By attaching roughness elements along the leading edge in order to accelerate the transition from laminar to turbulent boundary layer, they succeeded in delaying the cavitation inception in the tip vortex. The addition of the roughness caused only a marginal increase in the total drag of the hydrofoil; the higher the angle of attack the lower the drag penalty. Katz and Bueno Galdo (1989) measured the surface pressure around the tip, and Stinebring et al. (1991) measured the tangential velocities in a rolled up vortex. Both groups indicate that roughness on the tip of the hydrofoil reduces the strength of the tip vortex, but there are no inception observations to support these results. More recent studies by Maines and Arndt (1993) show that inception follows the relationship

$$\sigma_i = K \cdot C_L{}^2 \, Re^{0.4}$$

at low lift coefficients, C_L. In this relationship the variation of boundary layers at the tip, between different foils, at the same Reynolds number, is accounted for by the constant K. Flow visualization showed strong tipward deflection of the pressure side boundary layers, in support of McCormick's theory.

By now it has been well established that σ_i depends on the viscous flow in the tip region, which is a function of Reynolds number, but the influence of the air content of the water is still not clearly understood. Several researchers (Higuchi et al.1986, Arndt et al. 1991, Johnsson and Rutgersson 1991, Green 1991, Arndt and Keller 1992 and Gindroz and Billet 1994) have shown that σ_i increases with the dissolved air content (DAC) of the water. This observation can readily be explained: the higher concentration of dissolved air (measured in parts per million), and hence, higher partial pressure of the dissolved air, the smaller the reduction in test section pressure, p_∞, before the saturation pressure of the air is reached. Below this pressure the water is saturated with air, causing the air to diffuse and produce miniature bubbles that work as cavitation catalyzers, hereafter referred to as nuclei.

There are also more freestream nuclei associated with a higher DAC, even before the test section pressure is reduced, and therefore one requires a lower freestream velocity and hence, a higher cavitation index, to avoid cavitation.

Arndt et al. (1991) suggested that even with sub-saturated water in the test section, nuclei can be supplied from low pressure zones on the hydrofoil, like laminar separation bubbles, which would increase σ_i even further. Arndt and Keller (1992) found that, under otherwise identical conditions, σ_i followed a C_L^2 relation in saturated water and a $C_L^{1.4}$ relation in sub-saturated water. Assuming that the lift coefficient is directly proportional to the angle of attack, α, the $C_L^{1.4}$ relation then agrees with McCormick's results. The C_L^2 relation was suggested by Arndt and Maines (1994) as a universal scaling law for inception in *weak* (saturated) water. Gindroz and Billet (1994) have demonstrated how the inception index depends on the tension sustaining capacity of the water, which is a function of the nuclei distribution. Gindroz (1995) has summarized these results and shows how water conditions with equal saturation levels can sustain quite different tensions due to different nuclei sizes and populations. However, a scaling law for the inception that accounts for all water qualities has yet to be formulated.

1.2.2 Research on tip devices

The first systematic efforts to study the effect of tip devices on marine propellers were motivated by the desire to increase the speed of naval ships in the range of noise-free operation. Crump (1948) carried out experiments on model propellers with bulbs attached to the tips, which were based on a set of unsuccessful experiments at the David Taylor Model Basin in 1942. The new tests were motivated by the fact that the Germans, during the war, had achieved a 30% increase in speed on one of their submarines equipped with a propeller with bulbous tips. Crump tested two types of propellers with different configurations of propeller diameter, bulb diameter, pitch and numbers of blades. In two of the configurations, as much as a 25% increase in free stream velocity at inception was obtained with the bulbous tips attached, with only a marginal effect on the propeller

efficiency. Brown(1973) conducted experiments on model propellers with different numbers of blades, and showed that by dividing the total load on the propeller between a higher number of blades tip vortex cavitation inception was delayed substantially.

By the end of the 1970's, only a few reports were available on experimental work to alleviate tip-vortex cavitation. Platzer and Souders (1979) comment on the large number of reports on tip vortex suppression from aircraft wings - over 80% percent of the papers reviewed - as opposed to marine propellers. However, it was concluded that the following tip devices had a potential to delay tip-vortex cavitation in practical applications :

1. Bulbous tips
2. Porous tips
3. Linear mass injection tips

The bulbous tip had already been tested (Crump 1948) on model propellers and showed promising results. More recently it has been tested on a hydrofoil by Johnsson and Rutgersson (1991). No delay of inception was observed, but rather an accelerating effect. In addition, the bulbs caused a 15% increase in drag of the hydrofoil. However, the results of Johnsson and Rutgersson can hardly be regarded as representative of the performance of bulbs; first of all, as they have pointed out in their paper, the hydrofoil experiences a constant spanwise, axial incoming flow, while the tip of the propeller that it models, sees a radially varying, tangential incoming flow. The different incoming flow, and hence, a different spanwise loading may be the reason why Johnsson and Rutgersson could not reproduce Crump's results. A second weakness with the experiments of Johnsson and Rutgersson can be attributed to the flow direction relative to the bulb, for which very little information is given. The bulb is extending relatively far down along the leading edge of the highly skewed hydrofoil, and will therefore experience the incoming fluid as a cross-flow, which is likely to have suction peaks or cause flow separation that accelerates

the tip cavitation inception. There is in general a lack of consideration to the location and geometry of the bulb in their work.

Mani et al. (1988) found that the porous tip, however, substantially delayed inception, particularly at low *advance ratios*[1]. The porous tips did not affect the hydrodynamic performance of the propeller. The linear mass injection has been given a substantial amount of attention for the same reason; the likelihood of affecting the hydrodynamic performance is small as only minor modification to the propeller geometry is required. Fruman (1988) and Fruman and Aflalo (1989) were able to reduce the tip vortex cavitation inception index by 60% when a diluted polymer solution was ejected from an orifice at the tip of a hydrofoil. Simultaneous lift and drag measurements were carried out and showed that the hydrodynamic performance was unaffected by the polymer ejection. More recent experiments on a model propeller by Chahine et al. (1993) confirm the results of Fruman and Aflalo. These experiments also showed that there is an optimum polymer ejection ratio, and that the location of the ejection ports is salient to the delay of inception.

Several other methods to inhibit tip vortex cavitation have been tried. Two papers, by Itoh et al. (1986) and Itoh (1987), indicate that a model propeller fitted with small bladelets, equivalent to the Whitcomb winglets, delayed the inception of tip cavitation, and increased the propeller efficiency by 1 to 4%. These results contradict the findings of Goodman and Breslin (1980), who focused solely on the effects on the efficiency when bladelets are attached to a conventional outboard propeller. It was concluded that the bladelets reduced the efficiency of the propeller as well as created additional cavitation problems; sheet cavitation would emerge on the bladelets over most of the range of the conditions for which they were tested, and for one particular configuration tip vortex cavitation would emerge from the tip of the bladelet.

The discrepancy between the results of these two groups is likely to be found in the wealth of different configurations tested by Itoh and his research group as opposed to the limited combinations of geometry and orientation of the bladelets

[1] For a definition of the advance ratio, see Chapter 4.1.

tested by Goodman and Breslin. Although Itoh and his group succeeded in improving the efficiency for a number of bladelet configurations, they also tested configurations that resulted in substantial loss of efficiency. These are all *open-water* efficiencies, the effect of the bladelets were not tested in *behind* conditions, i.e. when the propeller is mounted on a boat, either full scale or model. There is, however, one distinct difference between the bladelet orientation of the tests of the two groups: the bladelets were all affixed perpendicular to the blade plan of the propeller tested by Goodman and Breslin, while Itoh et al. attached the bladelets to the blades at angles between 0° and 60°, called the *bend angle*. This means that the bladelets become a part of the effective lifting surface. There is a slight variation of both the blade area and maximum diameter, which might have caused the positive results. Nevertheless, the bladelets, both on the suction side and the pressure side of the propeller blades, can be installed to give added thrust and a counter rotating tip vortex, while the bladelets of Goodman and Breslin were installed solely to create counter rotating vortices. The lower bend angle may also reduce the mixing of the boundary layers on the bladelet and the blade itself, which is likely to create extra frictional drag. In addition, the bladelets of Itoh et. al. are in general installed with a substantial higher angle of attack than those of Goodman and Breslin, producing stronger counter rotating tip vortices.

Green et al. (1988) tested three different tip configurations on a hydrofoil and found that the so called *ring-wing tip* was very effective in reducing the inception index. These studies were further supported by Duan et al. (1992) who demonstrated an improved Lift/Drag (L/D) ratio, at high angles of attack, for an airfoil with the ring-wing tip. The results from the investigation of the ring-wing tip have been summarized by Green and Duan (1995), who attribute the improvement of the L/D ratio to redistribution of the shed vorticity in the Trefftz plane. The effect of the hydrofoil planform, with otherwise identical chord and cross sectional variation in the spanwise direction, has been investigated by Fruman et al. (1993). They found that a forward swept tip delays the onset of tip vortex cavitation,

suggesting that such a tip configuration could be of practical interest for marine applications.

1.2.3 Application of tip devices

Only a limited number of the tip appendages discussed here have been applied to full scale propellers. The only reported applications are of bladelets in the form of blade tips that are bent towards the suction side (Glover 1987) or the pressure side (Bystrøm 1996). For full scale propulsion systems, the focus has always been on improved fuel economy through an increased efficiency of the propeller. This improvement, it has been found, can more effectively be achieved with compound propeller configurations (e.g. contra-rotating propellers) and flow smoothing devices (e.g. Kort nozzles) than with tip devices. A number of these installations and their power savings relative to conventional propellers, are listed by Glover (1987), Manen and Oossanen (1988) and Breslin and Andersen (1994). Practical applications of some of these compound propeller configurations are described by Brophy (1986), Savikurki (1988) and Henriksen (1988).

1.2.4 Summary

Previous work aimed at reducing the strength of the tip vortices produced by marine propellers has demonstrated that any alteration to the geometry of the propeller will have a greater or lesser impact on the efficiency. Most of the tip appendages tested have been successful in terms of suppressing the tip vortices to an extent that tip vortex cavitation has been delayed, but not enough to compensate for the added parasitic drag. The cases where the tip devices have improved the efficiency of the lifting surfaces, including hydrofoils and airfoils in uniform incoming flows, seems to be the devices where special attention have been paid to the geometry with respect to reduction of both friction and profile drag. For example, Green and Duan (1995) found that a partial chord (0.65 c) ducted tip was superior to a full chord ducted tip.

The ducted tip appear to be the device where the best parasite drag characteristics can be achieved. Compared to a bulb of the same diameter, the duct will have a slightly higher friction drag, but on the other hand, a comparatively less profile drag. The duct will also be likely to interrupt more effectively the roll up process due to the flow through the duct, and therefore better reduce the strength of the tip vortex. The duct, as for the bulb, replaces a fraction of the span of the foil, and therefore keeps the added wetted surface to a minimum, while a winglet, or bladelet, effectively is an extension of the foil span, and is therefore a large source of added friction drag. The winglet can also, potentially, cause large profile drag if the correct profile or angle of attack not is chosen. In general, the ducted tip seems to the tip device that offers the best combination of geometric simplicity and efficiency.

1.3 Scope of work

This research is aimed at expanding our knowledge on the effect of attaching tip devices to the blades of full scale marine propellers. It is motivated and based on the results of Green and Duan (1995), which indicate that the ring-wing tip might have an application on propellers operating at very high loads, like propellers on tug boats and trawlers. The ring-wing tip has, when applied on marine propellers, adopted the name *ducted tip* propeller. It should not be confused with propellers mounted in nozzles, which are often referred to as *ducted* propellers.

Sea trials of a propeller installed on a fishing boat have been conducted in order to investigate the difference in 1) propeller efficiency and 2) tip vortex cavitation inception between a conventional propeller and a ducted-tip propeller. Chapter 2 describes the preparations and the experimental equipment as well as the procedure employed during the sea trials. Chapter 3 presents the results, Chapter 4 an analysis and a discussion, while a summary of this research is outlined as a conclusion and a set of recommendations in Chapter 5.

Chapter 2 - EXPERIMENTAL EQUIPMENT AND TECHNIQUES

A substantial part of the equipment needed for this project has been designed and built at the university, instead of buying stock products. This was done in order to satisfy, or rather compromise between, the following constraints for the instruments: 1) cost, 2) size, 3) range/resolution, 4) environment. The first three constraints affect each other, and depend on the size of the boat, engine and propeller. As soon as it was settled which boat to use for the sea trials, these constraints were essentially set. The last constraint, the environment factor, is a result of the nature of the experiments. When doing a sea trial, as opposed to laboratory tests, it is necessary make a greater effort to protect the instruments from the environment in which they are operating.

This chapter describes the features of the boat, the propeller and the ducted tips, and the transducers that have been applied to measure forces on the propeller shaft as well as the boat velocity and shaft rotational speed. It also describes the data acquisition system that goes with the transducers, the underwater video equipment, and finally, a description of the procedures adopted during the sea trials.

2.1 The boat, the propeller and the ducted tips

2.1.1 Pearl Sea

A 45 ft. wooden seine boat has been used for the sea trials (Figure 2.2). This boat is typical of a substantial number of seine boats that are operating in the coastal waters of British Columbia. At the time of the sea trials the stern roller, the net drum and the hydraulics associated with it were removed from the boat, making it substantially lighter than an operating seine boat. The width (beam) of the boat is 13 feet and it drafts 6 feet. The geometry of the hull can be described as having a very deep forebody with steep angles from the skegg and out towards the sides, changing sternwards into an afterbody that is fairly shallow and flat. A keel extends

all the way sternwards to the single screw propeller, and the rudder is an extension of the keel immediately aft of the propeller.

Pearl Sea is powered by a General Motors V6-71 diesel engine, rated to 200 HP at 2100 rpm at maximum engine output, and 180 HP at 1800 rpm at cruising speed. The transmission ratio is given to be approximately 2.5:1, reducing the maximum propeller rotation to 900 rpm. The propeller shaft has a diameter, D_S = 2.0 in. It sits horizontally between the transmission and the stern bearing, and the axis of the propeller is therefore essentially aligned with the incoming flow.

2.1.2 The propeller

To propel Pearl Sea, a Bronze-Manganese, 4 bladed, right hand screw propeller was chosen (Figure 2.3), with diameter, D = 36 in., and pitch, P = 29 in. The *expanded area ratio*, i.e. the total expanded area of the blades divided by the disc area, A_E/A_0 = 0.5. The area of the hub, which has a 5.5 in. diameter, is not regarded as a part of the expanded area.

The blades were modified from their original Kaplan shape, which is typical for propellers operating in a nozzle, to a slight skewed-back contour, which often is employed in order to reduce the impact from any leading edge cavitation (Bjørheden 1981). The profiles of the blade sections were also modified. Originally the blades had an ogival profile along their full spanwise length. They were reshaped according to equations and tables given for the Wageningen B-Screw Series (Manen and Oossanen 1988), to have an airfoil shape from the hub to $r = 0.8R$, and an ogival shape from $r = 0.8R$ to the tip of the blades, according to Troost (1937).

Preliminary propeller performance calculations carried out according to practical bollard pull estimations, outlined by Isin (1987), based on the Wageningen B-screw series, show that for cavitation free service, i.e. no surface cavitation, the propeller has to produce less than 4647 kg (10410 lb.) of thrust. Further calculations show that the maximum expected thrust produced by the propeller would be 2293 kg (5136 lb.) at 606 rpm. These numbers have not been corrected for Reynolds number effects; calculations based on the method of Isin (1987) apply

for $Re = 2 \cdot 10^6$ while for the sea trials typically $1 \cdot 10^6 < Re < 4 \cdot 10^6$, both at $r = 0.7R$. Due to lack of thickness of the original propeller, the thickness of the B-screw series could not be reproduced. Hence, the lift on the blades is reduced, and less thrust can be expected. A reasonable estimate of the maximum thrust would therefore be approximately 2000 kg (4480 lb.). These calculations are all based on bollard pull conditions, i.e. at zero velocity, $V = 0$.

2.1.3 The ducted tip

The ducted tip propeller is shown in Figure 2.4. The ducted tip design is geometrically similar to that used in the airfoil tests by Duan et al. (1992): duct-diameter/span, d/b = 0.05, and duct-length/chord, l/c = 0.65. The final dimensions are: d = 1.5 in. and l = 5.5 in. Each duct is built from a copper tube with wall thickness t = 0.06 in. that was bent into an arc with outer radius equal to the tip radius of the original propeller. The ducts have a completely circular cross section. The leading edge of the ducts have been formed into a spiral, or a lip, with the suction side of the duct extending furthest towards the blade leading edge. (Figures 2.5 to 2.7). The thickness of the duct leading edge was increased with epoxy body filler and rounded to delay leading edge cavitation, while the thickness of the duct trailing edge was filed down to reduce their wake. The ducts were attached to the blades by silver soldering, and aligned with the chord of the blades. The solder seams were covered with body filler and faired into a smooth transition between the ducts and the blades (Figure 2.8).

2.2 Instrumentation

In order to determine the efficiency of the propeller it is necessary to measure the torque and the thrust generated by the propeller, for example by measuring the stresses in the propeller shaft. The conventional method of measuring torque and thrust on any kind of a shaft is to cement strain gauges directly onto the shaft. Yet, measuring thrust on a propeller shaft can hardly be called conventional as it is done only on a very small number of sea going vessels,

according to Manen and Oossanen (1988), Haggarty (1994), McGreer (1994) and Towland (1994). The lack of thrust measurements on sea going vessels can partly be attributed to the fact that it is difficult to record the stresses in the shaft produced by the thrust, for reasons explained below. Nevertheless, while the torque, multiplied with the shaft rotation,

$$P_Q = 2\pi nQ$$

gives the power delivered to the propeller (neglecting losses through the stern bearing), there is currently no need to monitor the propulsive power, given by the thrust multiplied by the forward velocity of the boat relative to the water,

$$P_T = VT$$

Using strain gauges to measure forces in a solid circular bar, like a propeller shaft, is simple provided the bar is subjected to either pure thrust or pure torsion. However, on a propeller shaft there will always be a combination of axial and torsional forces, which complicates the measurements; the torque required to turn the propeller produce stresses that are an order of magnitude larger than the stresses produced by the thrust from the propeller. The shaft size necessary to withstand the high torsional stresses, will therefore allow only a minimum of shaft compression, resulting in very low magnitudes of axial strains. Millan (1993) found that the axial strains could be as much as 20 - 30 times less than the torsional strains. Three problems arise due to this large difference in strains:

1. Misalignment of the gauges, which in practice is impossible to avoid, will result in *cross talk* between the gauges. This implies that the axially oriented gauges (used to measure thrust) will register some torsional strain, which, because of the large difference in magnitude can substantial contaminate the thrust signals.

2. At low strain levels the errors introduced by temperature related apparent stresses as well as noise produced by the environment and the signal transmission from the rotating shaft to the stationary data acquisition system, will have a greater impact on the thrust measurements.
3. The minute axial strains are difficult to measure, although it can be done, by amplification of the signals. However, by amplifying the signals one would also amplify the errors.

To measure torque and thrust in a shaft, the strain gauges are arranged in two Wheatstone bridges, one for torque and one for thrust. In order to decouple the torque and the thrust, i.e. remove the cross talk, a technique has been developed that involves a modification of the thrust bridge. By replacing the single gauge in each of the two active arms of the bridge (Figure 2.1.*a*) with a rosette that contains two perpendicularly oriented gauges (Figure 2.1.*b*), a complete decoupling can be achieved (Millan 1993). Unfortunately the decoupling occurs at the expense of the axial strain being measured; using the rosettes reduces the sensitivity of the bridge by a factor of $(1 - \nu)$, where typically for steel Poisson's ratio $\nu = 0.28$, which is undesirable as the thrust strain already is very low.

The noise from the environment can to a certain degree be avoided by shielding the gauges from electromagnetic fields and radio frequency interference. The noise-to-signal ratio will also clearly depend on how the strain gauge signal is transferred from the rotating shaft: slip rings produce more noise than a telemetry or magnetic system. Furthermore, the signals can be amplified prior to the signal transmission to the stationary unit, which will improve the signal-to-noise ratio substantially, although this requires that the amplifier circuit be mounted to and rotates with, the shaft. The thermal-related apparent stresses are caused typically by gauge factor variation, gauge heating and thermal expansion coefficient mismatch between the gauge and the steel. The effects of the apparent stresses can be minimized through sophisticated electronic circuits, which together with the amplifier would have to be mounted to the shaft.

Obviously, by the time the torque and thrust have been decoupled and the errors have been minimized, the signal conditioning system has become very complex and expensive. A better technique of stress measurements involves mechanical decoupling and amplification of the strains. To decouple torque and thrust a section of the shaft could be replaced by a device consisting of links that experience either pure axial or torsional forces. A straight forward way to mechanically amplify the axial strains is by reducing the diameter over a short section of the shaft where the strain gauges are located. This section should preferably be incorporated as one of the links in the decoupling device. According to a patent search conducted in May 1994, few instruments exist that are capable of doing such a decoupling.

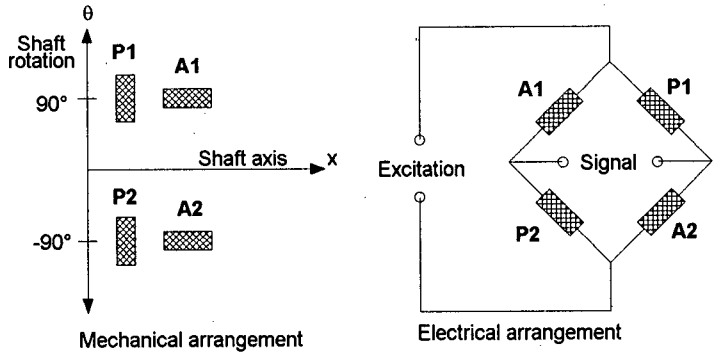

a) Conventional Wheatstone bridge

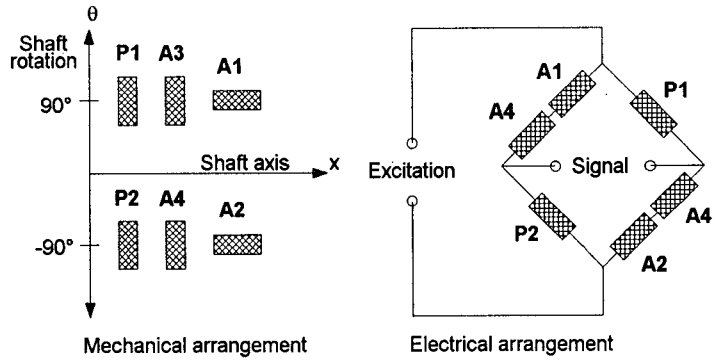

b) Wheatstone bridge with cross-talk compensation

Figure 2.1 Application of strain gauges for measuring thrust in a circular shaft.

2.2.1 Torque and Thrust Transducer (TTT)

For the sea trials described in this report, a torque and thrust transducer, hereafter referred to as TTT, was built that combines two of the above mentioned techniques: it consists of a set of links that decouples torque and thrust, where the diameter of the link that measures thrust has been reduced in order to mechanically amplify the thrust strain (Figures 2.9 and B.1). The transducer fits into the shaft line between the flanges of a previously existing coupling that connects the propeller shaft with the drive shaft, and hence slightly extends the shaft line (Figure 2.10). The axial length of the transducer had to be less than the maximum distance the coupling could be split apart, which was in turn limited by the distance between the propeller and the rudder.

The three main design constraints of the TTT were: maximum torque, maximum thrust and axial length of the transducer. Maximum torque was defined as maximum power (200 hp) divided by shaft rotation rate at cruising speed (700 rpm), giving Q = 2007 Nm (18042 lb.-in.). The shaft rotation at cruising speed instead of the maximum shaft rotation rate was chosen in order to build in an extra safety factor. We were not confident of the assumed engine shaft/drive shaft ratio. The design of the TTT started before the propeller was chosen, and therefore an estimate of the maximum thrust was based on the approximation that a well designed tug boat propeller should produce 15 kg of thrust per horsepower delivered to the propeller (Isin 1987). For a seine boat this number should be reduced, and for the design of the transducer 10 kg/hp was chosen, giving T = 19620 N (4480 lb.) at maximum power. This number is in accordance with preliminary calculations of the propeller performance described in Chapter 2.1.2. The axial length of the transducer was restricted to 4.5 in., which is the distance between the end of the propeller shaft and the rudder.

The transducer consists of two flanges, the same size as the coupling flanges, connected by means of three flat bars located circumferentially, at a radius of 2 in., around the centerline of the shaft axis. Each bar has one end connected to a support on the engine-side flange, while the other end is connected to a support

on the propeller-side flange. Because both ends of each bar are free to rotate around an axis parallel with the shaft, through the support, all of the bars will experience only pure tension when the propeller imposes a torque on the shaft during forward motion of the boat. During backwards motion the force will be purely compressive. One of the bars is equipped with strain gauges to form a load cell that measures the torque in terms of pure tensile or compressive strain.

The thrust is carried by a column located at the centerline between the two flanges. The diameter of the column has been reduced from a shaft size D_S = 2 in. to d_S = 0.5 in., thus increasing the strain by a factor of 16. Strain gauges are mounted to it and connected in a Wheatstone bridge to form a thrust load cell. The column is free to rotate around its own axis, and the friction between the shoulders of the column and the flange surfaces can be minimized by lubrication or, if necessary, a roller bearing. In this way it experiences no torque, and as a load cell it will measure pure compressive or tensile strain. Because the compression of the center column is small, the thrust imposes essentially no bending on the flat bars, and conversely, the flat bars carry no thrust.

The cross section of both the flat bars and the center column were chosen to give stresses equal to the design stress under maximum propeller torque and thrust. Throughout the design a minimum safety factor of 2 was used, allowing the stress levels in all members to reach a maximum of $\sigma_d = \sigma_y/2$. Steel code 4140 was chosen for the flat bars and the center column in order to minimize any hysteresis due to plastic elongation, and they were all heat treated to give a yield stress σ_y = 680 N/mm^2.

Calibration of the TTT was carried out on campus using facilities in both the Departments of Mechanical and Civil Engineering. The thrust cell was calibrated in a materials testing machine that exerted a pure axial force through the center of the transducer. The force, starting at zero, was increased in small steps to finally equal the maximum thrust expected to be produced by the propeller. The transducer was then unloaded with equal but opposite increments in order to test for hysteresis,

correlating the loads registered by the materials testing machine and the signals produced by the transducer after each force increment.

The torque cell was calibrated in a test bench set up on a lathe, where one flange is fixed in the lathe and the other is exposed to a pure torque through a load on an 18.5 inches arm. The load on the arm was recorded with a ring load cell, described later in this chapter. As for thrust, the torque was increased in steps to match the maximum expected torque produced by the engine, for then being released again with equal and opposite increments. The torque was registered and correlated with the signals from the transducer in order to plot a calibration curve and calculate a calibration factor. The calibration data for both the torque and thrust cells are presented in Figures A.1 and A.2 of this report.

Further testing has confirmed that the transducer responds linearly to both torque and thrust, with no discernible cross-talk; the torque cell responds linearly when a pure torsional force is applied, while the thrust remains constant at a preset magnitude. Following the same trend, when a pure axial force is applied, the thrust varies linearly while the torque remains constant at a preset magnitude.

Both the torque and the thrust load cell are equipped with strain gauges arranged in a full Wheatstone bridge. The Wheatstone bridge consists of two active gauges, oriented in the direction of the principal stresses in the load cell, and two inactive gauges, oriented perpendicular to the direction of the principal stresses. With this arrangement the inactive gauges will automatically compensate for apparent stress due to thermal expansion of the load cells. The difference in temperature between calibration and the sea trials will therefore have no effect on the TTT and the results of the efficiency measurements.

Provided a bolted flange coupling exists, and the distance to the rudder allows for the propeller shaft to be displaced, the TTT has a number of advantages and is more versatile than strain gauges mounted directly on the shaft:

1. All preparations involving machining of parts, cementing strain gauges onto load cells, and in particular, the calibration, can be done in a machine shop or a

laboratory instead of onboard the boat. Only the final installation, bolting the transducer to the coupling, has to be done on site.

2. By avoiding modifications of the shaft, the damage done to the shaft itself, as well as the alignment difficulties, are minimized.
3. It can be scaled up to fit different shaft sizes.
4. The load cells can be replaced if greater resolution is desired or if more strength is required, or in case of damage.
5. The parts are easy to machine, resulting in low manufacturing costs.

2.2.2 Ring load cell

Drogues of varying drag were constructed of bundled car tires. These drogues were towed behind the boat. The drogue drag was monitored by a 5000 lb. ring load cell. In this way any variation in the thrust from the propeller could be correlated to variations of the drag force on the drogue. The ring load cell was calibrated by loading it in pure tension in the materials testing machine, following the same procedure as for the TTT. The calibration data are presented in Figure A.3.

2.2.3 Velocity transducer

An industrial turbine flow meter for recording mass flow in pipes was adapted to measure the velocity of the boat. Compared to a standard velocity meter of the paddle wheel type, the turbine flow meter can measure lower velocities, although at low velocities it is non-linear due to bearing friction in the turbine. The lowest velocity it is capable of measuring is approximately V = 0.5 m/s. In order to measure the true velocity of the boat relative to the water, the flow meter had to be located away from the flow field induced around the hull. This was done by attaching the flow meter to one of the stabilizer poles, extending 17 ft. out to the side of the boat. The stabilizer poles can be seen on Figure 2.2, located midship and brought up to a vertical position.

The calibration of the velocity transducer was carried out in the towing tank of BC Research by attaching the velocity transducer to the carriage of the towing tank. The carriage was run at a constant velocity along the full length of the towing tank, and an average signal from the flow meter sampled throughout the run, disregarding the acceleration phase at the start, was associated with that particular velocity. This procedure was repeated for a number of different velocities. The calibration data are presented in Figure A.4.

2.2.4 Tachometer

The propeller shaft rotation was measured by a MAXI-MAG magnetic sensor. The sensor counts the passage frequency of gear teeth on a gear (4 inches in diameter, with 60 teeth) connected to the propeller shaft (Figure 2.10). The tachometer was calibrated in a lathe in the Department of Mechanical Engineering, equipped with a tachometer of similar type, and a digital display. The gear was fixed in the chuck of the lathe, the sensor was mounted at a prescribed distance from the gear, and the signals from the magnetic sensor was correlated with the chuck rotation registered by the lathe. The chuck rotation was double checked with a hand held tachometer. The calibration data are presented in Figure A.5.

2.3 Signal conditioning and data acquisition system

A schematic diagram of the experimental set-up for the sea trials is shown in Figure B.2. The signals produced by the torque and thrust load cells are conditioned separately by two printed circuit boards that each have an amplifier, an analog-to-digital (A/D) converter and a radio transmitter. Both boards, approximately 2 in. by 2 in., are installed and sealed together with two 9V batteries for power supply, in a plastic box that is mounted on, and turns with the shaft. After being conditioned the signals from the torque and thrust load cell are transmitted simultaneously, at a rate of one signal a second, on two separate channels to a stationary receiver. The receiver is connected directly to a computer, which, by using commercial software, can log the data for any length of the sampling period.

The signals from both the torque and thrust load cells are received as *radio transmitter units* between 10 and 1023. To obtain, for example, the thrust measured by the TTT, the average radio transmitter unit sampled on the thrust channel over a period of 30 seconds during a test, minus the units recorded at zero shaft rotation, is multiplied by the respective calibration factor to give the thrust in Newtons (N). The *zero-load offset* (N = 0) can be set to any desired value between 10 and 1023.

The signal from the ring load cell is amplified (BN3031) before it is sampled by the computer through a 12 bit, 1 MHz, ISC-16 A/D card. Both the velocity transducer and the shaft rotation transducer produce signals in the form of pulses with frequencies proportional to the rotation of the turbine and the gear, respectively. These signals are therefore first sent through a frequency-to-voltage converter (LM2407), and then, amplified (A07) before they are sampled through the ISC-16 A/D card.

110 VAC was supplied by a Briggs & Stratton/Homelite 2500 Watt generator with a VARIAC voltage regulator.

2.4 Underwater video recording

Visual recordings of the tip cavitation were obtained with a Sony Hi8 CCD-V99 video camera with a maximum shutter speed of 1/10000 second. The video camera is mounted in a water tight, cast aluminum housing, and powered by either a 9 volt battery or 110 volts from the surface. Light was supplied by two 650 watt underwater lights and a 100 feet cable for 110 volt power supply from the surface.

2.5 Procedure for sea trials

The sea trials consisted of two sets of experiments; the first for the conventional propeller, and the second for the ducted tip propeller. Each set was divided into sub-experiments: first efficiency measurements at five different advance ratios, followed by cavitation observations at zero velocity.

The efficiency measurements involved sampling of torque, thrust, velocity, shaft rotation and tow load data for 5 different drogue sizes:

1. Free running - no tow load
2. Light drogue - 14 tires in one bundle
3. Medium drogue - 30 tires in two bundles (14+16)
4. Heavy drogue - 48 tires in two bundles (37+11)
5. Bollard pull - pulling against the dock, zero velocity

For each drogue size data was collected from approximately 180 rpm up to maximum shaft rotation; in steps of 10 from 180 to 260 rpm, in steps of 20 from 260 to 300 rpm, and in steps 50 from 300 to maximum rpm, depending on the drogue size. For each increment conditions were stabilized before data were acquired over a period of 30 seconds. Every data point presented in this report is an average of the data sampled over 30 seconds, unless otherwise stated. At maximum shaft rotation the boat was turned 180° and the measurements were retaken. In this way the effect of the tide, wind and waves could be determined.

Cavitation observations were carried out by a diver taking video recordings of the turning propeller while the boat was tied to the dock. The diver was harnessed to the dock, filming from a 30 - 60° angle, approximately 10 feet aft of the propeller. Before the filming was started, the shaft rotation rate at cavitation inception was determined by increasing the shaft rotation in as small as possible increments until the diver could see the first white bubble of the tip vortex cavitation on the tips of the propeller. The shaft rotation was then reduced and video recordings were carried out for shaft rotations from 250 rpm up to the maximum; in increments of 10 up to 300 rpm, 25 between 300 and 400 rpm, and increments of 50 from 400 up to maximum shaft rotation.

Figure 2.2 Pearl Sea up for painting prior to the sea trials.

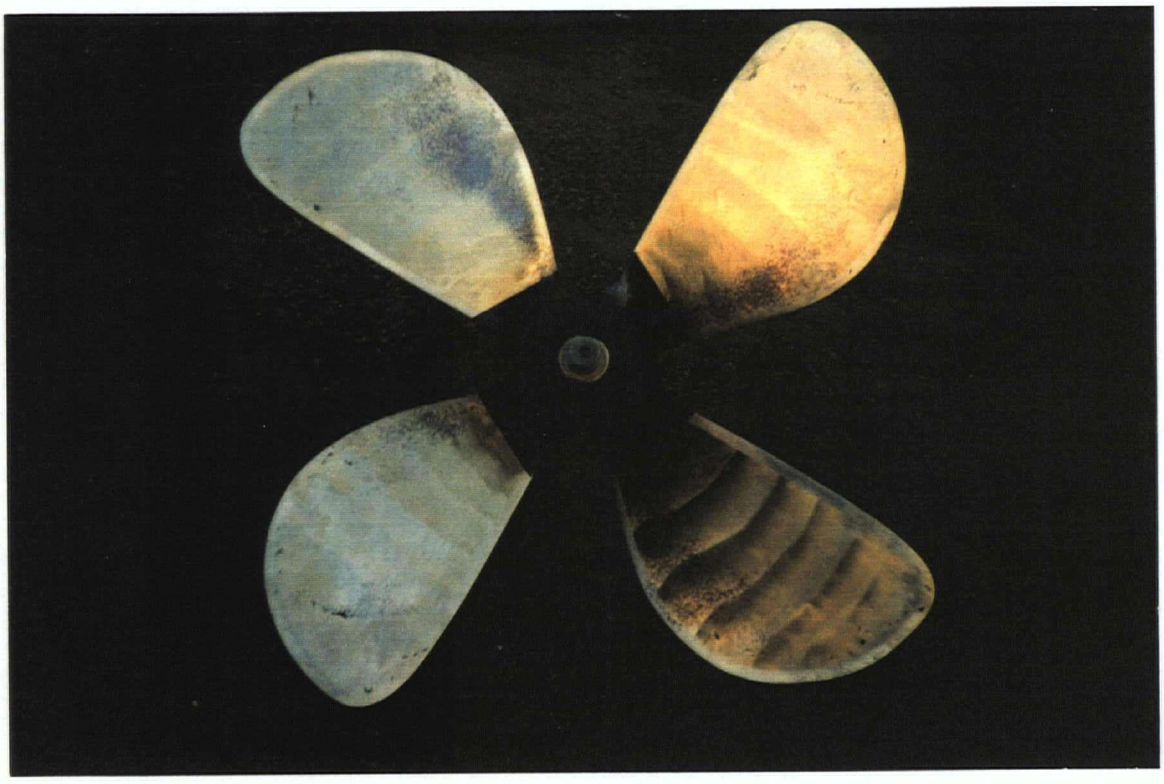

Figure 2.3 The conventional propeller.

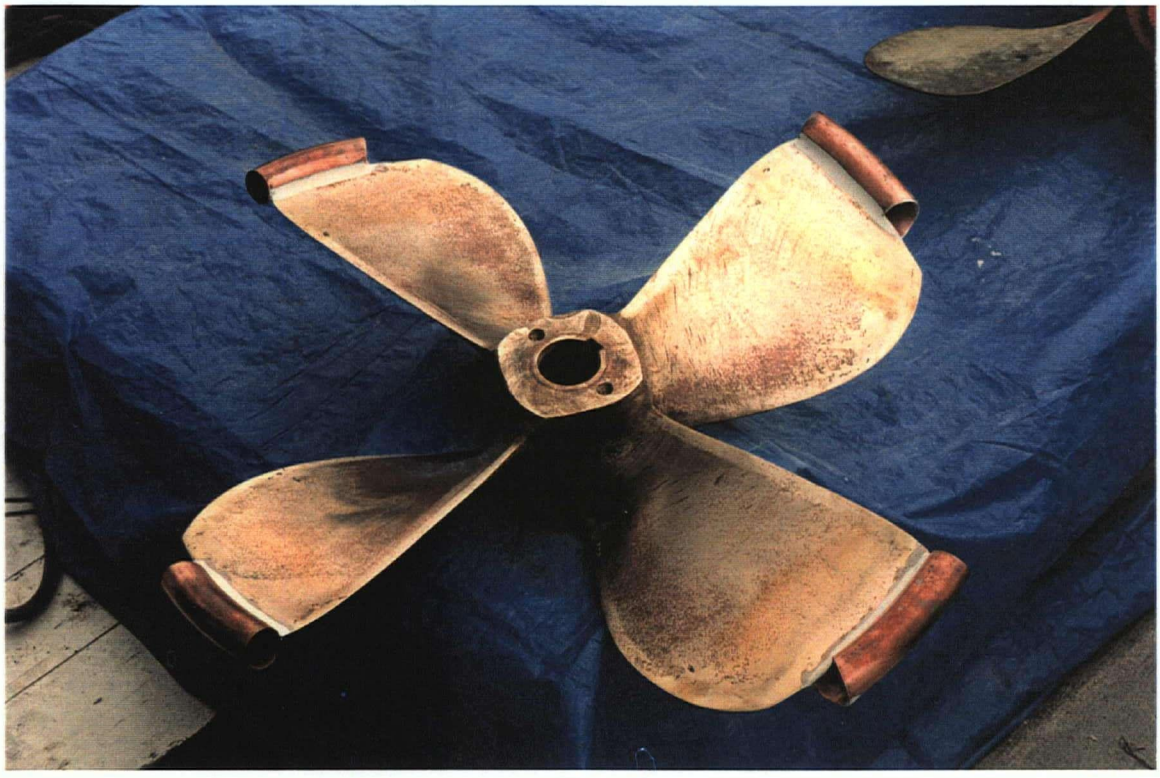

Figure 2.4 The ducted tip propeller.

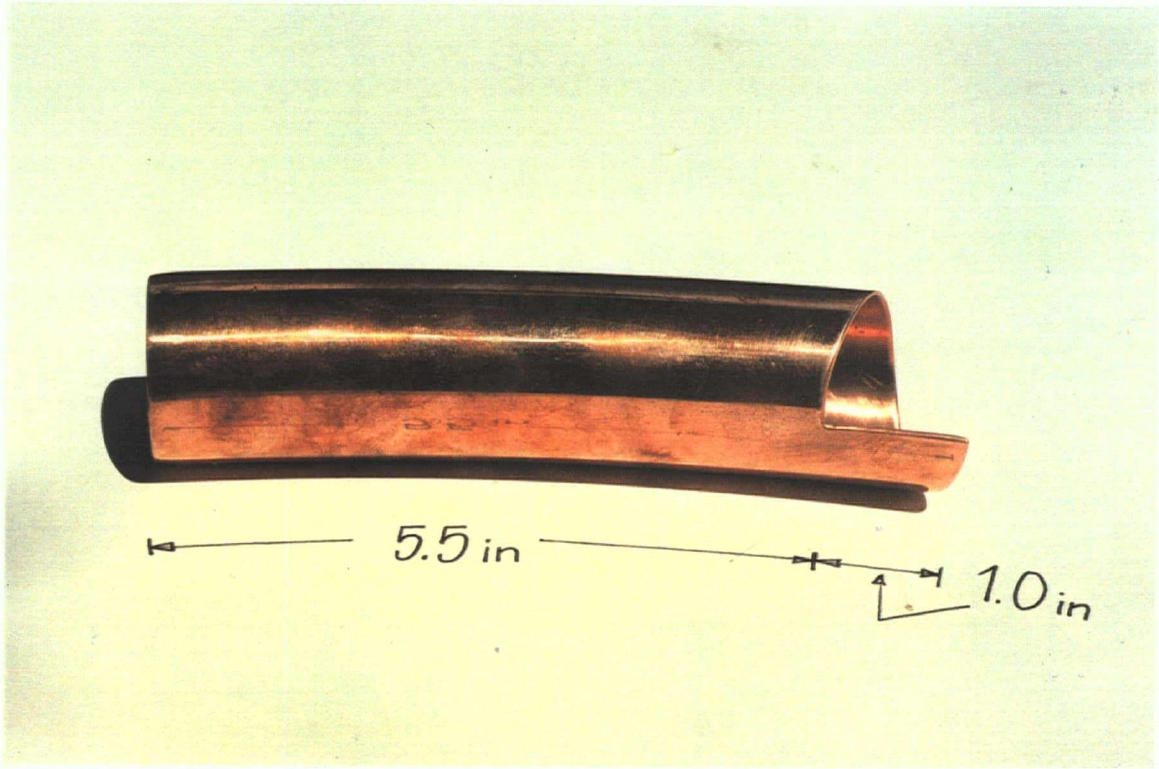

Figure 2.5 Details of the ducted tips: Size and geometry.

Figure 2.6 Details of the ducted tips: Seen in proportion to the rest of the blade.

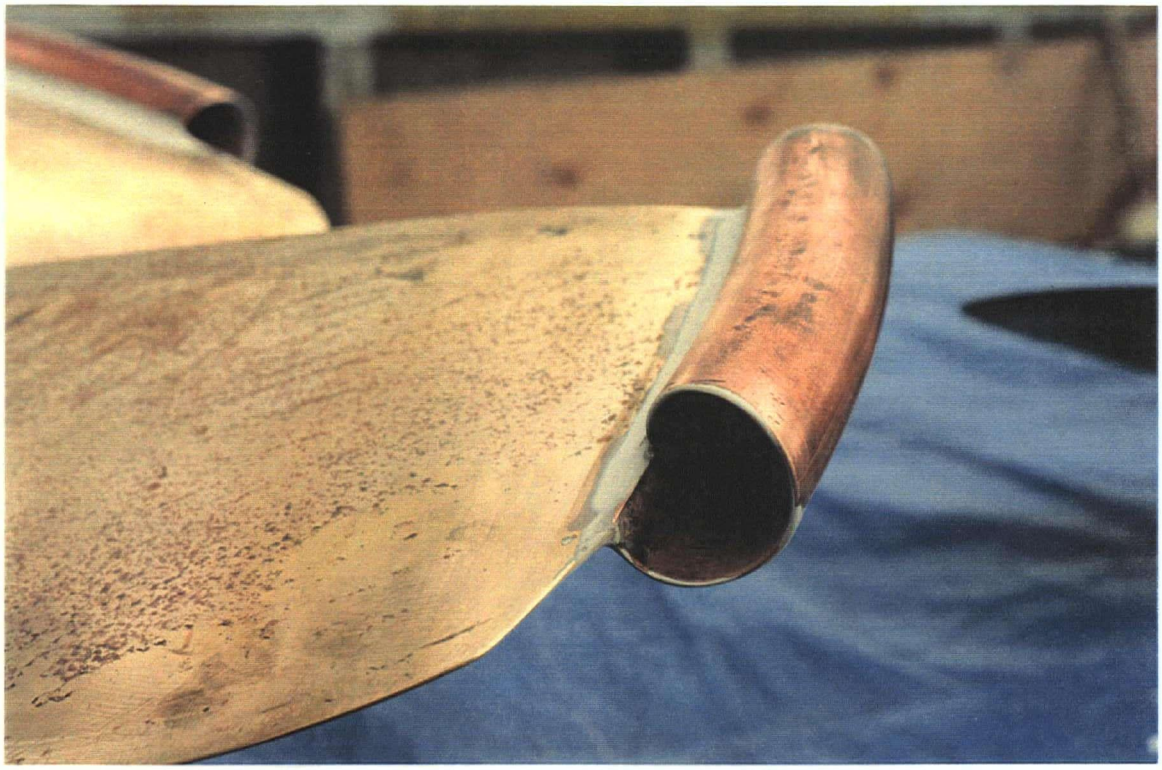

Figure 2.7 Details of the ducted tips: The entrance of the duct from the pressure side.

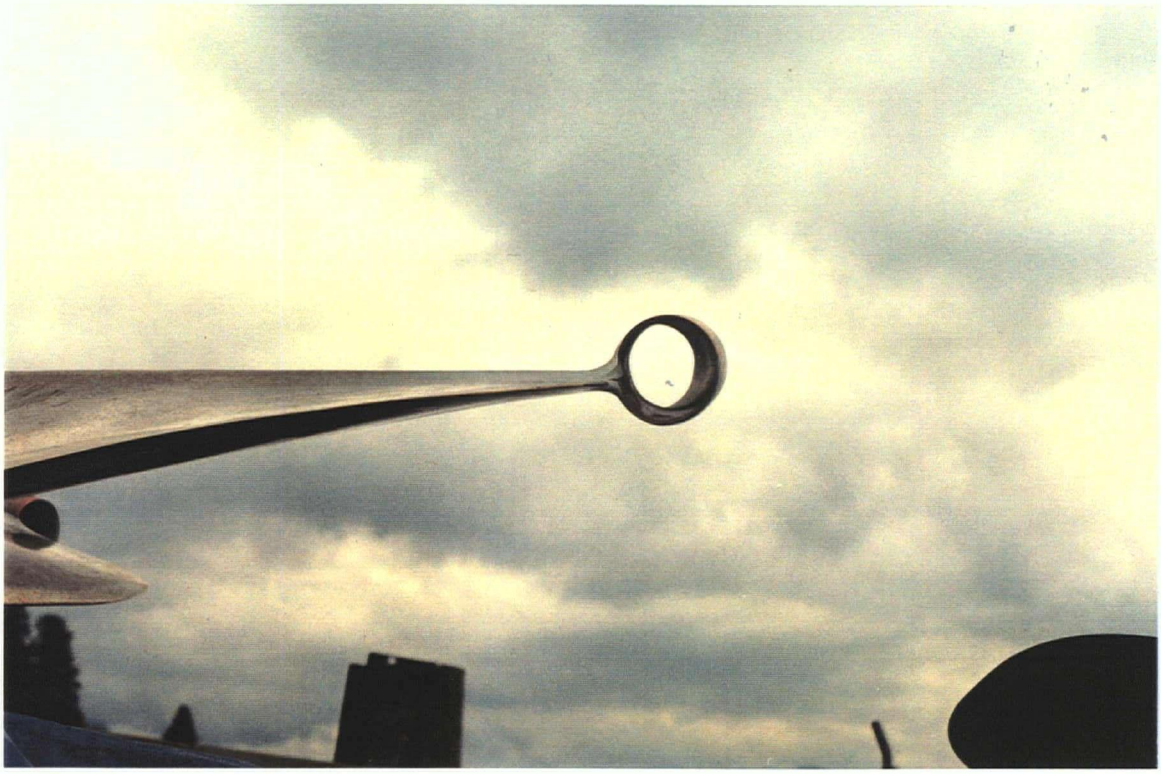

Figure 2.8 Details of the ducted tips: View through the exit of the duct.

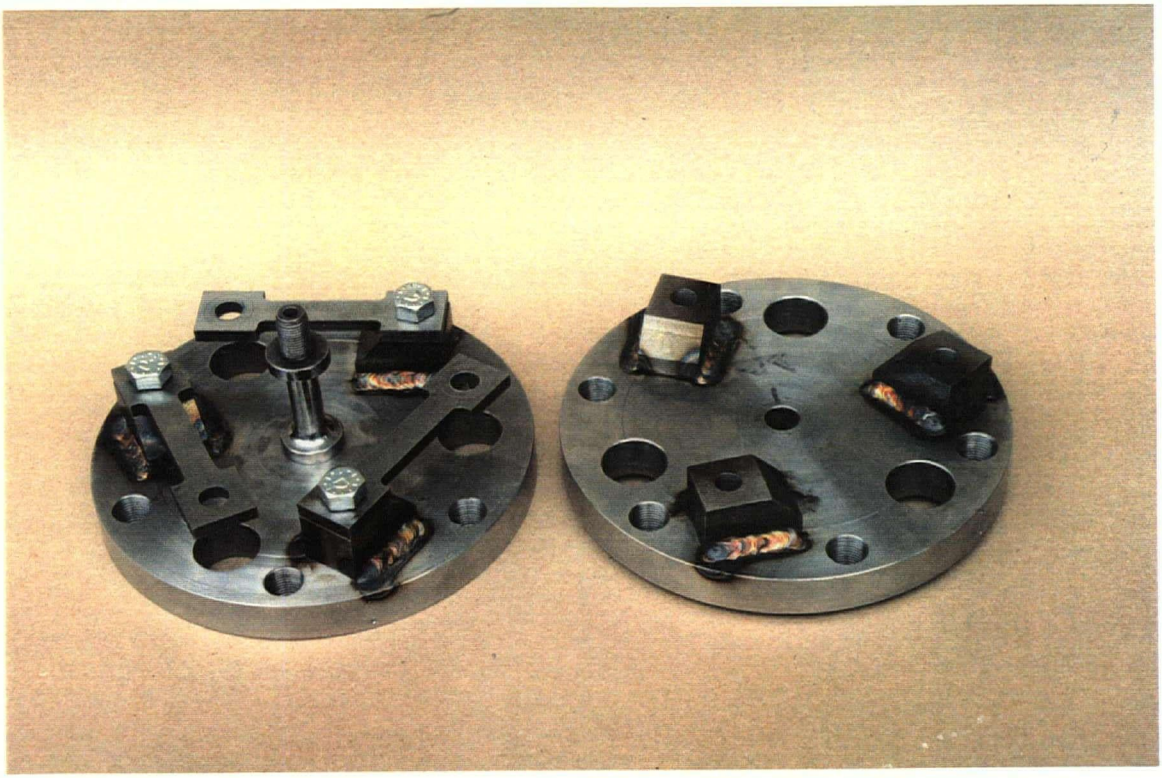

Figure 2.9 Details of the Torque and Trust Transducer (TTT).

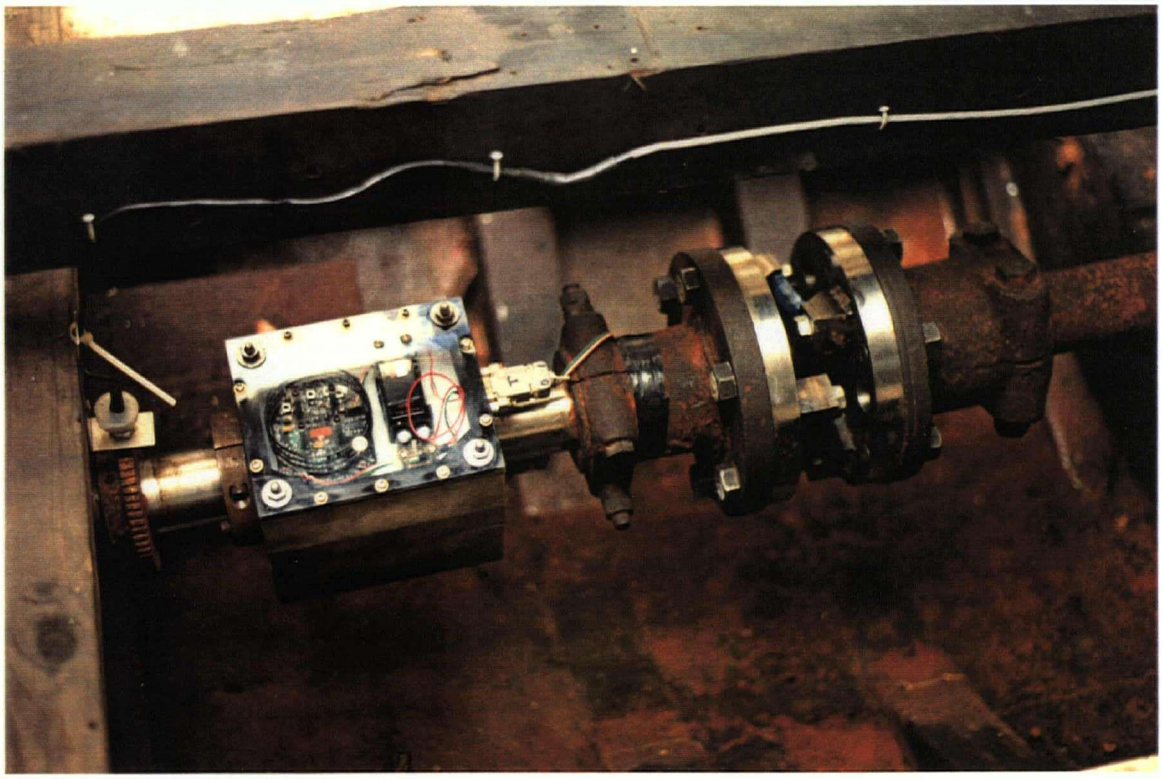

Figure 2.10 The TTT installed on the propeller shaft of Pearl Sea.

Chapter 3 - RESULTS

This chapter commences with a report on some general observations of the performance of the test equipment, followed by a section describing the method used to estimate the errors introduced by the instruments, and finally, the results of the sea trials.

3.1 Performance of the test equipment

The mechanical performance of the TTT (U.S. patent no. 5,445,036 of August 29, 1995) has been closely observed. Interest was first focused on the strength of the device. No problems have occurred even though the transducer has experienced substantially rougher service conditions than anticipated, especially associated with landing of the boat, when at times abrupt shifts into high reverse thrust has been necessary. No sign of fatigue in load cells and bolts, or loosening of bolts, has been observed. Misalignment of the transducer, and its potential to amplify any of the harmonic vibrations of the shaft line, received close attention, particularly because of the transducers weight and its position far from the shaft support points on each side (Figure 2.7). However, the installation of the TTT did not result in extra vibrations. The effect on vibrations of displacing the propeller 4.5 in. sternwards, and thus increasing the distance between the propeller and the stern bearing was considered and partly compensated for by shortening the shaft by two inches prior to installing the TTT.

As a part of the strength considerations, the measured torque and thrust was compared with the predicted values. The maximum measured torque was 9.5% less than the predicted maximum value, while the maximum measured thrust was 10.8% less than the prediction. For the purpose of this comparison, only data for the conventional propeller has been considered. The accuracy of the predictions implies that the TTT was appropriately designed for the torque and thrust measured.

Prediction of the torque was based on the maximum power delivered at the crank shaft. However, no losses were taken into consideration, i.e. losses through the gear box and one bearing, which would cause the power transferred through the TTT to be less. In addition the maximum expected shaft rotation of 900 rpm was never achieved, mainly as a result of the gear ratio being higher than expected. Some reduction in maximum shaft rotation can be attributed to an excessively high pitch of the propeller. The boat owner commented that the engine struggled to achieve the same top shaft rotation rate as for his own propeller, which has a 0.625 in. larger diameter but with 2 in. less pitch. This indicates that the engine never was able to deliver the maximum power. The maximum power transmitted through the transducer was measured as 152 hp at 587 rpm. See Table 3.1.

Conditions at maximum:		P_Q **[Hp]**	N **[rpm]**	Q **[Nm]**	T **[N]**
Power	**predicted**	**200**			
	measured	**152**	587	1817	15459
Shaft rotations	**predicted**		**900**		
	measured	152	**603**	1770	13249
Torque	**predicted**	200	700	**2007**	
	measured	152	587	**1817**	15459
Thrust	**predicted**	200	606		**19620**
	measured*		459		**17504**

Table 3.1 Predicted and measured torque and thrust produced by the propeller. *Maximum thrust was measured during cavitation observations.

While the prediction of the maximum torque was based solely on the power that the engine can supply, the prediction of the maximum thrust was in addition based on the size and shape of the propeller. Because the propeller was manually reshaped, the shape and profile of the B-screw series were only moderately well adopted. This may have influenced the prediction of the maximum thrust to a certain extent, although the main deviation is caused by basing the prediction on a too high value for maximum power (Table 3.1). On the other hand, the propeller was capable of delivering 13.9 kg/hp at ordinary bollard pull (N = 459 rpm, Q = 1795 Nm and T = 15969 N) instead of the 10 kg/hp that was used in order to dimension the load cells of the TTT. In other words, the lack of power available was compensated for by the higher thrust producing capacity of the propeller.

In spite of a well designed transducer, seen from a mechanical point of view, it was concluded that the concept needs to be improved with regards to the signal transmission. The dynamic response of the transducer is limited by the transmission rate (1 signal/second). A better dynamic response would be useful in order to determine if the load variations on the shaft are caused by varying hydrodynamic and aerodynamic forces, or if they are caused by vibrations of the shaft line. However, the lack of dynamic response will only be a problem if a set of torque or thrust data is very stable, indicating that the transmission ratio coincides with the frequency of the varying load. In such a situation we could not determine if the average value we are reading is too high, too low or is the true average. This situation has not been encountered with the data collected during the sea trials.

During the sea trials of the conventional propeller the magnetic pickup of the tachometer was positioned too far from the inducing gear, resulting in unsteady measurements at idle shaft rotations (N = 145 rpm). The problem was corrected for the ducted tip propeller, although this problem was not a concern as efficiency data was not recorded for shaft rotation rates less than 180 rpm.

The velocity transducer gave unsteady readings at low velocities. This is caused partly because of its non-linear behavior at the bottom end of its operating range, but mainly because of the relatively higher impact of the vertical movement

as the boat were rolling due to waves. In extreme cases the flow meter, positioned approximately 2 ft. below the surface in still water, would be elevated out of the water, which not only gave zero velocity readings, but also disconnected the ground for the data acquisition equipment. Data collected when this is known to have happened have all been discarded.

Both when pulling the drogues and at bollard pulls, a force perpendicular to the tow direction was introduced on the tow line. When towing at a forward motion asymmetric hydrodynamic forces could be the reason for this. However, as confirmed at bollard pull, there is a sideways force (similar to "prop walk") acting on the drogue due to the tangential momentum of the water in the propeller wake, which, because of equilibrium, will act with an equal magnitude but opposite direction on the hull. At drogue pulls this side force caused the tow line to always have a small angle relative to the centerline of the boat, in the opposite direction of the propeller rotation, and at bollard pulls, it pushed the boat in the direction of the propeller rotation. This effect should, however, have no impact on the thrust measurement, whereas it will cause the tension in the tow rope to be 0 - 2% higher than the resistance of the load.

Between the last test with the conventional propeller and the first test with the ducted propeller, a misalignment was introduced in the shaft line, causing the TTT to register varying zero-load offsets for both torque and thrust, depending on the tangential position of the shaft. The misalignment affected the torque load cell the most, by varying its reading by 28 radio transmitter units (54.6 Nm) between the maximum and minimum offset, positioned approximately 180° apart. The difference between the maximum and minimum thrust offset was measured to be 10 radio units (178.3 N), positioned approximately 180° apart, with a 135° phase angle to the maximum torque offset. The variation in offset was not discovered until all the tests with the ducted propeller had been terminated, and therefore all the torque and thrust offsets recorded prior to each run, measured only at one tangential position, had to be adjusted. The tangential position of the shaft at the time of the offset recordings is, however, known: between 0 and 45° from the position of maximum

torque offset and 0 to 45° from the position of minimum thrust offset. A conservative adjustment was therefore made by assuming that the recorded offset values were equal to maximum torque offset and minimum thrust offset, which means subtracting 14 radio units from the recorded torque offsets, and adding 5 radio units to the recorded thrust offsets. Both adjustments contribute to reduce the measured propeller efficiency, and consequently, to present a conservative result of the ducted tip propeller sea trials.

The offset variations were discovered because of a drift in the signals from both the torque and the thrust load cell, which first were assumed to be the reason why the signals did not return to the same zero-load offsets. When analyzing the data, the drift was found to have been introduced after the completion of the test of the ducted tip propeller pulling the heavy drogue. The tests with the medium and light drogue, as well as at free running speeds, were all conducted on the same day, 5 days after the heavy drogue. The drift is known to occur when the supply voltage of the radio transmitter falls below 7.5 volts. In this case the voltage of the batteries for both the torque and thrust channel was 8.8 volts. However, after replacing the same batteries subsequent to the voltage check, the signals stabilized, suggesting that the battery poles may have been contaminated by the humidity as they remained on the shaft between the tests. This contamination would cause an erratic voltage supply to the radio transmitter. Because every signal from the TTT is associated with a time value (in seconds) supplied by a counter in the radio receiver, the drift can be calculated by dividing the difference of the first and last measurement for each drogue size, both at $N \approx 180$ rpm, by the time between these two measurements. Every recorded value for torque and thrust has subsequently been adjusted by adding the drift, multiplied by the time associated with that particular measurement.

The maximum error due to incorrect offset recordings has been estimated as 6% at N = 180 rpm, and less than 1% for N > 500 rpm. The error due to drift is estimated to be 5% at N = 180 rpm, and less than 0.5% for N = 550 rpm. These errors will add to the inaccuracy of the instruments, described in the following

chapter. However, because every data point has an associated individual error, no error bar representing drift or incorrect zero-load offset has been included with the results.

3.2 Instrumentation error

The accuracy of the instruments used during the sea trials is based on the deviation from the calibrated value of the instrument at a particular signal. This requires a more detailed explanation: during calibration, the individual instruments were *excited* by a second device for which the excitation was known and assumed to be the *true* value. The true value was plotted as a function of the signal from our instrument. A least-squares fit curve was plotted through these points, being the calibration curve of our instrument. The standard deviation, S_x, of the instrument is given by the deviation of the true values from the calibration curve. The error is equal to $\pm 2S_x$ (95% confidence interval) plus the resolution of the analogue to digital conversion.

Finding the error of the efficiency measurements is more complex. The efficiency is a product of four parameters (velocity, shaft rotation, torque and thrust) that all have a separate error associated with them. A method described by Bevington (1969) has been used to determine the square of the deviation for every efficiency point,

$$\frac{S_{\eta j}^2}{\eta_j^2} = \frac{S_V^2}{V_j^2} + \frac{S_T^2}{T_j^2} + \frac{S_N^2}{N_j^2} + \frac{S_Q^2}{Q_j^2} + \frac{2S_V S_T}{V_j T_j} - \frac{2S_V S_N}{V_j N_j} - \frac{2S_V S_Q}{V_j Q_j} - \frac{2S_T S_N}{T_j N_j} - \frac{2S_T S_Q}{T_j Q_j} + \frac{2S_N S_Q}{N_j Q_j}$$

from which the standard deviation can be determined,

$$S_\eta = \sqrt{\frac{1}{M-1}\sum_{j=1}^{j=M} S_{\eta j}^2}$$

and, as for the individual instruments, the error is set to $\pm 2S_\eta$ in order to stay within a 95% confidence interval.

3.3 Efficiency measurements

The results of the sea trials with both the original and ducted tip propeller are presented in Figures 3.1 - 3.10. Figure 3.1 shows the results from the bollard pull trials. Bollard pulls were carried out only for the conventional propeller. Figures 3.2 - 3.5 present the results for the heavy, medium and light tows, as well as free running condition, respectively. Part *a*, *b* and *c* of each figure contains the torque, thrust and velocity, respectively, for both the conventional and ducted tip propeller, plotted as a function of the shaft rotation. To each set of data from the conventional propeller, a third order, *least-squares fit* polynomial curve has been drawn through the points in order to visually enhance the trend of the data. This curve has also been forced through the origin as it is expected that all parameters are zero at zero shaft rotation. Part *d* of each figure, contains the efficiency

$$\eta = \frac{VT}{2\pi nQ} = \frac{30VT}{\pi NQ}$$

for both the original and ducted tip propeller, plotted as a function of the advance ratio

$$J = \frac{V}{nD} = \frac{60V}{ND}$$

Figure 3.6 contains all the previous efficiency points plotted in the same diagram, again as a function of the advance ratio, while Figures 3.7 and 3.8 show the corresponding torque and thrust coefficients,

$$K_Q = \frac{Q}{\rho n^2 D^5} \qquad \text{and} \qquad K_T = \frac{T}{\rho n^2 D^4}$$

respectively.

Figures 3.9 and 3.10 shows the torque and thrust data recorded during a typical run with the conventional propeller and the corresponding set of data recorded with the ducted tip propeller, both sampled over a period of 30 seconds.

3.3.1 The conventional propeller

Throughout this sub-chapter all references to Figures 3.1 trough 3.10 are only concerned with the data for the conventional propeller.

The results from the bollard pulls, shown in Figure 3.1, display more scatter of the data than seen for any of the drogue pulls. A combination of shifting wind and the propeller trying to pull the boat sideways as well as creating local currents, caused highly unsteady pulling conditions. It was difficult to keep a constant tension on the tow line, as seen from the tow load data. Despite a rubber damper on the tow line, the line seems to have experienced impact loads during two of the sampling runs ($N \approx 275$ and 330 rpm), probably as the propeller thrust picked up slack on the line. The high tow loads also could be a result of sharp pull angles due to the side forces. The trust measured during the cavitation observations, when the boat was moored alongside the dock, produced less scatter around the regression line, confirming that the variation of the tow line data is a result of the unstable pulling conditions. This is less of a problem during the drogue pulls as the forward velocity keeps the boat on a steady bearing.

The tests at free running speeds and with the light drogue (Figures 3.4 and 3.5) were used to determine how the equipment performed and which external factors had to be considered, in order to establish a test procedure for the remaining sea trials. Hence, there is no repeated pattern to the amount of points and the interval between them for the data collected during these two test runs. Based on these runs it was decided that more points were needed at low shaft rotation rates as the variation of the test conditions, such as wind, waves and tidal currents, have a larger impact on the measurements in this range.

The impact of variable test conditions is seen in the data from the heavy drogue. After sampling data while traveling in one direction, the boat was turned around to return to the dock along the exact opposite bearing and the measurements were re-taken (Figures 3.2 and 3.3). This run was carried out on a day with small waves (< 30 cm), negligible tidal currents, and light wind. With the heavy drogue there is a slight deviation of the thrust (Figure 3.2.*b*), particularly at low shaft rotations. The low thrust values, for N < 300 rpm, are all measured on the returning leg, with a simultaneous trend of higher velocity in that direction (Figure 3.2.*c*). The deviation is probably caused by the changing aerodynamic drag as we headed straight into the wind on the departing leg and straight out of it on the returning leg.

Figures 3.4 and 3.5 show that the spread of the velocity data decrease as the drogue size is reduced, especially at low shaft rotations. This is because lighter drogues imply higher forward velocities at the same shaft rotations, which diminishes the effect of boat rolling and pitching on the velocity measurements. It should also be mentioned that the non-linear velocity of the boat at free running speeds (Figure 3.5.*c*) is caused by the sharp increase in wave resistance as the Froude number exceeds 0.3. At V = 4 m/s, Fr = 0.38.

There is, on the other hand, an increasing variation of torque and thrust as the drogue size is reduced, indicating that the drogue acts as a stabilizing load against impacts from the external forces such as waves. However, the variation of the data introduced by the external conditions, such as the aerodynamic drag, seems to have had no effect on the efficiency (Figures 3.2 to 3.5, part *d*, and Figure 3.6) other than resulting in a wider spread of the points, particularly the points recorded at low velocities at free running speeds. Thus, the test conditions can be assumed to not have affected the outcome of the sea trials[1].

[1] The ducted tip propeller was tested under similar, but slightly less rough, sea conditions than was the conventional propeller.

3.3.2 The ducted tip propeller

The data from the measurements of the ducted tip propeller follow the same general pattern as the data for the conventional propeller, but with slightly increased gradients for both the torque and thrust when plotted as functions of the shaft rotation (Figures 3.2 to 3.5, part *a* and *b*). The position and gradient of the individual torque and thrust curves do not tell us anything about how the propeller performance has changed; any changes merely indicate that the blade characteristics have been altered. The relationship between the thrust and torque curves will, however, indicate if the propeller efficiency has increased after the installation of the ducted tips. It is therefore of interest to notice that the gradients for the thrust curves seems to have increased more than those of the torque curves, particularly as the drogue size is reduced. This observation is in accordance with the actual efficiency calculations, which show that the highest improvement was achieved at high advance ratios. The torque and thrust measurements are compiled into K_Q and K_T curves, plotted as functions of J (Figures 3.9 and 3.10). From these two diagrams it first of all can be seen how the thrust in particular, has increased towards higher advance ratios after the installation of the ducted tips. It also appears that the ducted tips caused a loss of both torque and thrust at low advance ratios. An equivalent trend can be seen for a number of the propellers tested with bladelets by Itoh et al. (1987). This effect is probably caused by flow separation, and will be discussed in Chapter 4.3.

The difference in velocity between the conventional and ducted tip propeller is in general within the instrumentation error, implying that the ducted tips do not affect the speed of the boat. However, the results from pulling the heavy drogue (Figure 3.2.*c*) indicate an increased velocity at high N. Higher velocity at the same shaft rotation suggests that the efficiency of the propeller has improved, but the efficiency diagram (Figure 3.2.*d*) shows that there is little or no improvement of the efficiency at these advance ratios.

A reduction of the top shaft rotation rate was anticipated because of the increased parasite drag associated with ducted tips. However, the measured

reduction of less than 2% in N at free running speeds is very encouraging. Installation of the ducted tips does not reduce the shaft rotation rate and therefore does not cause the engine to run at off-peak efficiency, i.e. a boat retrofitted with a ducted tip propeller would not require installation of a new transmission.

During the sea trials a number of other factors caught our attention with respect to the performance of the ducted tip propeller: there was no noticeable changes to the maneuverability of the boat, a factor that was put to a test every time the boat was maneuvered in and out from the dock. According to the skipper the propeller still had a good *bite*, i.e. high acceleration in either direction, when needed. The owner also commented on how the wake was different at low and moderate velocities. With the ducted tip propeller, the tip vortices were visible in the surface wake substantially further behind the transom than is the case with the conventional propeller. Although this does not prove that the propeller performance is improved, it should be regarded as an indication that the tip vortices have been suppressed.

Finally, the addition of the ducts did not seem to intensify the vibration onboard the boat. This implies that the ducted tips have been installed with more or less identical orientation, resulting in an even loading on the four propeller blades. In addition, any weakening of the tip vortices as a result of installing the ducted tips will also contribute to reduce the vibration. Some amplification of the torsional vibration may be expected due to increased resistance of the ducts passing through the different regions of the hull wake. Torsional vibration is harder to detect by simply being onboard the boat, first of all because of the nature of the vibration - tangentially around the shaft axis - but also because one would expect a higher frequency due to a stiffer system. Nonetheless, torsional vibration is as damaging with respect to engine wear as is the off-axis vibration. The variation of the torque with time, sampled over periods of 30 seconds (Figures 3.9 and 3.10), indicates that there has been an increase of the amplitudes of the torsional vibration, although this was almost certainly caused by the torque load cell picking up the shaft misalignment (refer to Chapter 3.1).

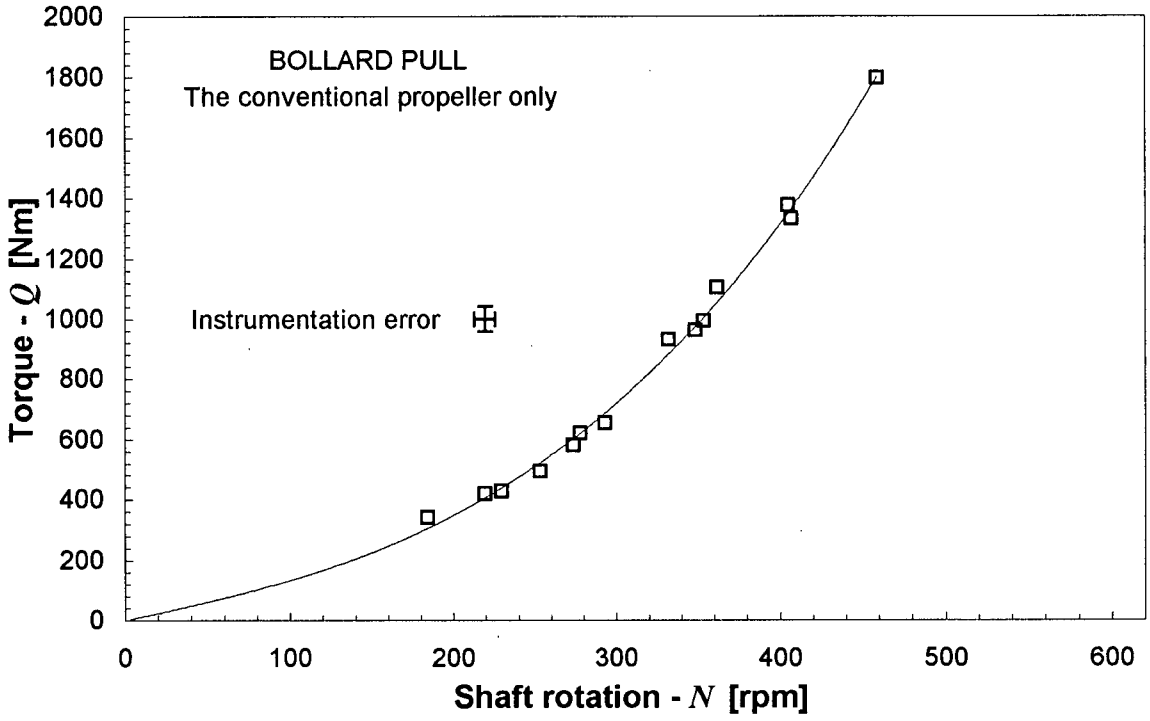

Figure 3.1.*a* Torque measured during bollard pulls. Conventional propeller only.

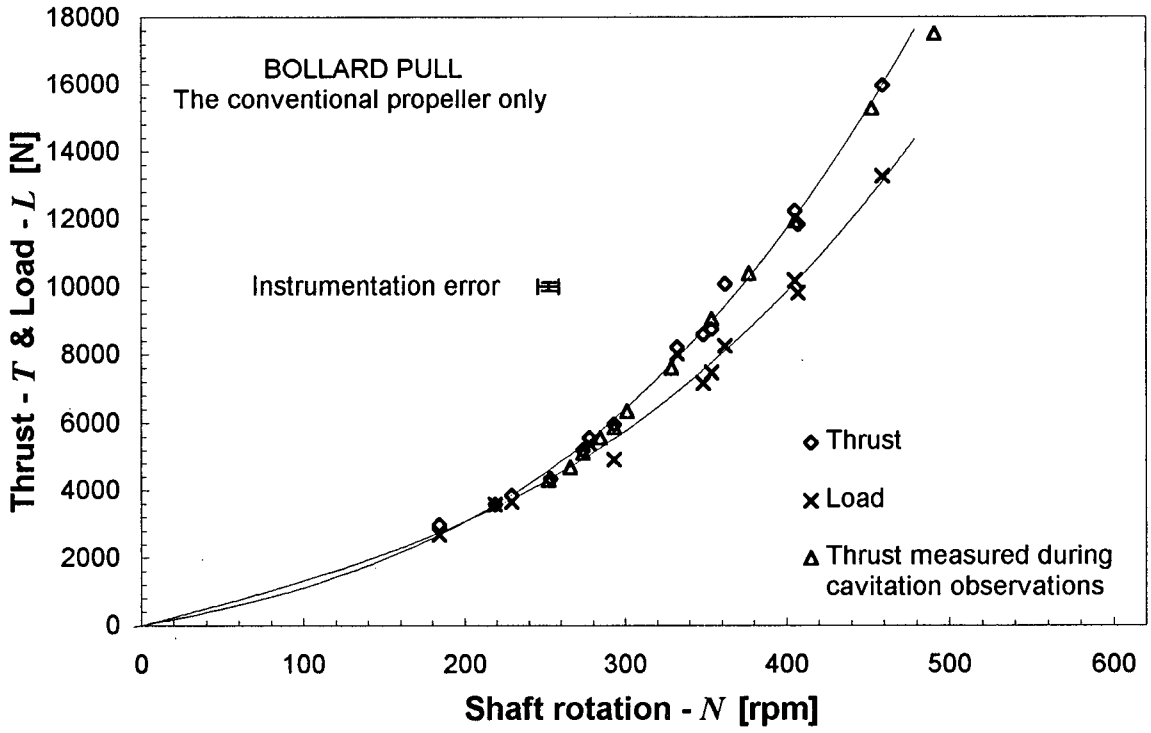

Figure 3.1.*b* Thrust and tow load measured during bollard pulls. Conventional propeller only.

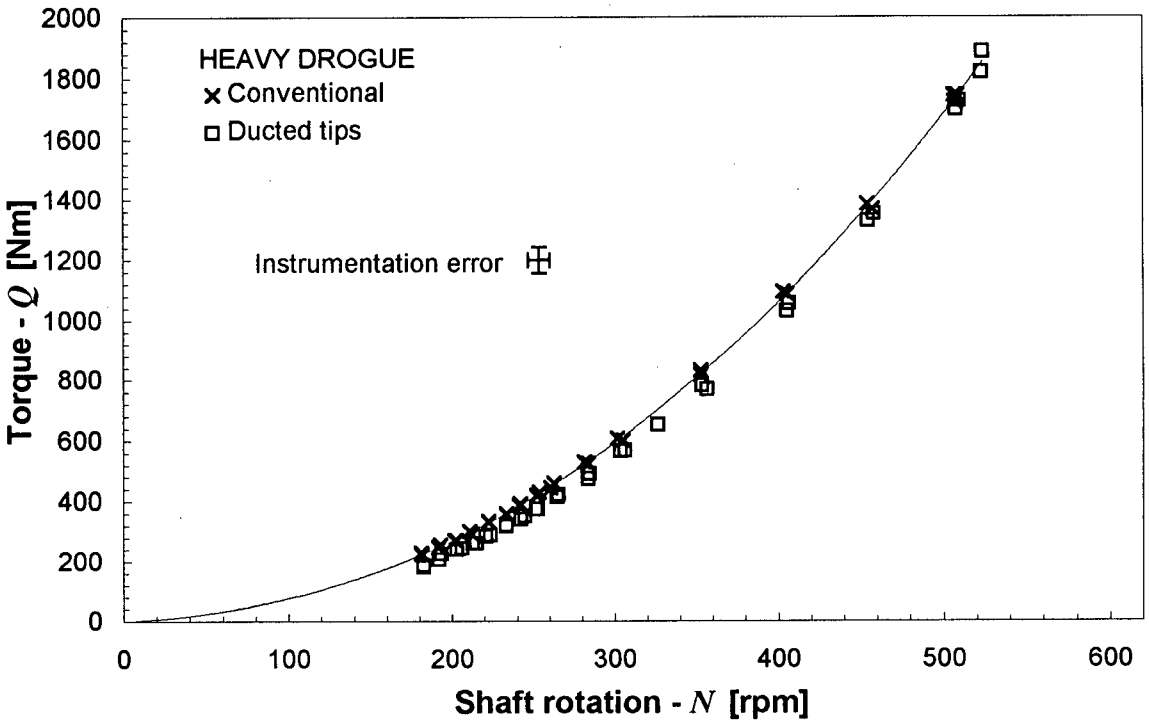

Figure 3.2.*a* **Torque measured when pulling the heavy drogue.**

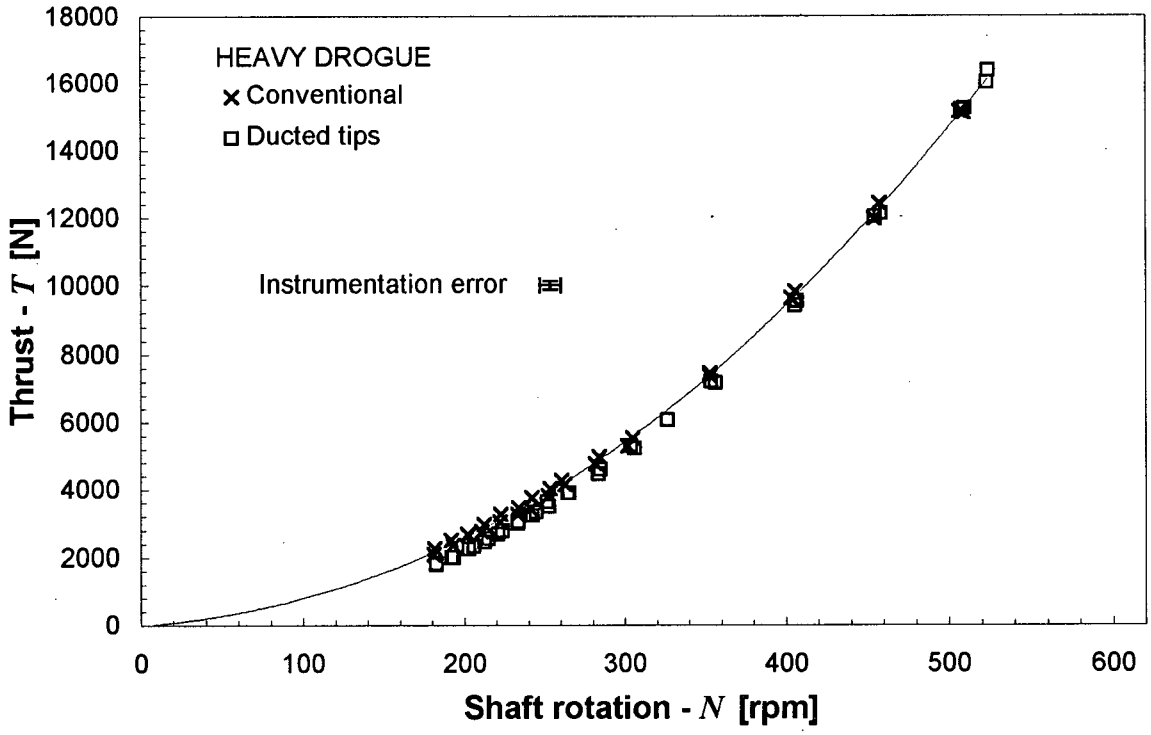

Figure3.2.*b* **Thrust measured when pulling the heavy drogue.**

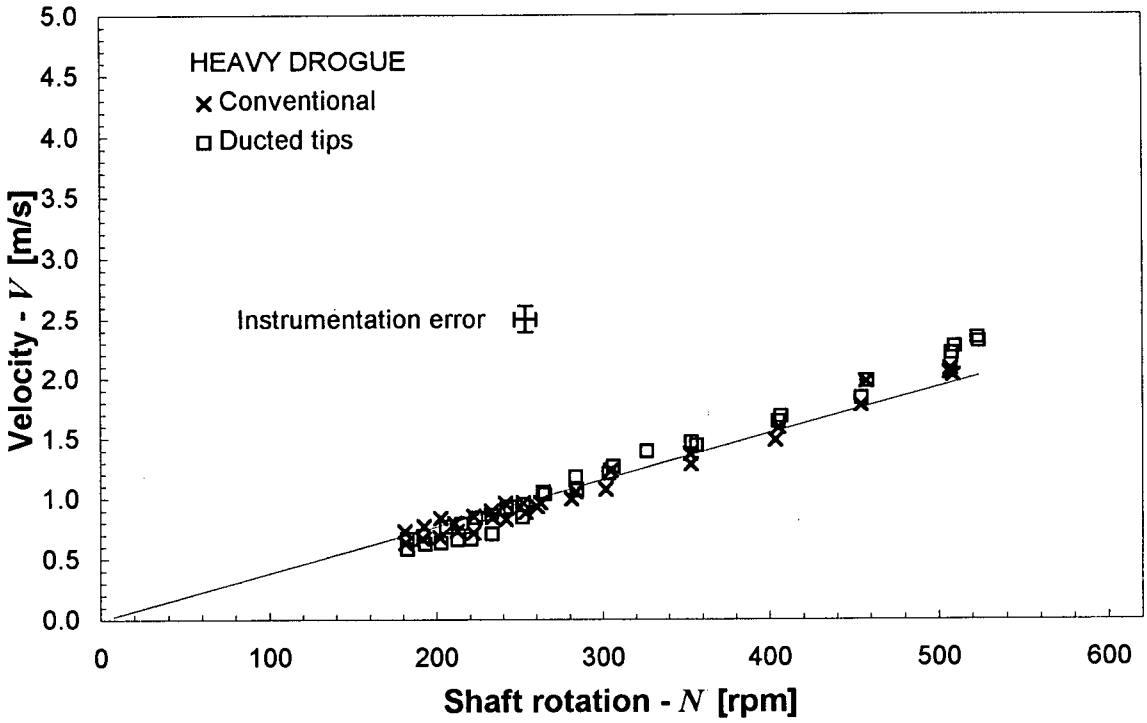

Figure3.2.c Velocity measured when pulling the heavy drogue.

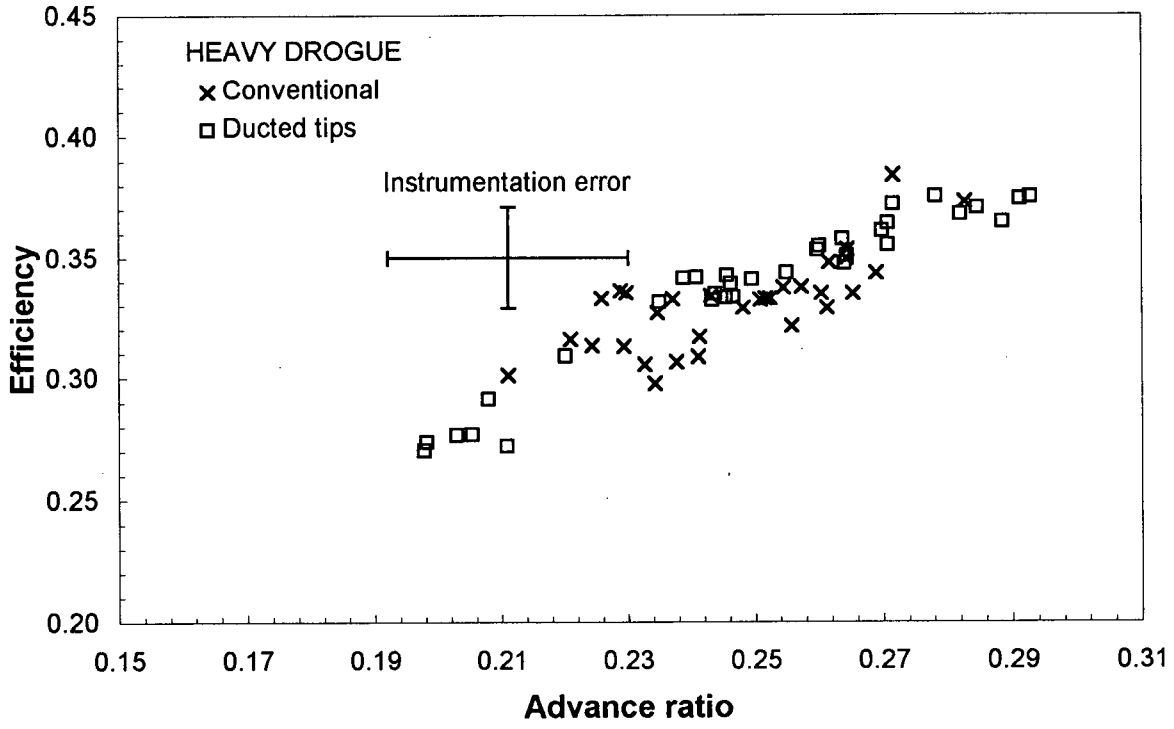

Figure 3.2.*d* Efficiency measured when pulling the heavy drogue.

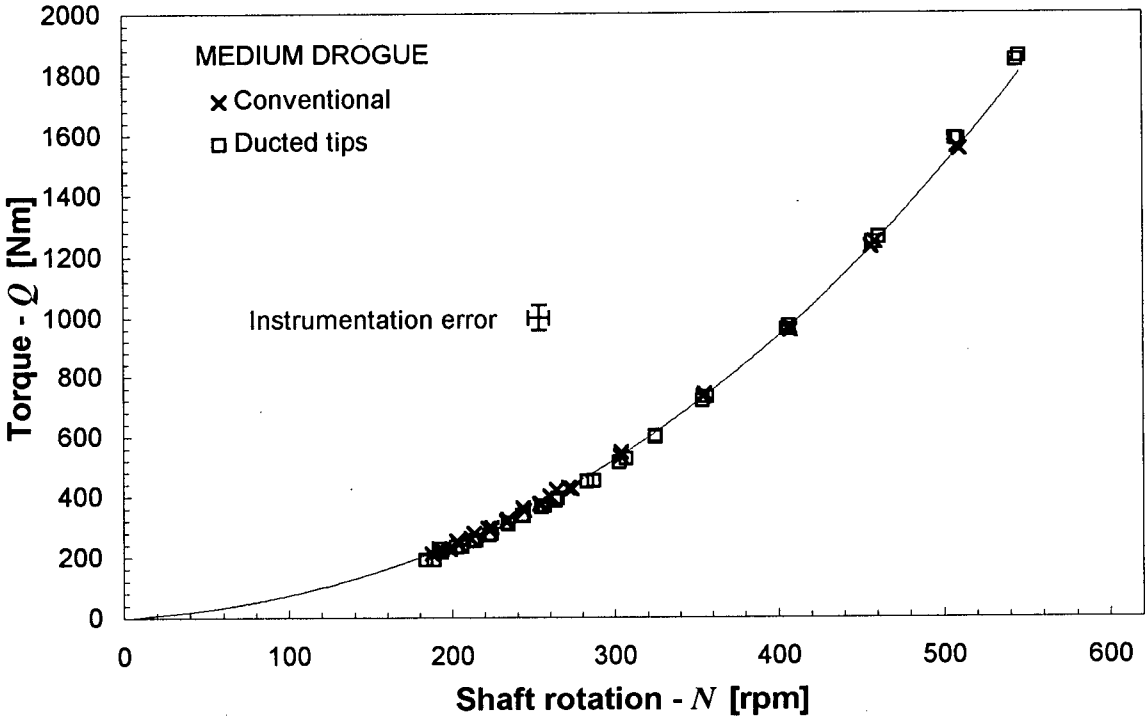

Figure 3.3.*a* Torque measured when pulling the medium drogue.

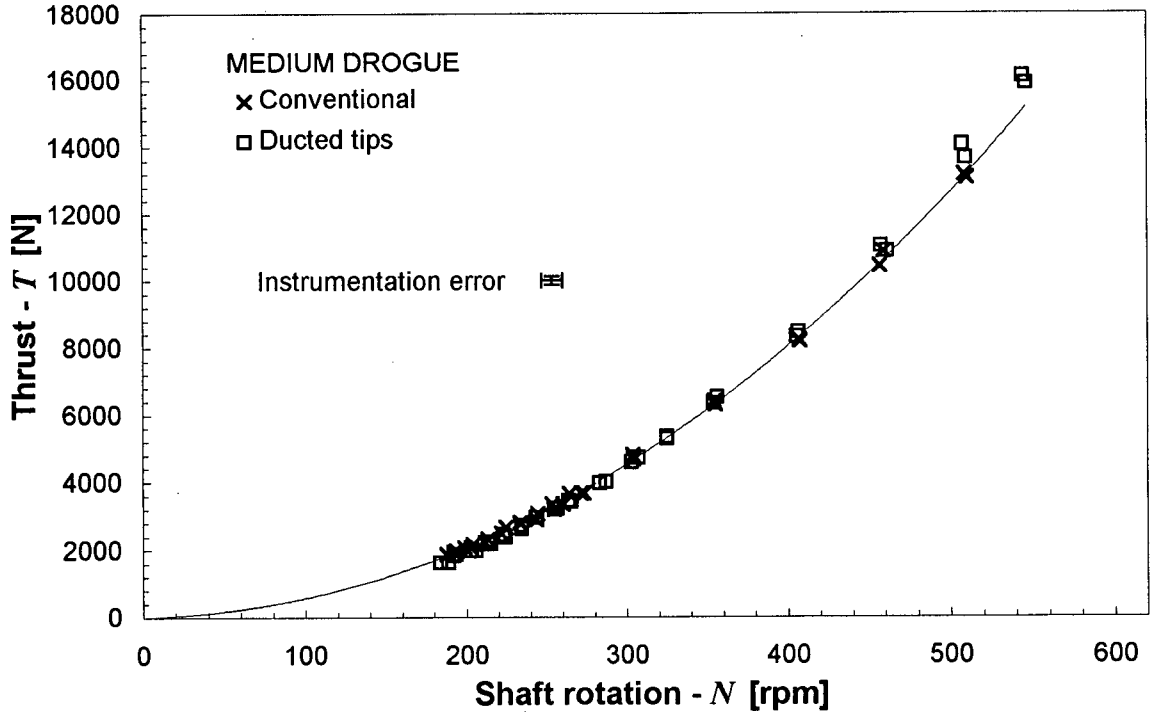

Figure 3.3.*b* Thrust measured when pulling the medium drogue.

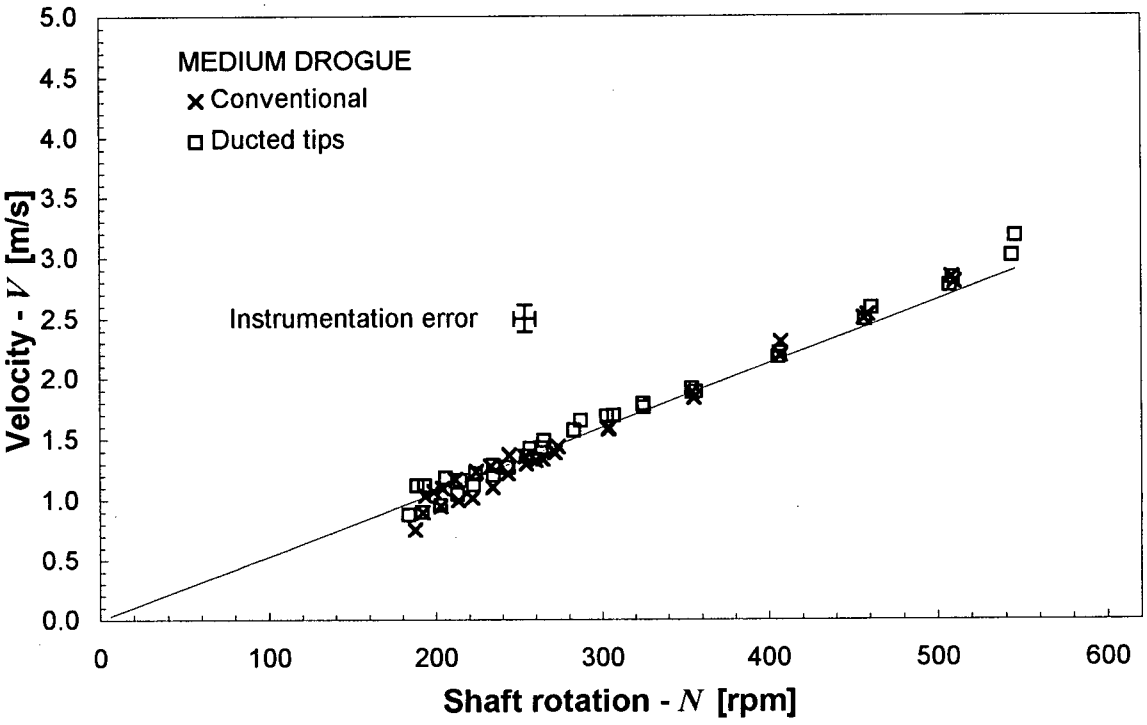

Figure 3.3.*c* Velocity measured when pulling the medium drogue.

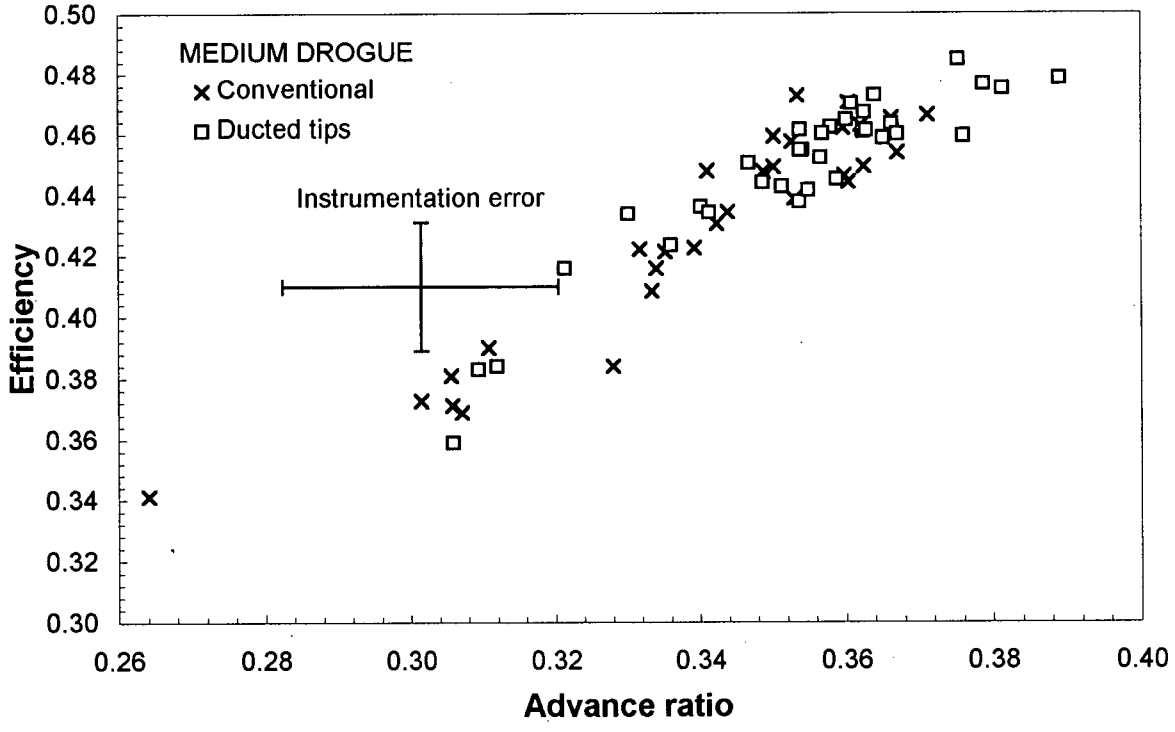

Figure 3.3.*d* Efficiency measured when pulling the medium drogue.

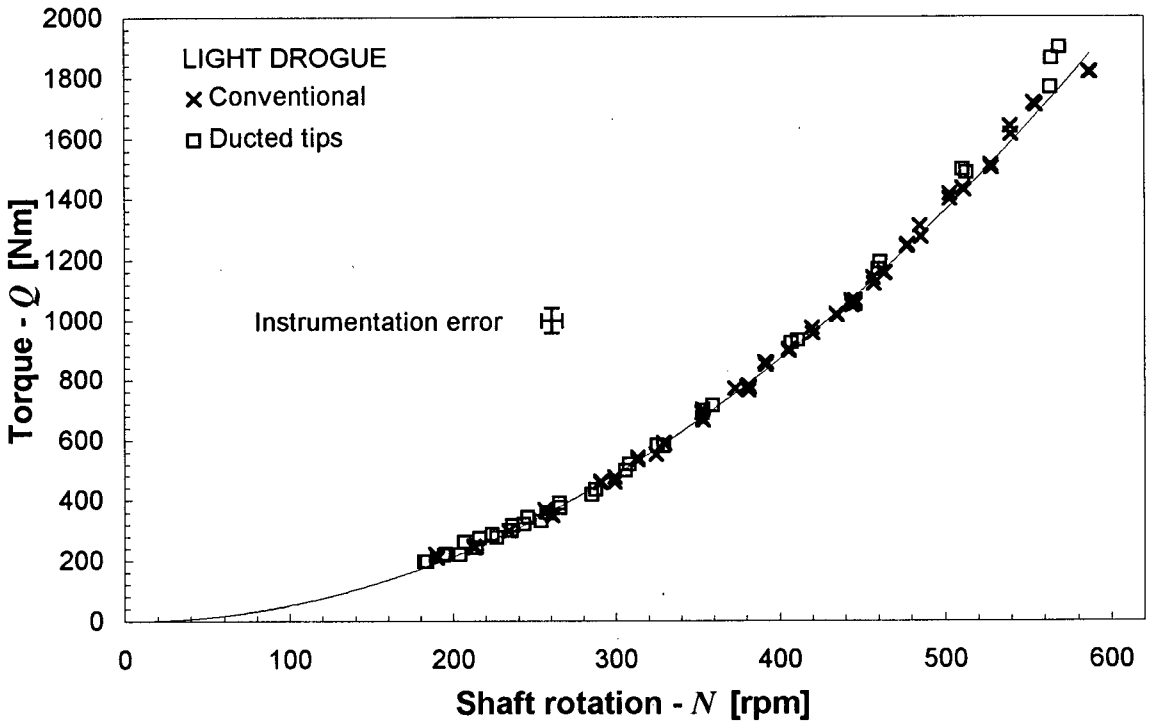

Figure 3.4.*a* Torque measured when pulling the light drogue.

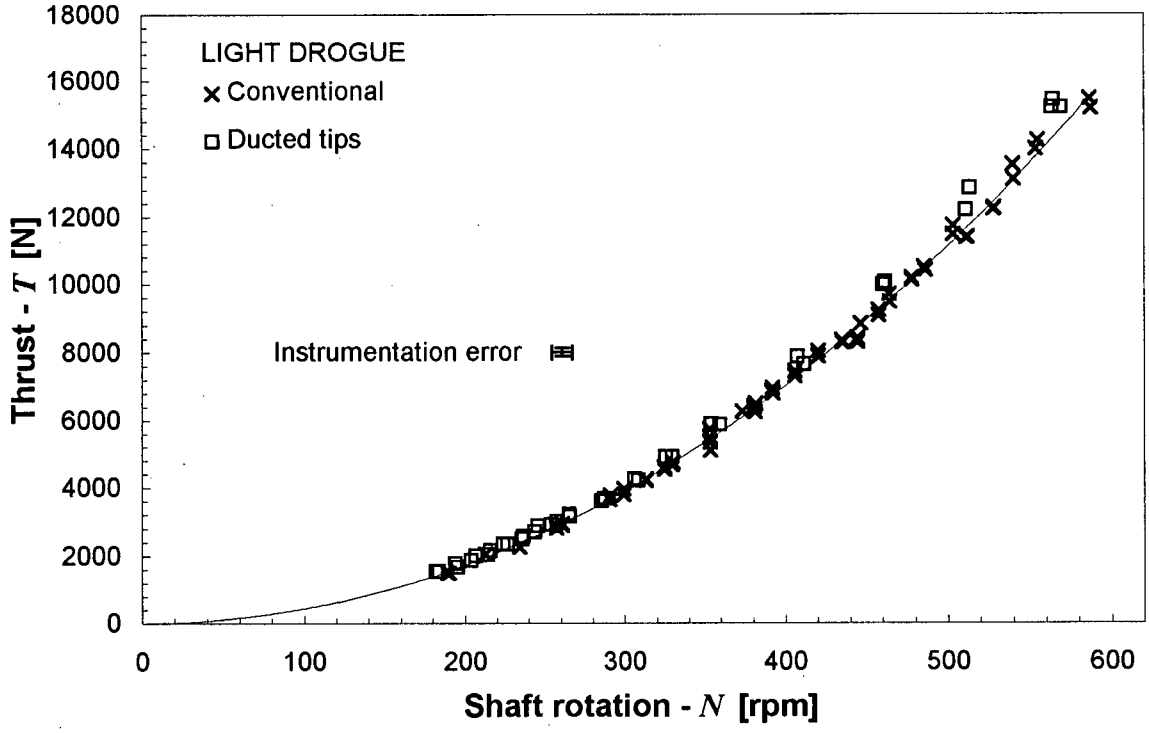

Figure 3.4.*b* Thrust measured when pulling the light drogue.

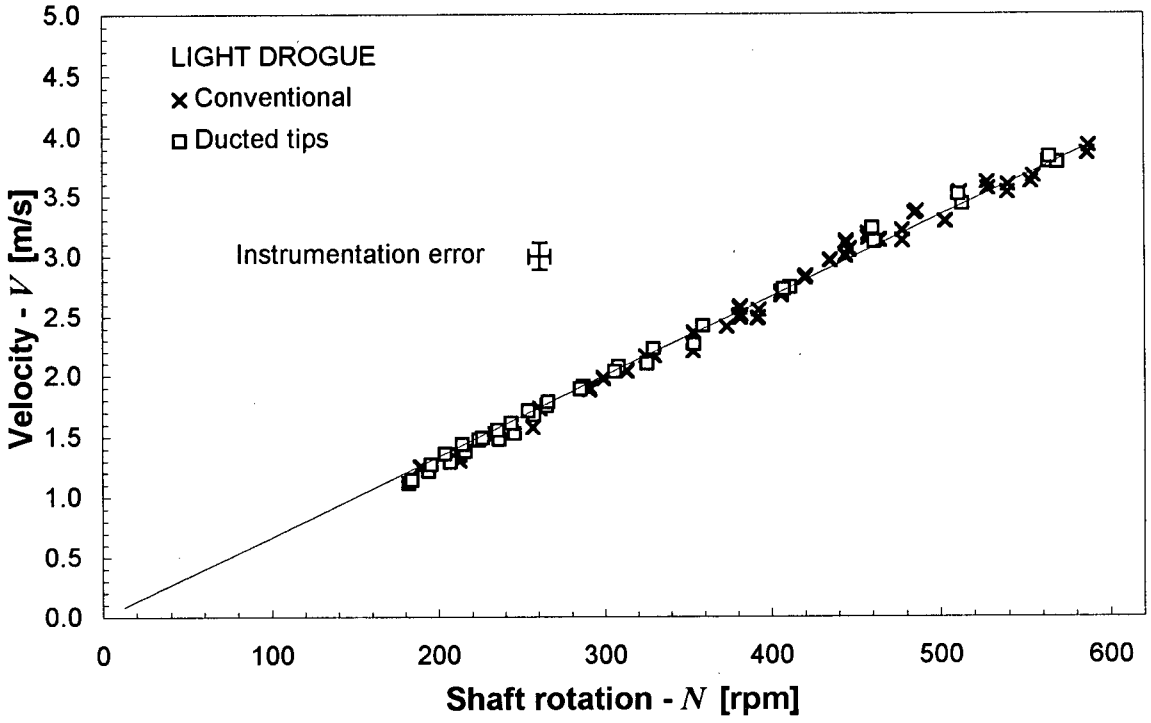

Figure 3.4.*c* Velocity measured when pulling the light drogue.

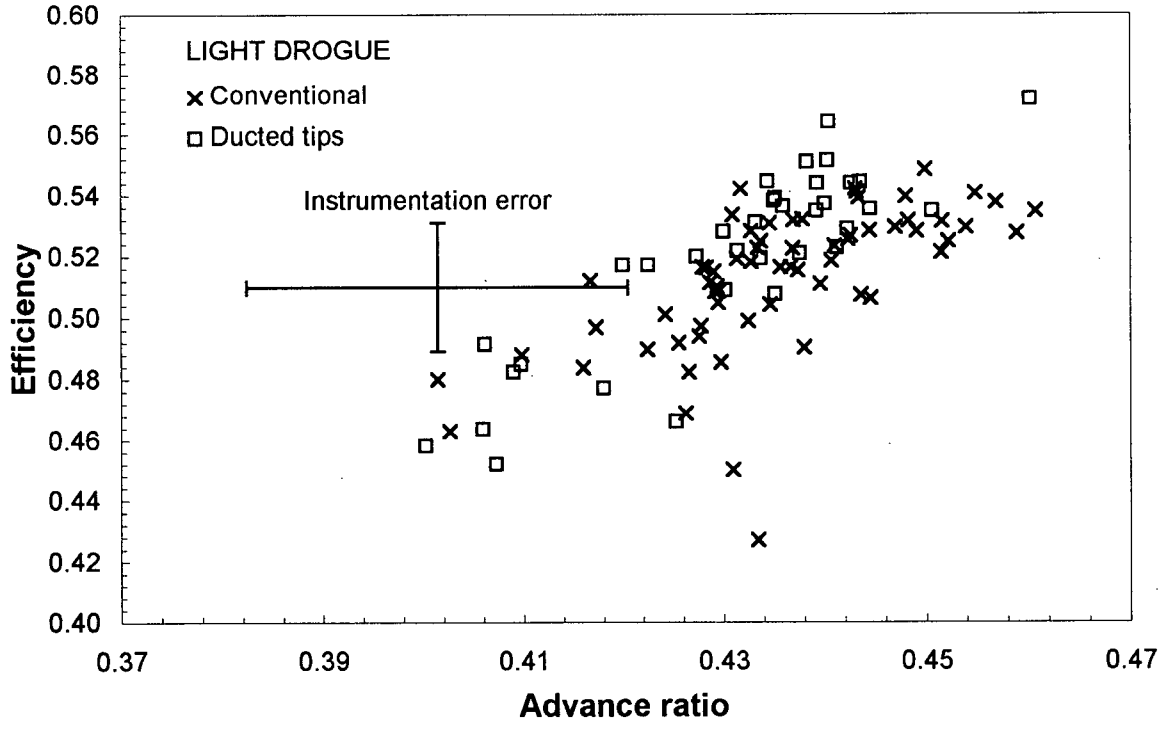

Figure 3.4.*d* Efficiency measured when pulling the light drogue.

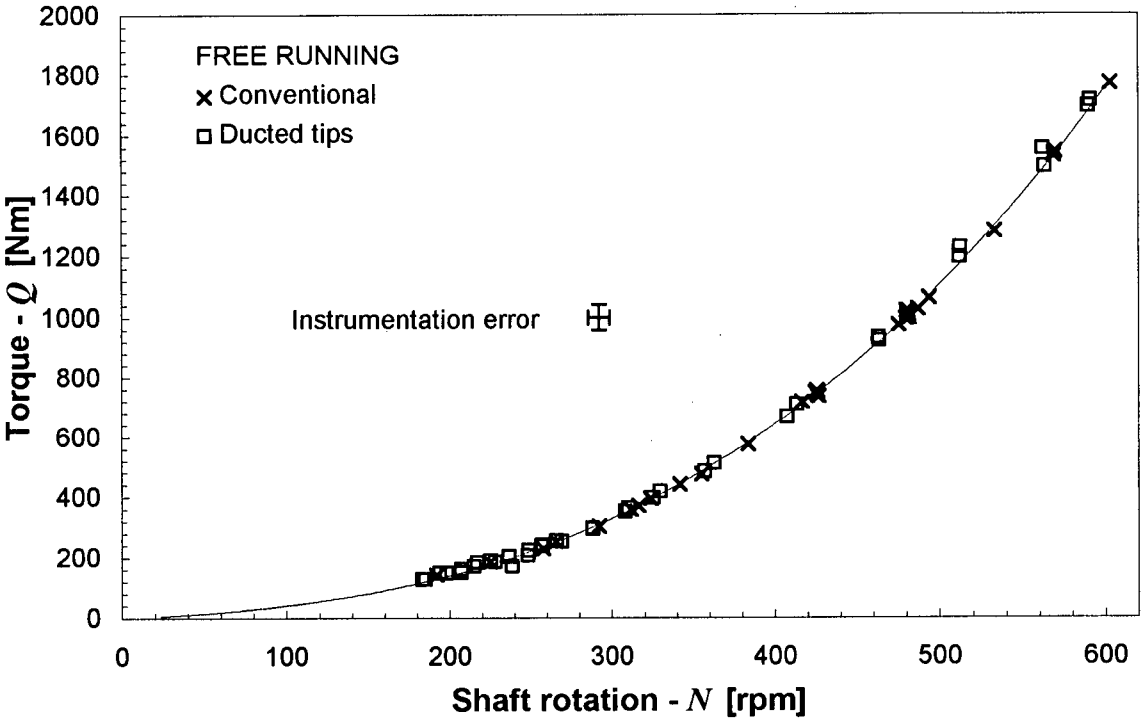

Figure 3.5.*a* Torque measured at free running speeds.

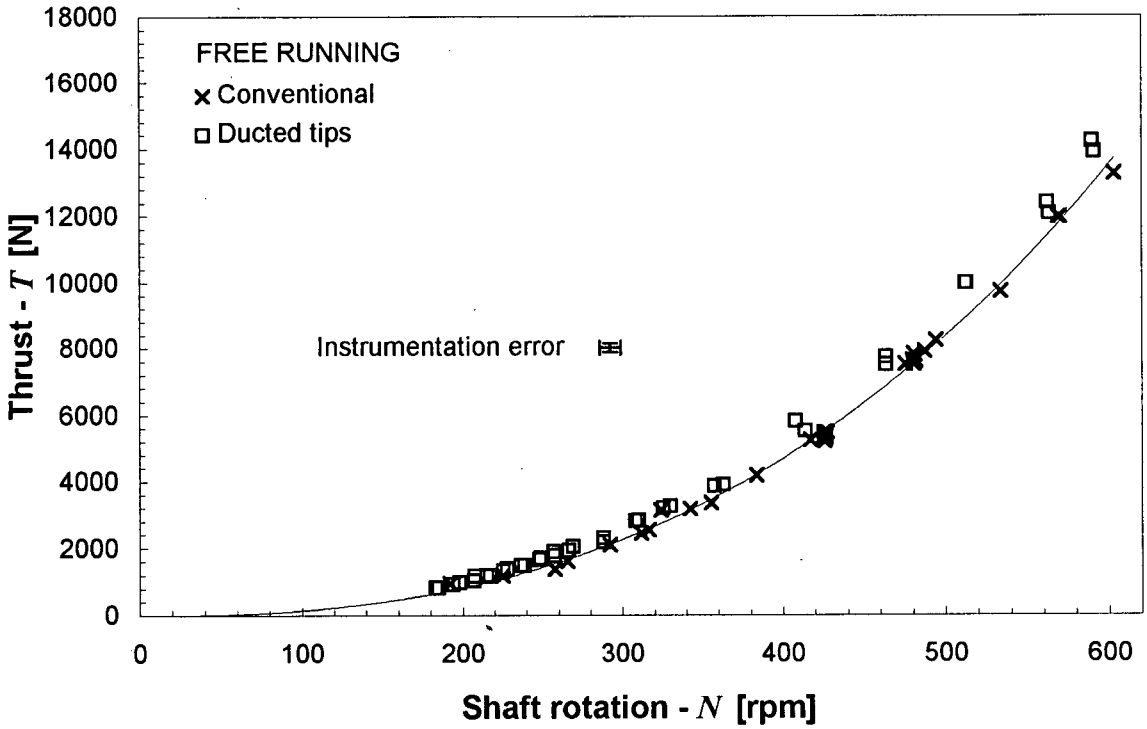

Figure 3.5.*b* Thrust measured at free running speeds.

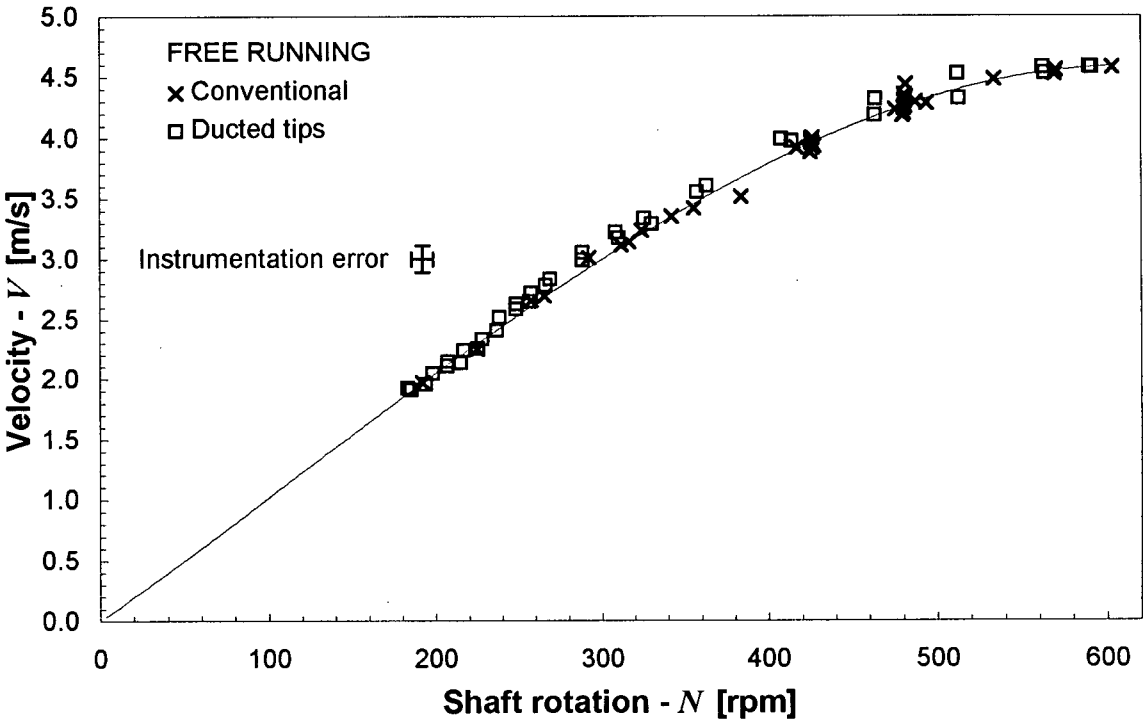

Figure 3.5.*c* Velocity measured at free running speeds.

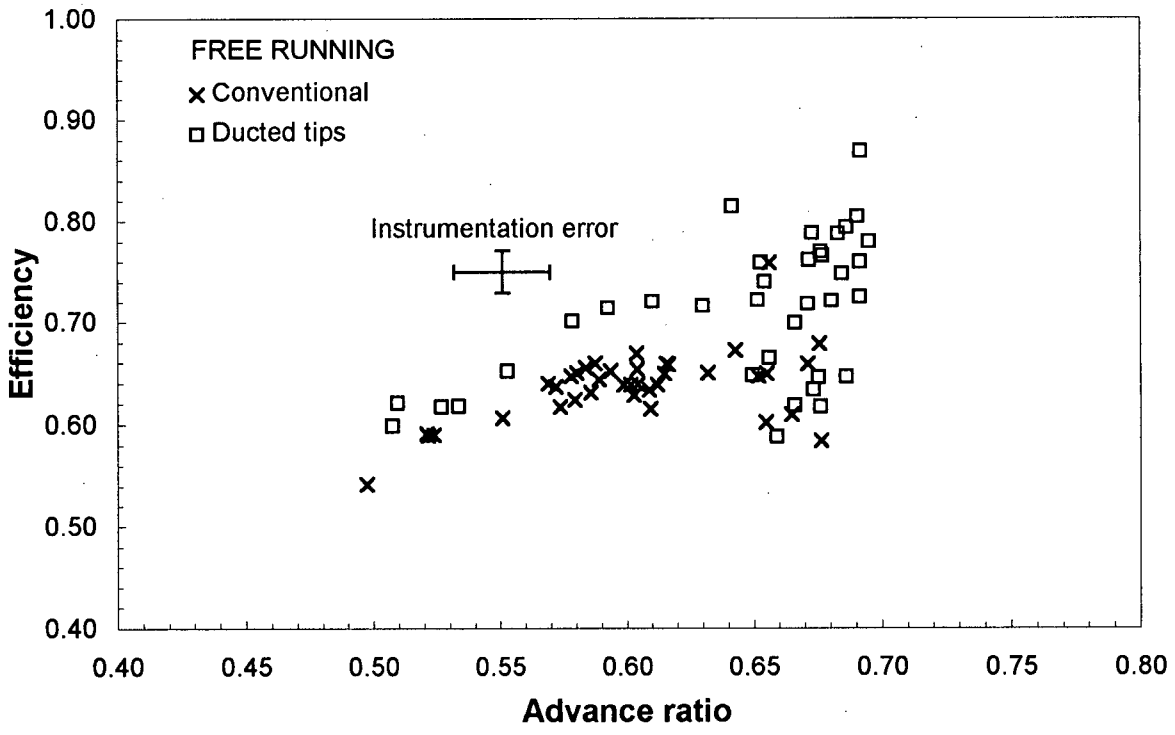

Figure 3.5.*d* Efficiency measured at free running speeds.

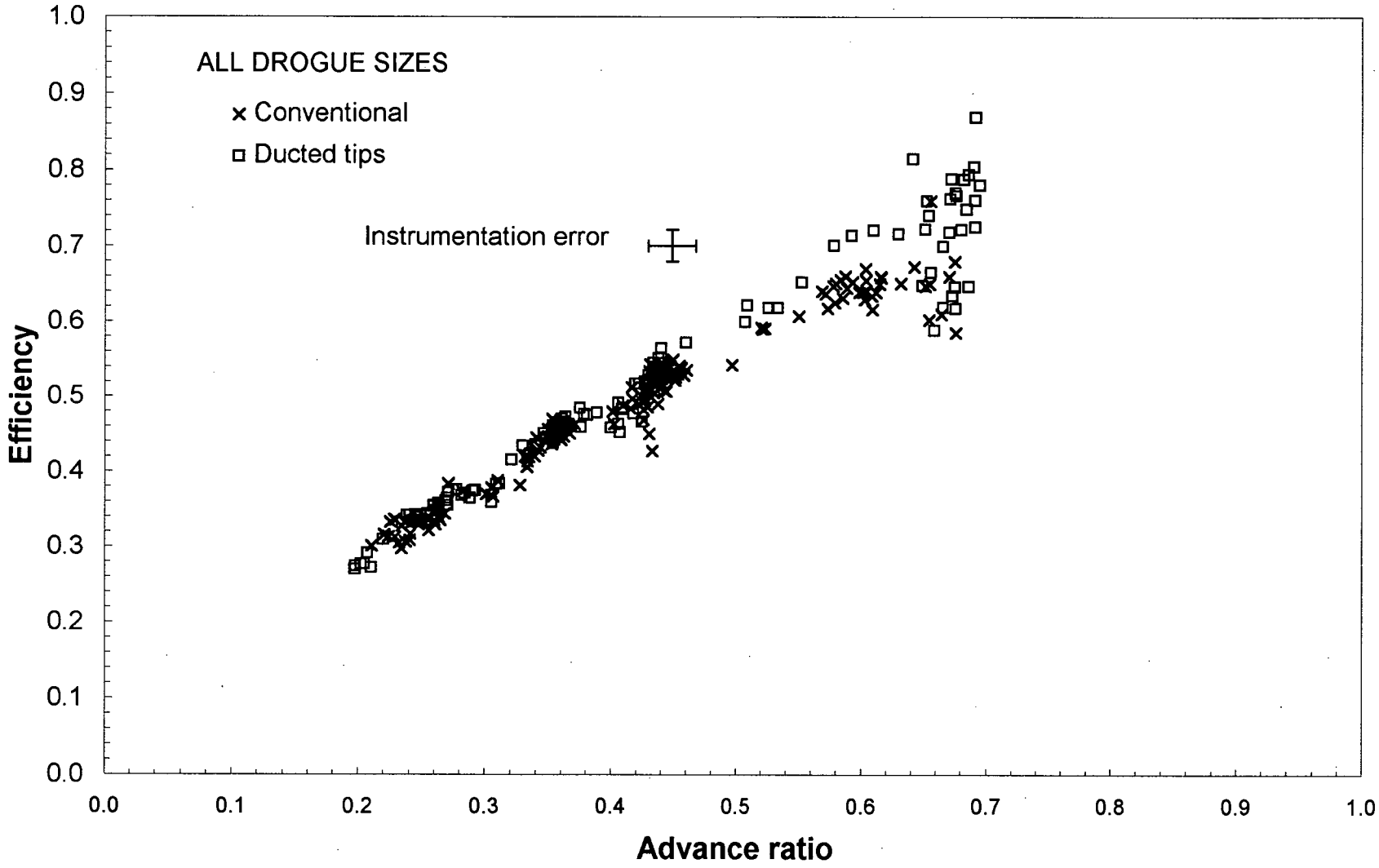

Figure 3.6 All previous efficiency data plotted together.

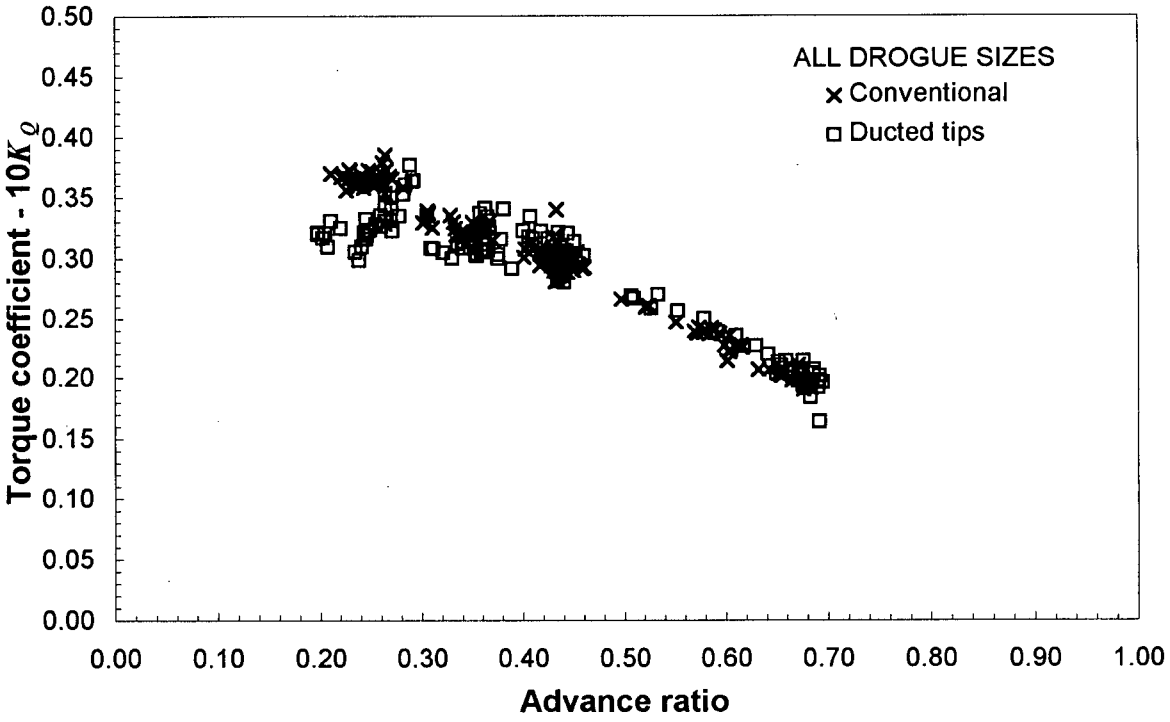

Figure 3.7 Torque coefficients for the conventional and ducted tip propeller.

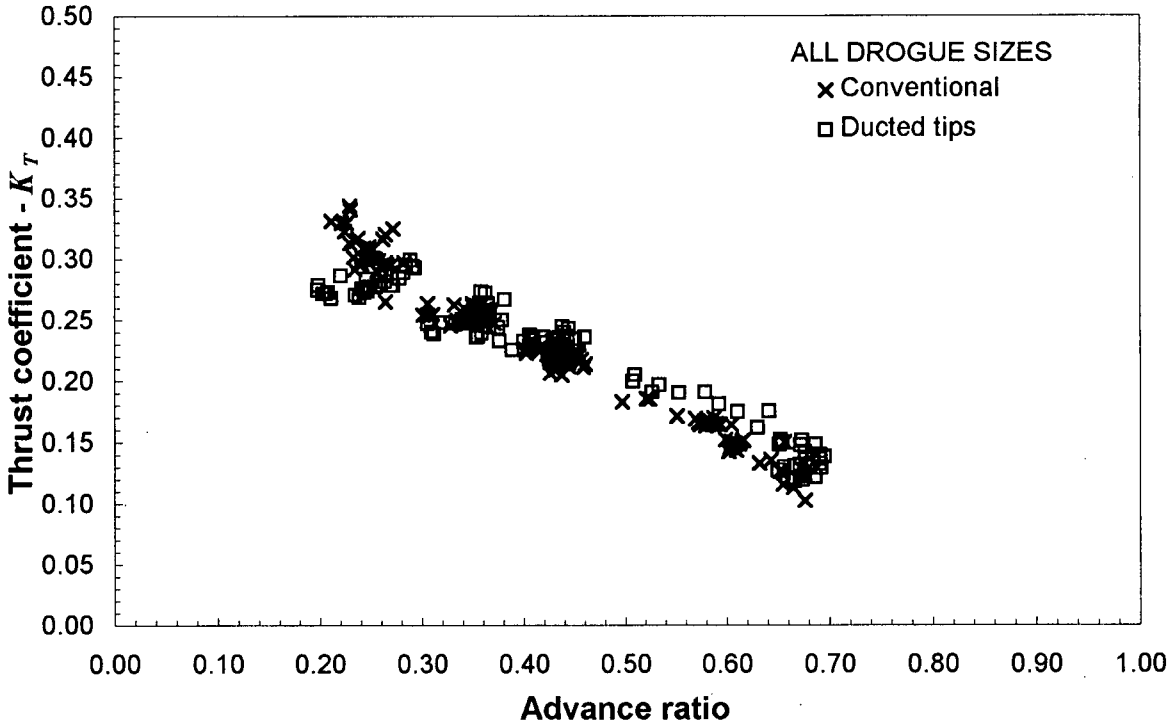

Figure 3.8 Thrust coefficients for the conventional and ducted tip propeller.

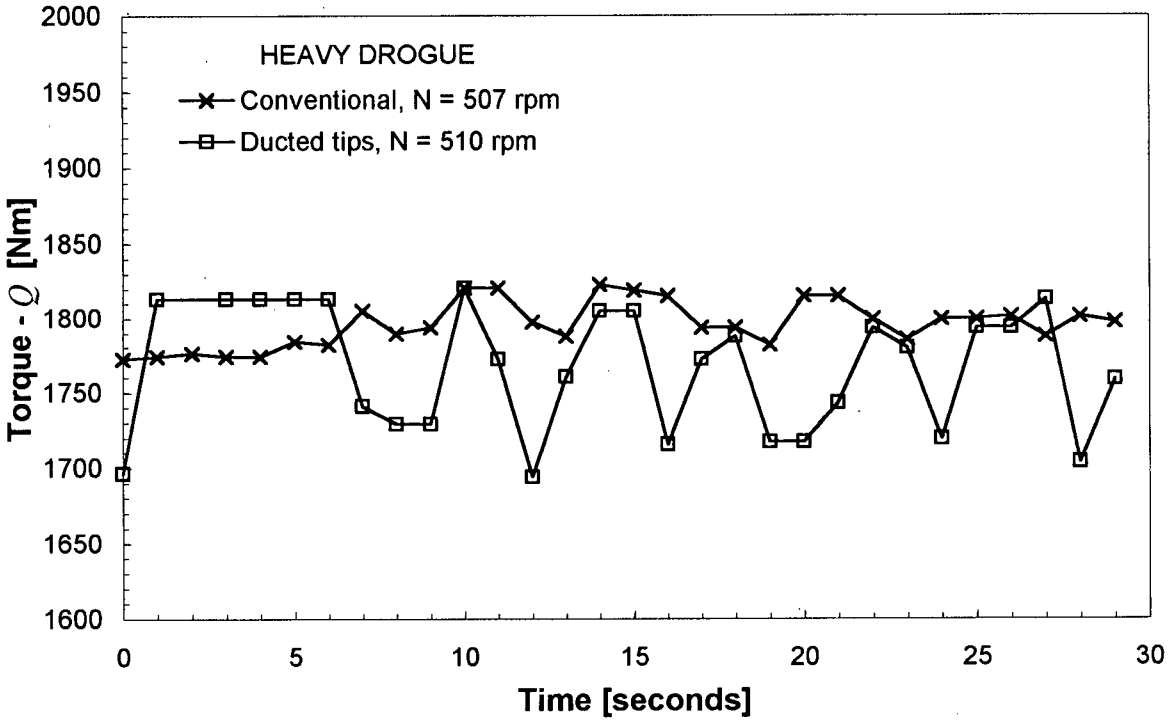

Figure 3.9 Variation of torque during a sampling period of 30 seconds.

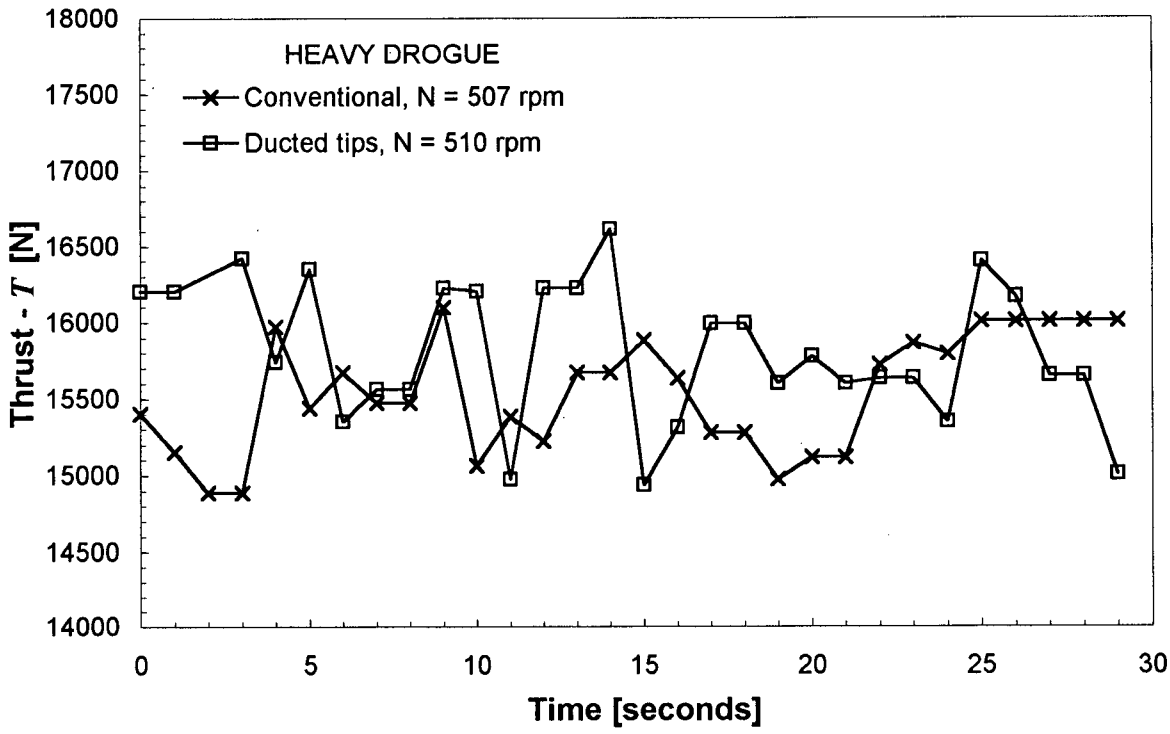

Figure 3.10 Variation of thrust during a sampling period of 30 seconds.

3.4 Cavitation observations

Video recordings from the cavitation observations of the conventional and ducted tip propeller is submitted as an appendix to this report on a VHS cassette titled *Tip Vortex Cavitation on Marine Propellers*. For a summary, see Table 3.2.

N rpm	Conventional propeller	N rpm	Ducted tip propeller
252	No cavitation.	252	No cavitation.
266	A few infrequent bubbles can be observed.	259	No cavitation.
274	Intermittent cavitation from two of the blades.	274	No cavitation.
285	Continuous cavitation from two of the blades and intermittent cavitation from the remaining two.	283	No cavitation.
293	Same as for N = 285	292	No cavitation.
301	Continuous cavitation from all blades.	305	The propeller wake becomes visible. No cavitation.
329	The propeller wake becomes visible. Strong sternwards race aft of the propeller.	314 324 335	No cavitation.
354	Cavity helices are emerging from the tips of the propeller.	346 355	No cavitation.
377	Extension of the helices.	365	No cavitation.
405	Extension of the helices.	404	Leading edge cavitation emerging from the duct entrances.
452	Extension of the helices.	457	A vapor cloud is trailing from the exit of the ducts, forming very diffuse cavitation helices.
491	Maximum shaft rotation. Strongly cavitating helices trailing behind the blade tips.	463	Maximum shaft rotation. Same as for N = 457.

Table 3.2 Content of the video recorded during the cavitation observations.

Chapter 4 - DISCUSSION

This chapter contains the discussion of the results obtained during the sea trials of the conventional and ducted tip propeller, starting with a definition of the dimensionless numbers used in the subsequent discussion.

4.1 Dimensionless numbers

This report uses two different definitions for the propeller efficiency:

1. Measured efficiency, $$\eta = \frac{VT}{2\pi nQ} \quad (4.1)$$

2. Open-water efficiency, $$\eta_o = \frac{V_A T_o}{2\pi n Q_o} \quad (4.2)$$

where T_o and Q_o are the thrust and torque, respectively, of the propeller in the absence of the hull of the boat. In a similar fashion, two definitions for the advance ratio has been used:

1. Measured advance ratio, $$J = \frac{V}{nD} \quad (4.3)$$

2. True advance ratio, $$J_A = \frac{V_A}{nD} \quad (4.4)$$

In general V_A is less than V owing to the boat wake. At bollard pull conditions, V_A is finite even though V is zero, owing to the fluid velocity induced by the propeller.

Non-dimensional numbers for torque and thrust are defined as:

Measured torque coefficient, $$K_Q = \frac{Q}{\rho n^2 D^5} \quad (4.5)$$

Measured thrust coefficient, $$K_T = \frac{T}{\rho n^2 D^4} \quad (4.6)$$

where the corresponding open-water coefficients can be obtained by replacing Q and T by Q_o and T_o.

The Reynolds number for the propeller is based on the relative blade velocity, U, and the chord, c, at $0.7R$ of the blade:

$$Re_{0.7} = \frac{Uc}{\nu} \tag{4.7}$$

Unless otherwise specified, U and c will always refer to $r = 0.7R$.

It has also been necessary to use two definitions for the cavitation inception index; one for comparison to other propellers, based on the boat velocity, V, and a second for comparison to hydrofoils in a uniform flow, based on the relative blade velocity, U.

1. Propeller cavitation inception index, $\sigma_i = \frac{p_\infty - p_v}{\frac{1}{2}\rho V^2}$ **(4.8)**

2. Blade cavitation inception index, $\sigma_{ir} = \frac{p_\infty - p_v}{\frac{1}{2}\rho U^2}$ **(4.9)**

4.2 Comparison to the open-water efficiency

Figure 4.1 shows the efficiency, torque and thrust coefficients for the conventional propeller plotted together with the corresponding open-water curves of the Wageningen B4-50 propeller, with P/D = 0.8. The digits in the B-series designation represent the number of blades and the expanded area ratio, respectively. The open-water curves are based on the experiments of Troost (1937) on the 4-bladed B-screw propeller series, to which a polynomial was fitted by Lammeren et al. (1969). This polynomial is a function of A_E/A_0, P/D and J, and has later been expanded by Oosterveld and Oossanen (1975) to include terms that account for different numbers of blades (Z). Terms can also be added that will adjust

for $Re > 2 \cdot 10^6$ and different blade thickness. In this report no corrections have been made either to the Reynolds number or to the blade thickness. During the sea trials $10^6 < Re < 4 \cdot 10^6$, even with the same size drogue. Therefore it does not make sense to adjust for the Reynolds number. The blade thickness could not be measured with an accuracy that would justify any corrections to the open-water curves.

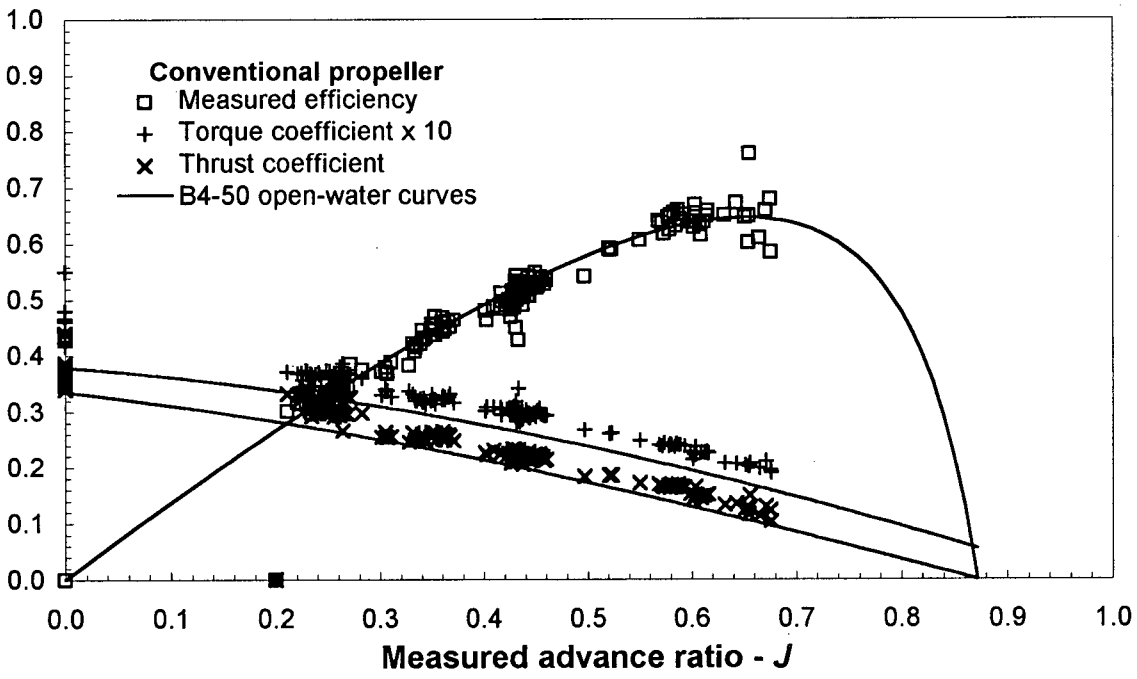

Figure 4.1 Comparison of the measured propeller performance of the conventional propeller and the open-water curves of the B4-50 propeller.

Figure 4.1 shows that the conventional propeller has high efficiency, although the measured and open-water performance can not be compared directly. The measured efficiency is based on the boat velocity, V, while the open-water efficiency is based on the speed of advance, V_A. Because a propeller operating in the wake of a boat it sees a different water approach velocity than an open water propeller, it can be at the same operating point and yet measure a different η and J. If the Taylor wake fraction, w = 1- V_A/V, of Pearl Sea was known, η and J could be

adjusted to obtain a true comparison. If $T/T_o = Q_o/Q = 1$, η could be adjusted down by ηw and in by Jw to give η_o and J_A for the conventional propeller. However, such an analysis of the data of Figure 4.1 indicates that all the measured efficiency points will remain on top of, or close to the B4-50 curve even after such an adjustment. Thus, it is fair to say that the propeller studied here was well represented by the B4-50, with its similar geometry, diameter, pitch and area ratio.

In the same manner K_Q and K_T can be adjusted in by Jw to give the open-water coefficients, K_{Qo} and K_{To}, for the conventional propeller. In situations where it is known that the full scale propeller is geometrically identical to a model propeller for which the open-water curves are plotted, K_Q or K_T can be used to actually determine w for the boat. Because w is constant the propeller should produce K_T equivalent to those shown in Figure 4.2.

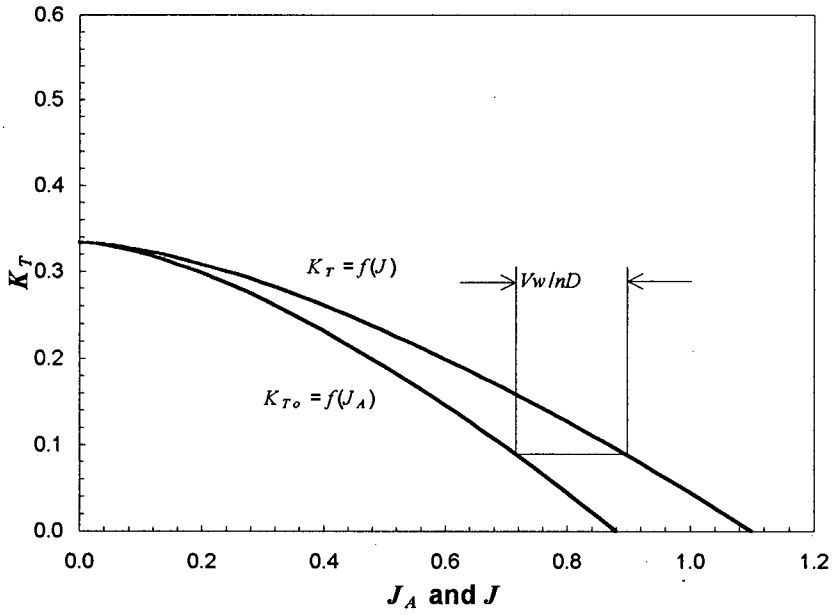

Figure 4.2 The difference between the measured (K_T) and open-water (K_{To}) thrust coefficient for identical propellers.

This is clearly not the case for the conventional propeller used during the sea trials, confirming our suspicions that the manual rebuilding of the propeller was not precise enough to achieve geometric similarity to the B-series. Particularly the much

higher torque and thrust at bollard pulls imply that P/D > 0.8 for the conventional propeller, although there are other factors that could result in the same effect, such as differing blade thickness and blade contour. These deviations from the B-series performance should have no consequence for the comparison of the conventional and ducted tip propeller discussed next .

4.3 Hydrodynamic performance of the ducted tip propeller

According to blade element theory, the torque and thrust experienced by a radial section of a propeller blade located at radius r and dr wide (Figure 4.3) can be expressed as:

$$dT = dL\cos\beta_I - dD\sin\beta_I$$

$$dQ = (dL\sin\beta_I + dD\cos\beta_I)r$$

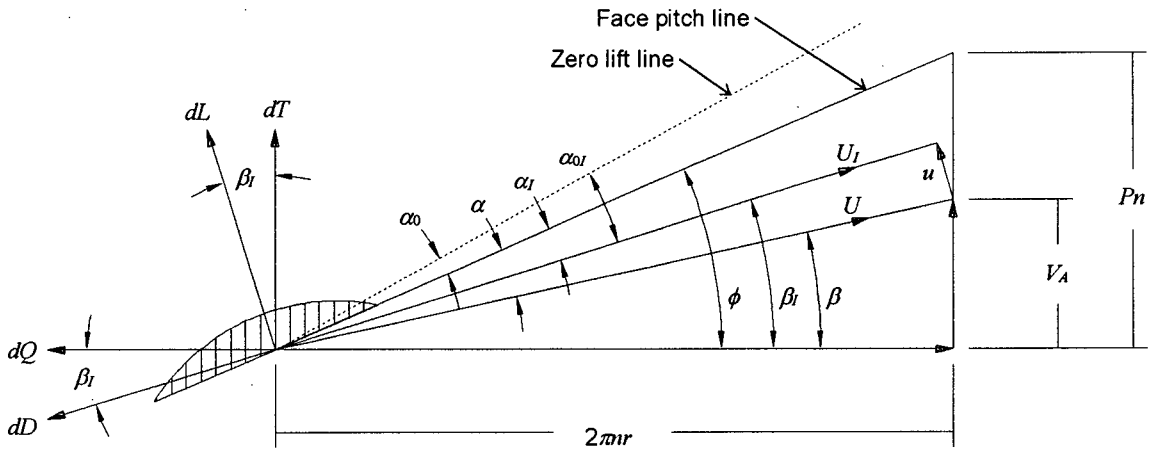

Figure 4.3 Force and velocity diagram for a blade element.

Furthermore, according to previous definitions of propeller efficiency, the blade element efficiency can be written

$$\eta = \frac{dTV_A}{2\pi ndQ}$$

By substituting for dT and dQ, it can be shown (Manen and Oossanen, 1988) that the element efficiency becomes a function of the Lift/Drag ratio:

$$\eta = \frac{\tan\beta}{\tan(\beta_1 + \gamma)} \qquad \text{and} \qquad \tan\gamma = \frac{D}{L}$$

Hence, an increase in the L/D ratio of the blades of a propeller should result in an improved propeller efficiency. In addition, and more significantly, any reduction of the induced velocity, u, will reduce β_1 and therefore improve the efficiency.

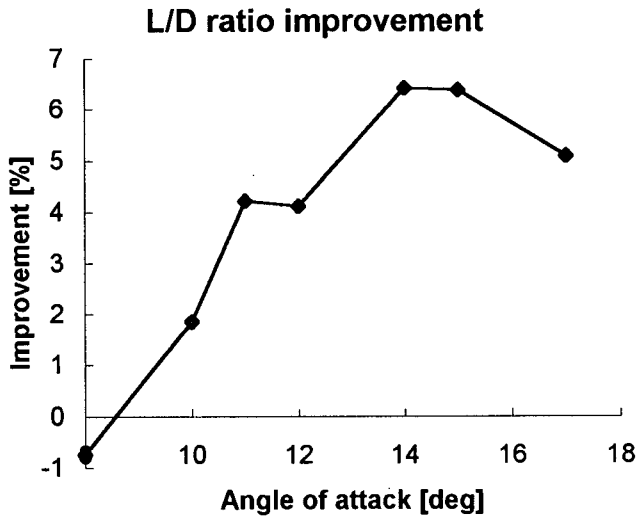

Figure 4.4 Lift/Drag ratio improvement of the ducted tip on a rectangular, untwisted, constant NACA 66-209 profile airfoil. Source: Green and Duan (1995).

When Green and Duan (1995) showed that the L/D ratio of a *ducted tip hydrofoil* is superior to that of a conventional hydrofoil for angles of attack larger than 8° (Figure 4.4), it was expected that any efficiency improvement of a *ducted tip propeller* would occur when the blades operate at high angles of attack, i.e. at low advance ratios. At higher advance ratios, towards maximum efficiency, a loss of efficiency was expected, or at best no change at all. The results from the sea trials of the ducted tip propeller are therefore somewhat surprising. Figures 3.2.*d* to 3.5.*d*

indicate only a marginal efficiency improvement at low and moderate advance ratios, with increasing improvement towards higher advance ratios.

However, due to the large experimental error combined with a large spread of the data, resulting from other sources (aerodynamic drag, wave loads, etc.), the percentage increase in efficiency is not readily observed. In order to better visualize the trend of the efficiency of the propeller before and after the ducts were attached, the efficiency has been plotted as a function of the advance ratio, where, instead of using the measured values for Q, T and V, the regression lines $Q = f(N)$, $T = f(N)$ and $V = f(N)$ have been used as input in Equation (4.1) and (4.3), giving $J = f(N)$ and $\eta = f(N)$. The efficiency based on the regression lines for both the conventional and ducted tip propeller is shown in Figure 4.5.

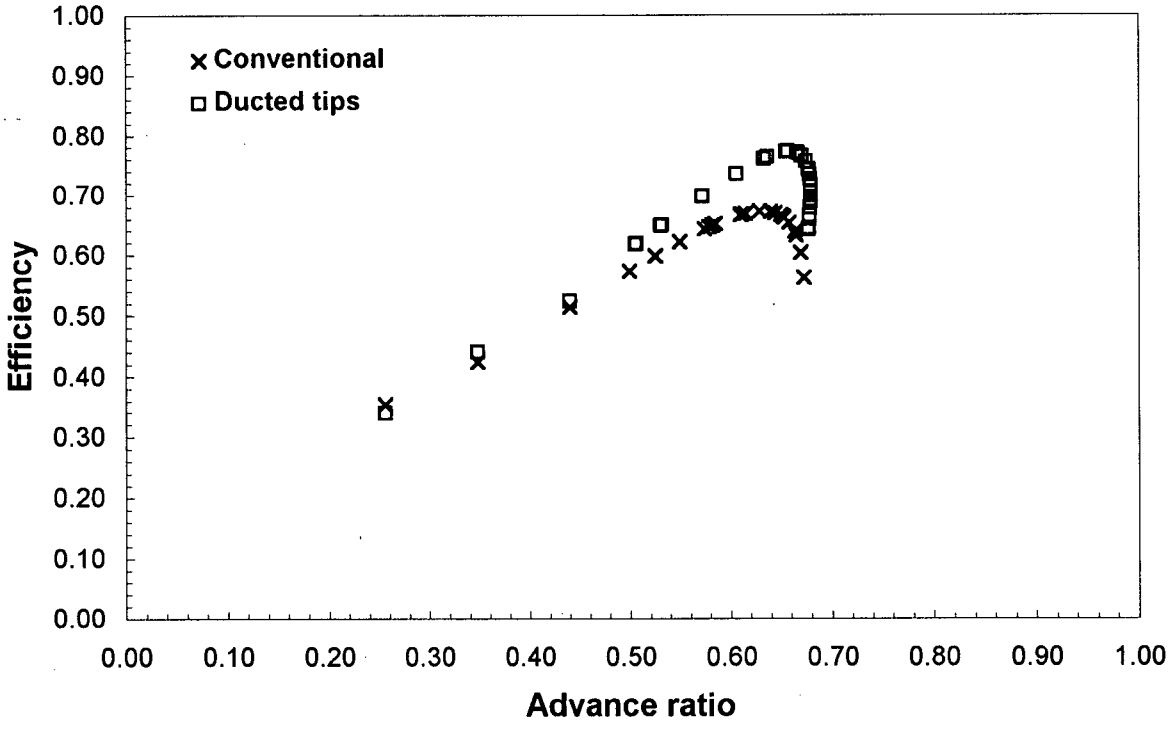

Figure 4.5 The efficiency of the conventional and ducted tip propeller plotted with the measured values for Q, T and V replaced by their regression lines in the efficiency equation. The points at J = 0.26, 0.35 and 0.44 describe the tests with heavy , medium and light drogues, respectively, while all the remaining points describe the free running speeds; the lowest advance ratios correspond to the highest shaft rotational speeds.

For the heavy, medium and light drogues a linear regression line has been found for the velocity as a function of the shaft rotation, N. With V directly proportional to N, J becomes a constant, and a plot of $\eta = f(N)$ therefore appears as a number of points spread vertically at a constant advance ratio. These points have been reduced to an average efficiency, one for the conventional and one for the ducted tip propeller, for each of the different advance ratios associated with the three drogue sizes. Figure 4.5 *suggests* that there could be as much as a 10% improvement for the ducted tip propeller at maximum efficiency.

4.3.1 Comparison to propellers with other tip devices

For the two propeller types tested by Crump (1948), the installation of bulbous tips had dissimilar effects on the efficiency, owing either to the different propellers, or to the different bulbs. The first propeller, with three blades and P/D = 1.1, was designed for service at high advance ratios on a destroyer. The bulb had a cylindrical shape, rounded off at the nose and the tail, with a diameter equal to 3.5% of the propeller diameter. This propeller showed a marginal increase in efficiency ($\approx$ 1%) at high advance ratios after the bulbs had been installed, but no change at low advance ratios. The second propeller had four blades, P/D = 1.1, and were designed for service over a wider range of advance ratios on a submarine. The bulbs attached to this propeller were smaller, with diameters equal to 2% of the propeller diameter, and were faired into the tips to be an integral part of the propeller, looking more like a continuous increase of blade thickness towards the blade tips. After installation of the bulbs, this propeller had a noticeable reduction of the efficiency (4 - 5%) at high advance ratios, but there was some indication of increased efficiency at low advance ratios. Crump (1948) concluded that bulbous tips will be more effective on propellers operating at low advance ratios, although there is no data presented for $J < 0.4$. With the bulbous tips installed the freestream velocity could be increased by 25% for both propellers before the onset of tip vortex cavitation, which implies that both bulb configurations suppressed the tip vortices.

The experience with bladelets is somewhat similar. Goodman and Breslin (1980) found that bladelets have a detrimental effect, or at the best, no effect at all, on the propeller performance. Itoh et al. (1987), however, found that the *typical* behavior of their bladelets would be a noticeable reduction of the efficiency at high advance ratios, but a marginal increase at moderate and low advance ratios, with the best bladelets proving a 4% performance improvement. Due to a much larger number of different bladelets tested, the results of Itoh et al. (1987) better represent the potential bladelets have on marine propellers.

Although the results described above show that typically one obtains improved efficiency at low advance ratios and reduced efficiency at high advance ratios with tip devices installed, the experiments of Crump (1948) also indicate that the opposite may occur. Between the bulb and the bladelet, it is probably more relevant to compare the ducted tip with the bulb, owing to its similar geometry. The ducted tips used in the sea trials have a diameter equal to 4.2% of the propeller diameter, and therefore, bear some resemblance to the largest bulb tested by Crump (1948). This is the bulb that saw a slight efficiency increase at high advance ratios, which leads to the conclusion that bulbous and ducted tips with larger diameters, up to an unknown limit, are more effective as vortex suppressing devices. Crump also commented on the cavitation emerging from the base of the bulbs and attributed this to incorrect location or fairing of the bulbs into the blades. The presence of cavitation indicates that local flow separation occurs along the base of the bulbs, which would have caused extra drag and loss of lift. This observation suggests the importance of choosing a favorable combination of tip size, tip shape and the way it is faired into the blade in order to avoid large detrimental effects on the propeller efficiency as a consequence of tip device installation.

4.3.2 Blade area and duct geometry

Assuming that an efficiency improvement is possible provided a favorable tip configuration is chosen, the next step will be to explain why the improvement would

occur at high rather than low advance ratios in contrast with what one would expect based on the airfoil tests of Green and Duan (1995). In order to explain the unexpected result, we will first examine how the blade area was altered with the installation of the ducts.

The ducted tips on the propeller were designed to be a geometrically similar to the ducted tip on the airfoil of Green and Duan (1995). Thus, as was the case for the airfoil studies, the length of the ducts was equal to 65% of the average blade chord. However, due to the swept back leading edge, the planform area of the ducted tips, relative to the lifting surface they replace, is substantially larger on the propeller; for the airfoil the projected area of the ducted tip covered 65% of the surface it replaced, while the corresponding number for the propeller is approximately 100%. According to Green and Duan (1995), ducted tips redistribute the shed vorticity in the Trefftz-plane into a line and a ring formation (Figure 4.6), assuming that the ducts contribute to the shed vorticity, and therefore also generate lift. Obviously, the more lift a duct can generate, the better it will redistribute the circulation uniformly across the rest of the airfoil, and consequently, both increase the lift and reduce the induced drag of the lifting foil.

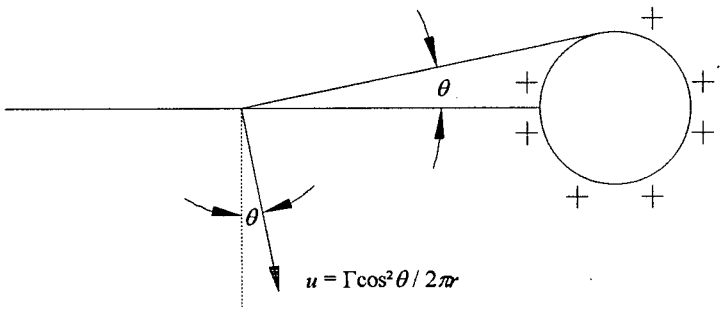

Figure 4.6 The *line and ring* model for the reduction in induced velocities (downwash) of the ducted tip geometry.

Because the installation of ducted tips on the propeller did not result in a reduced planform area, the propeller may have experienced a smaller net loss of lift in the tip region than did the airfoil. This in itself may have improved the effectiveness of the ducted tips when installed on the propeller. If, in addition, they more efficiently redistributed the circulation, we would expect to see the positive effects of the ducted tips at an earlier stage on the propeller than on the airfoil. Hence, the range of angles of attack at which the ducted tips improve the L/D ratio will be expanded to include $\alpha < 8°$, resulting in an increase interval of advance ratios where a better propeller performance could be expected.

On the other hand, the larger wetted area of the ducts may also result in a large drag penalty. The ducted tip added approximately 10% surface to the total wetted area of the airfoil, while the corresponding value for the propeller is 14%. The potential improvement in performance due to high lift might therefore be lost due to extra drag.

4.3.3 Radial variation of α

An explanation based solely on the duct geometry is not sufficient to explain why the ducted tips increased the peak performance of the propeller. It is necessary to associate the efficiency with the radial variation of the lift and drag coefficients, and hence, the angle of attack, as a function of the propeller radius and the advance ratio. At radius r a blade element (Figure 4.3) will experience the effective angle of attack α_I. However, the lift and drag data of Green and Duan (1995) are presented in terms of the geometric angle of attack, α, where the effects of the induced velocity, u, is disregarded, giving $\beta_I = \beta$, and hence

$$\alpha = \phi - \beta = \arctan\frac{Pn}{2\pi rn} - \arctan\frac{V_A}{2\pi rn}$$

or expressed in terms of P/D and J

$$\alpha = \arctan\frac{\left(P/D\right)}{\pi\left(r/R\right)} - \arctan\frac{J(1-w)}{\pi\left(r/R\right)} \qquad \textbf{(4.10)}$$

The airfoil tested by Green and Duan (1995) had a rectangular, untwisted, constant NACA 66-209 profile. The flow across a propeller blade is considerably more complex than the flow across such an airfoil. Nevertheless, by plotting α as a function of r/R for the values of J that characterize the heavy, medium and light drogues as well as the free running speeds at high and low shaft rotations (Figure 4.7), the results from the airfoil should give an indication of which radial sections of the propeller can be expected to operate with an improved efficiency after the ducts are installed.

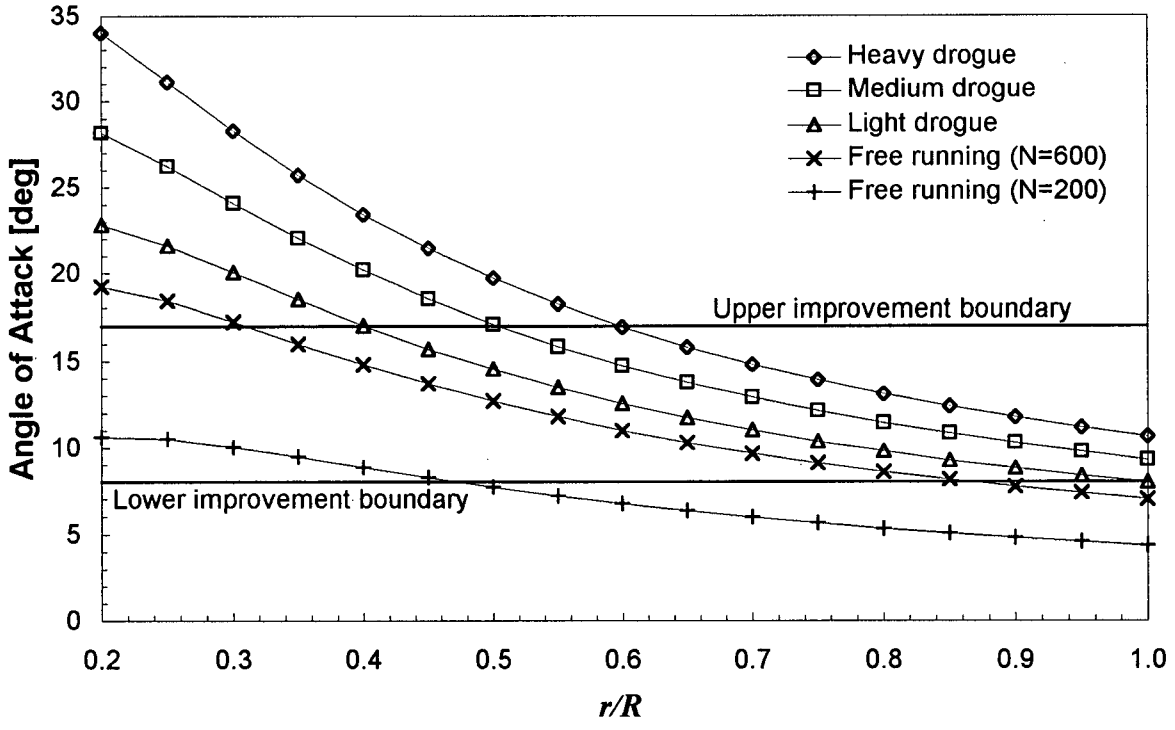

Figure 4.7 The angle of attack, α, plotted as a function of the propeller radius for six different advance ratios, ranging from J = 0.20 (heavy drogue) to J = 0.55 (free running, N = 200), for a Taylor wake fraction w = 0.20. The induced velocity has been neglected.

As mentioned in the previous chapter, the wake fraction, w, could not be determined for Pearl Sea. Single screw ships with moderate blockage coefficients, have Taylor wake fractions between 0.2 and 0.3 (Manen and Oossanen, 1988); w = 0.2 was chosen in order to plot Equation 4.10. Two extra lines have been plotted to indicate the upper and lower boundary of the region of possible improvement of the L/D ratio, hereafter referred to as the *improvement envelope*. The upper and lower boundary for the improvement envelope has been chosen to coincide with the lowest and highest angles of attack at which an improvement of the L/D ratio for the NACA 66-209 airfoil was measured by Green and Duan (1995). Figure 4.7 indicates that an improvement of the L/D ratio at free running speeds is possible only for the highest N. The figure also indicates that an improvement would not necessarily occur at high advance ratios, as a large radial section of the blades would be operating at conditions beyond stall. The improvement envelope shown in Figure 4.7 is not truly representative of what one would expect for the propeller blades, owing to the radial variation of both profile and relative velocity. The effects of these factors are examined below.

4.3.4 Blade thickness and camber

Both the blade thickness and camber will affect the shape of the improvement envelope. The upper boundary is determined by the stall of the blade. Stall occurs, in general, at higher absolute angles of attack (α - α_0) the thicker a hydrofoil is, and hence, the decreasing element thickness towards the tip of the propeller blades will therefore reshape the improvement envelope by decreasing the upper boundary from a stall angle α = 22° at 21% blade thickness close to the hub, to α = 12° at 3% blade thickness towards the tip.

The lower improvement boundary is determined by the lift coefficient, C_{Limpr}, at which the ducted tip reduces the induced drag to the extent that it compensates for both the extra parasite drag and loss of lift. This lift coefficient is a function of the absolute angle of attack, α - α_0. According to thin airfoil theory, the geometrical angle of attack, describing the lower improvement boundary, will therefore be

$$\alpha_{impr} = \frac{C_{Limpr}}{2\pi} + \alpha_0 \qquad \text{where} \qquad \alpha_0 = -2\varepsilon\,[\text{rad}]$$

where ε is the camber, as a fraction of the chord, of a blade element at radius r. The zero-lift angle of the NACA 66-209 profile is approximately -1.5°, giving ε = 0.013, or 1.3%. For the propeller ε > 1.3%, and hence, assuming C_{Limpr} is the same as for the airfoil, α_{impr} < 8° at all radii (Table 4.1).

r/R	**0.2**	**0.3**	**0.4**	**0.5**	**0.6**	**0.7**	**0.8**	**0.9**	**1.0**
t [%]	21.0	15.5	12.0	8.5	6.5	5.0	4.0	3.0	
α_{stall}[deg]	20	19	18	17	16	15	14	13	12
ε [%]		3.6	3.5	3.4	3.0	2.6	2.1	1.5	
α_{impr} [deg]		5.4	5.5	5.6	6.1	6.5	7.1	7.8	

Table 4.1 Radial variation of blade thickness and camber and the approximate angles of attack between which an improvement of the Lift/Drag ratio can be expected.

4.3.5 Reynolds number effects

Together with the reduced blade thickness towards the tips, the increased Reynolds number will reduce the parasite drag on the propeller blades. Typical values of $Re_{0.7}$ during the efficiency measurements are $1.0 \cdot 10^6$ to $3.5 \cdot 10^6$, respectively at minimum shaft rotation with the heavy drogue and maximum shaft rotation at free running speeds, respectively. The airfoil tests (Green and Duan, 1995) were conducted at Re = $0.6 \cdot 10^6$. All other things being equal, higher Re is associated with less parasite drag. Hence, at higher Re the reduction of induced drag will have a greater impact on the total drag of the blades, and therefore require a smaller lift coefficient before the L/D ratio improvement due to the ducted tips can

be observed. This is true for the extent of the blades that are operating at Re > $0.6 \cdot 10^6$, i.e., the outer radial sections of the blades, which carry the highest loads.

The effect of a higher Re can be demonstrated by some simple calculations, which are summarized in Table 4.2: part *a* contains the C_D and C_L measured with the NACA 66-209 airfoil at α = 8° and Re = $0.6 \cdot 10^6$ (extracted from Duan 1995), and part *b* an estimation of the results if the same airfoil had been tested at the same α and at Re = $3.0 \cdot 10^6$. The drag has been split into two parts: the total, measured, drag is equal to the sum of the parasite and the induced drag,

$$C_D = C_{DP} + C_{DI}$$

$C_{DP} \approx 0.0105$, with the conventional tip at Re = $3.0 \cdot 10^6$, is given by Abbott and Doenhoff (1959). C_{DP} at Re = $0.6 \cdot 10^6$ can be estimated, crudely, using a ratio of the drag coefficients, C_{DF}, for turbulent flow on a flat plate:

$$C_{DP}(Re = 0.6 \cdot 10^6) = 0.0105 \frac{C_{DF}(Re = 0.6 \cdot 10^6)}{C_{DF}(Re = 3.0 \cdot 10^6)} = 0.0132$$

$C_{DP} \approx 0.0145$ and 0.0116 for the ducted tip, were found by adding 10% to the drag of the conventional tip, equivalent to the percentage wetted surface added by the duct. By knowing C_D and C_{DP}, C_{DI} can now be estimated for both the conventional and ducted tip at Re = $0.6 \cdot 10^6$. Assuming that C_{DI} and C_L are independent of Re in this range, C_D and L/D can be calculated for Re = $3.0 \cdot 10^6$. Table 4.2 shows that the increased Re has increased the L/D improvement of the ducted tip from -0.7% to 0.5%, which implies that the positive effects of the ducted tips installed on the propeller can be expected to occur at a lower α than on the airfoil.

Tip type	C_{DP}	C_{DI}	C_D	C_L	C_L/C_D	Improve.
***a*) NACA 66-209 airfoil at α = 8° and Re = 0.6·10^6**						
Conventional	0.0132	0.0051	0.0183	0.4864	26.58	
Ducted	0.0145	0.0038	0.0183	0.4828	26.38	-0.7%
***b*) NACA 66-209 airfoil at α = 8° and Re = 3.0·10^6**						
Conventional	0.0105	0.0051	0.0156	0.4864	31.18	
Ducted	0.0116	0.0038	0.0154	0.4828	31.35	0.5%
***c*) Propeller at $\alpha_{0.7R}$ = 8° and $Re_{0.7}$ = 0.6·10^6**						
Conventional	0.0132	0.0215	0.0347	0.4864	14.02	
Ducted	0.0150	0.0160	0.0310	0.4828	15.57	11%

Table 4.2 The effect of higher Reynolds numbers and a larger fraction of induced drag.

4.3.6 Spanwise loading

According to the lifting line theory, the induced velocity at the radius $r = a$ can be expressed as

$$u_a = -\frac{1}{4\pi}\int_{-R}^{R}\frac{(\partial\Gamma/\partial r)dr}{a-r}$$

Hence, a lifting surface with large radial, or spanwise variation of the circulation, Γ, will therefore generate the highest induced velocities, and consequently, induced drag. Table 4.2.*c* shows the results of *LID* calculations based on a lifting surface that generates the same amount of lift and parasite drag as the NACA 66-209 airfoil, but substantially more induced drag, such as a propeller blade, where the load is concentrated towards the tip due to the radial distribution of blade chord and relative velocity (Figure 4.8). C_L and C_{DP} have been adopted from

part *a*, and C_{DI} has been calculated for the conventional tip as if produced by a propeller blade with elliptic distribution of the load:

$$C_{DI} = \frac{C_L^2}{\pi AR}$$

where AR = 3.5, which is the aspect ratio of the blades of the conventional propeller. The ratio of C_{DI} for the ducted and conventional tip (≈ 0.75) is also adopted from part *a*. By knowing C_{DP} and C_{DI}, C_D can be calculated. In part *a* the induced drag accounts for 28% of the total drag, while the corresponding number in part *c* is 62%. Owing to the larger induced drag for the propeller geometry, installation of the ducted tips results in an 11% increase in the L/D ratio. This finding suggests that the load distribution will have a large impact on the effectiveness of the ducted tips at different angles of attack, and hence, the improvement envelope of the propeller.

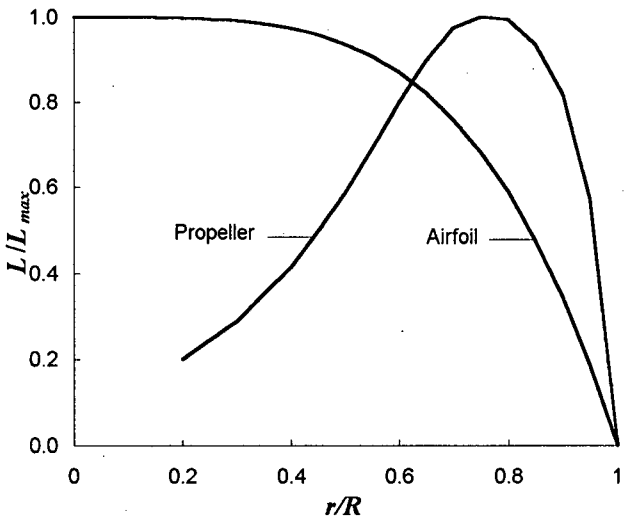

Figure 4.8 Typical radial/spanwise loading of a propeller blade and a rectangular, untwisted, constant profile airfoil.

4.3.7 3D effects

The improvement envelope have been replotted in Figure 4.9 where all the factors discussed above have been taken into consideration. The combined effect of the duct size, blade thickness and camber, Reynolds number and spanwise loading will move the lower improvement boundary down to an approximate, estimated value of α = 4°. This modification of the lower boundary results in a substantially larger improvement envelope that includes the complete span of the blades only when the propeller operates at free running speeds, which explains why the largest improvement of propeller efficiency was observed at free running speeds. At lower advance ratios parts of the propeller still operate within the improvement envelope, implying that a certain improvement is possible.

The principle of the ducted tip, however, is to reduce the induced velocities, and consequently, increase the effective angle of attack, which will move more of the α-lines for the heavy, medium and light drogue above the upper improvement boundary (Figure 4.10). The efficiency improvement obtained towards the tip of the blades will therefore be lost because a larger radial section towards the hub operates at stall.

4.3.7 Degradation in the marine environment

Prior to installing the propeller on the boat, the blade surfaces were sanded to a finish equivalent to that delivered by propeller manufacturers. Because of delays between installation and the first test runs of the conventional propeller, a certain degradation of the surface due to growth of marine micro organisms might have influenced the efficiency measurements, although frequent use and visual inspections refute this. At the time of installation of the conventional propeller, the hull of Pearl Sea was sanded down and given a new coat of bottom paint. During the next nine months it took to complete the test program, the hull stayed essentially free of barnacles and other marine growth. We have therefore assumed that the marine environment had only a negligible effect on the efficiency measurements.

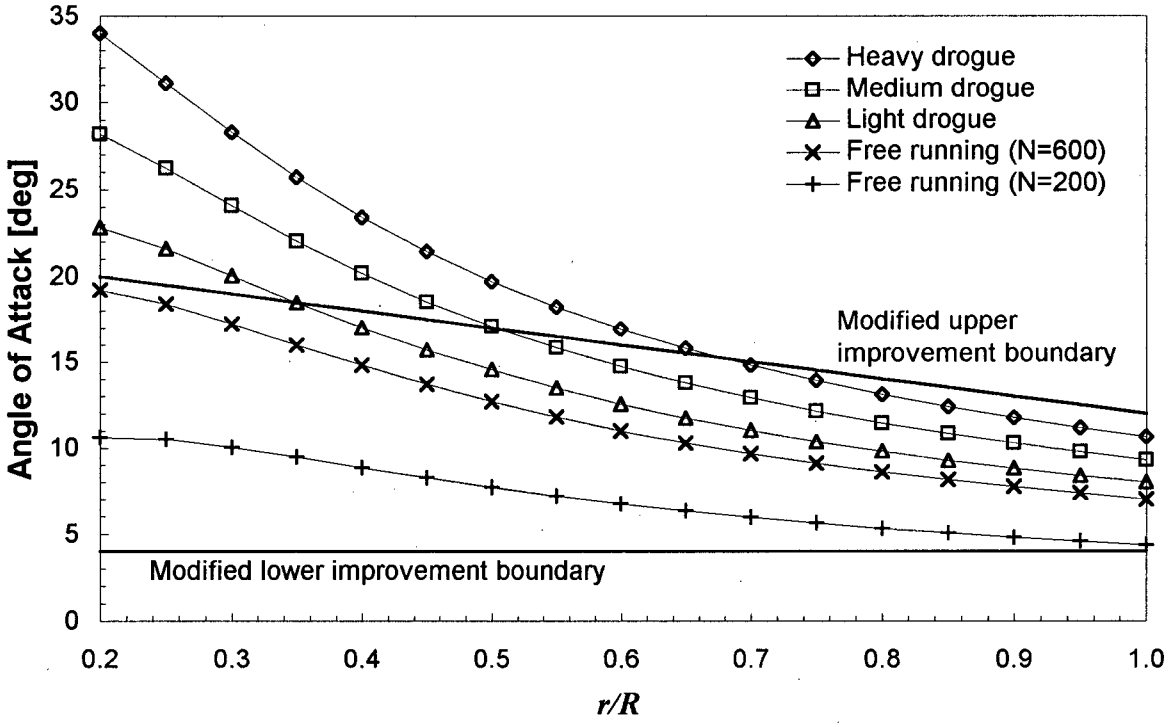

Figure 4.9 Replot of Figure 4.7 with a modified improvement envelope.

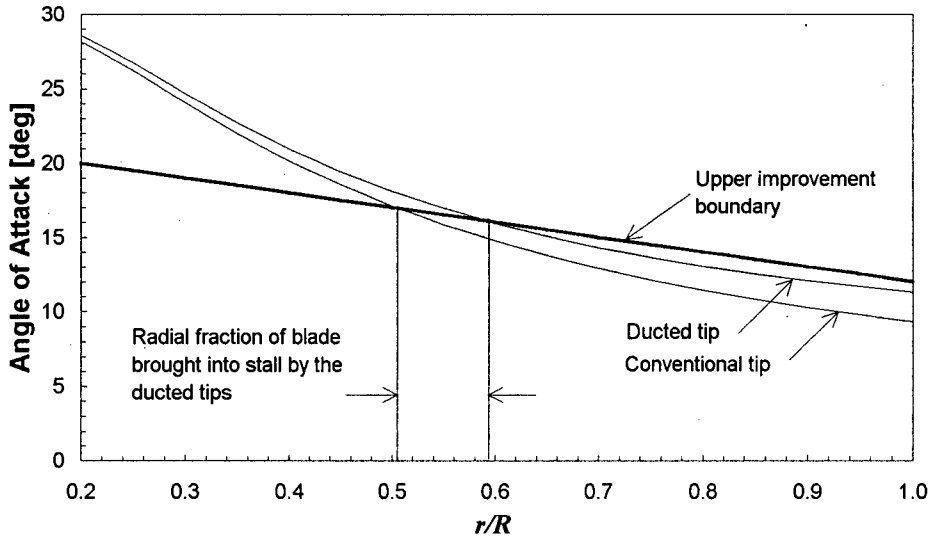

Figure 4.10 The effect of the ducted tips when the propeller operates at low advance ratios.

4.3.8 Summary

Previous research has shown that the effectiveness of a tip appendage as a L/D ratio improving device depends on its geometry, location and orientation. Wind tunnel tests have shown that the ducted tip is a geometry that has a large potential as such a device in marine applications. The current research has proven that installation of ducted tips can improve the efficiency of a marine propellers, possibly by as much as 10%. The ducted tips improve the efficiency of the propeller for advance ratios where a sufficient fraction of each blade operates within an angle of attack improvement envelope. This region is larger for the propeller blades, including smaller angles of attack, than that found in wind tunnel tests of ducted tip airfoils, in part because of the different loading of the propeller blade. Due to the larger spanwise variation of the loading, the propeller blades generate substantially more induced drag than the more uniformly loaded airfoil. A lower lift coefficient, and consequently, angle of attack, was therefore needed for the propeller blades to obtain an C_{Di}/C_D ratio where a certain percentage reduction of the induced drag resulted in an improved L/D ratio. The large camber (i.e. large zero-lift angle) and high Reynolds number (i.e. reduced parasite drag) also contributed in this direction.

4.4 Cavitation performance

4.4.1 Conventional propeller

When moored to the dock, the inception of tip vortex cavitation on the conventional propeller was determined to occur at shaft rotation rates between 266 - 274 rpm. N_i = 274 rpm will be referred to as the inception rotation rate in the subsequent discussion. It is also worth noting that the video recordings reveals that cavitation did not occur simultaneously on the four propeller blades. At N = 274 rpm cavitation seems to have reached an intermittent mode, but on still pictures it can be seen how only two of the blades, two consecutive blades, are trailed by a small cavitation bubble. This pattern remains for the next two increments in shaft rotation at which video recordings were made. Continuous cavities could, for the first time, clearly be seen emerging from all four tips at 301 rpm (Table 3.2.).

There are two reasons, that are more likely than others, why the onset of cavitation did not happen simultaneously on the four blades:

1. Two blades have a slightly higher pitch towards the tip than the other ones.
2. Two of the blades have a rougher surface in the tip region, causing a slight delay of cavitation inception.

The true explanation could involve a combination of these; both pitch and surface finish was done manually, in accordance with the methods that are practiced in small propeller shops, where precision tools are not available.

In order to determine the propeller cavitation inception index, σ_i, it is necessary to define a boat velocity $V > 0$. It is reasonable to assume such a V exists in the bollard pull data; there is a discrepancy between the thrust measured on the shaft and the load on the tow line (Figure 3.1.*b*), indicating that the propeller induces a flow that creates an extra drag on the boat (Figure 4.11). By plotting V at N = 274 as a function of T for the different drogue sizes, a linear relationship between V and T is obtained (Figure 4.12). This line can be extrapolated to give V = 0.55 m/s at bollard pull conditions ($T \approx$ 5330 N, see Figure 3.1.*b*). For the purpose of determining the blade cavitation inception index, σ_{ri}, it can be assumed that $V_A = V$. The cavitation inception index σ_i and σ_{ri} as well as the associated $Re_{0.7}$, J and α are listed in Table 4.3.

N_i	V_A=V	U	$Re_{0.7}$	J_A=J	α	σ_i	σ_{ir}
274 rpm	0.55 m/s	9.20 m/s	$1.6 \cdot 10^6$	0.14	16°	745	2.7

Table 4.3 Conditions at inception of tip vortex cavitation.

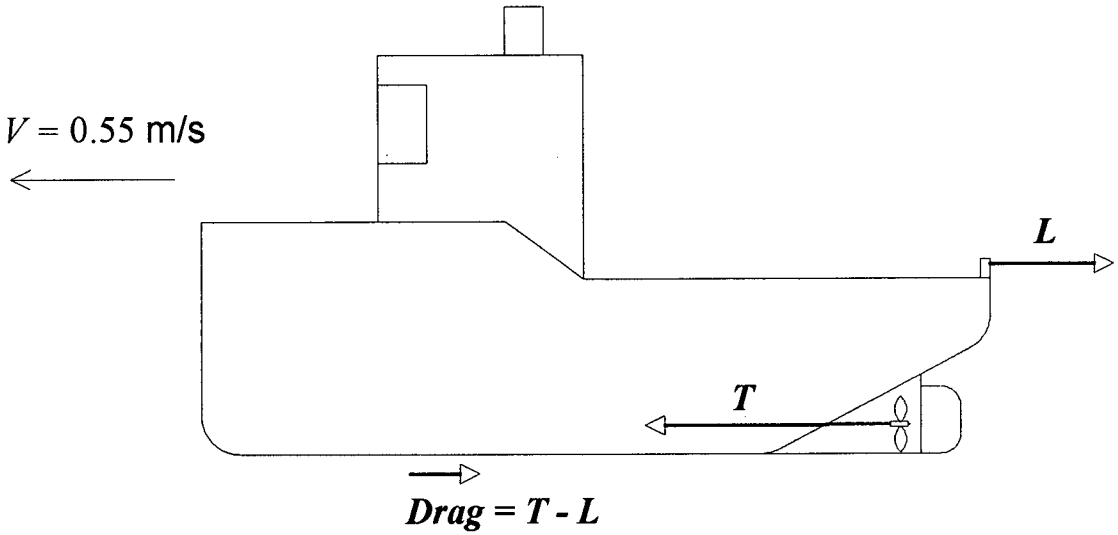

Figure 4.11 Forces acting on the boat during bollard pulls.

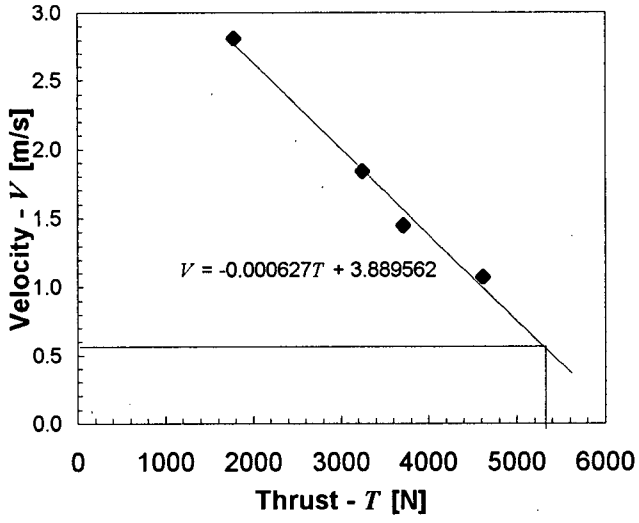

Figure 4.12 The boat velocity, V, at N = 274 rpm, plotted as a function of T for all drogue sizes in order to find V at bollard pull condition (T = 5330 N).

Now that σ_i and σ_{ir} has been established for the conventional propeller, it is of interest to compare them to values given in the literature. In order to avoid all the uncertainties associated with the flow relative to the propeller blades, the inception index for propellers, σ_i, is usually related to the freestream velocity, as defined by Equation 4.8, which in the case of sea trials is the forward velocity of the boat relative to the water. However, basing the analysis on σ_i as opposed to σ_{ir} is not free of complications. Due to the limited amount of information that exists on inception on propellers, it is difficult to compare propellers with different geometries, operating at different Reynolds numbers and advance ratios. This is demonstrated in Table 4.4, which shows the vastly different σ_i for model propellers operating at different advance ratios. There is a trend of increasing σ_i with decreasing J, which is what one would expect as reduced advance ratios increase the angles of attack.

The large σ_i found for the sea trials can therefore be attributed to the extremely low J, which is confirmed by a scaling equation, suggested by Strasberg (Mani and Arakeri, 1984), that relates σ_i to the slip ratio, S:

$$\sigma_i = 1.9e^{6.6S} \qquad \text{where} \qquad S = 1 - \frac{J_A}{\left(P/D\right)_{0.7R}}$$

Strasberg's equation and Equation 4.8 both give $\sigma_i \approx 605$ for $V_A = V = 0.61$ m/s, suggesting that the previous estimate giving $V = 0.55$ m/s is a little low. Nevertheless, together with the trend in Table 4.4, Strasberg's equation indicates that the conventional propeller had cavitation characteristics representative of propellers of similar size and geometry.

Although several papers present full scale cavitation observation only Jessup et al. (1993) have determined an inception index. Curiously, in that work σ_i for the full scale propeller is lower than σ_i for a model of the same propeller, in spite of a much higher Reynolds number. There has been no reason suggested for this unexpected scaling (recall that McCormick's studies (1962) on hydrofoils showed

that σ_i increases with Re). However, it is likely that failing to properly model the hull wake, despite a geometric identical model, has a major influence on the result. This could happen if the model is tested in a laminar flow, while the full scale propeller operates in turbulent flow. The nuclei content variation from the model tank to the sea may also have an effect on the scaling .

Author	Re	$P/D_{0.7R}$	J	σ_i
Lodha and Arakeri (1984) * model propeller * Strasbergs equation	$1.1 \cdot 10^6$	0.83 1.15	0.50 0.14	33 626
Chahine et al. (1993) * model propeller	$6.6 \cdot 10^5$		0.86	19.5
Jessup et al. (1993) * model propeller * full scale propeller	$4.0 \cdot 10^6$ $5.0 \cdot 10^7$		1.26 1.26	2.3 1.7
This report	$\mathbf{1.6 \cdot 10^6}$	**1.15**	**0.14**	**745**

Table 4.4 Comparing σ_i with values from previous research on propellers.

With respect to studies on hydrofoils (Table 4.5), σ_{ir} is comparable to those of previous research, although one would expect a higher value for the propeller than for the hydrofoils due to the stronger tip vortices generated by the propeller blades. The semi-empirical analysis of McCormick (1962) also suggests a higher value for the propeller. However, $Re_{0.7}$ and $\alpha_{0.7}$ may not be representative for the propeller blades for use with such an analysis.

The discrepancy between hydrofoil results and these propeller tests is most likely caused by the different flow conditions. While hydrofoils experience uniform incoming fluid velocities, the propeller blades has to encounter a much more complex flow structure due to its rotational motion. The rotational motion will, for example, result in a centripetal acceleration of the water, due to viscous effects, which might force more water to enter the tip vortex, increasing the vortex core-

pressure, and thereby delaying cavitation inception. To add to the complexity, every blade operates in the wake of the previous blade, causing the tip vortices to interact and influence the roll-up process, which could potentially delay cavitation inception to a greater or lesser extent.

Author	Re $\cdot 10^6$	α [deg]	σ_{ir}
Fruman et al. (1993) * elliptic hydrofoil no.1 (ENCT) * elliptic hydrofoil no.2 (ICT)	 1.2 1.2	 10 10	 1.8 2.9
Green (1991) * rectangular hydrofoil	1.0	14	4 - 5
Green and Duan (1995) * rectangular hydrofoil	1.4	15	3.2
McCormick (1962) * $\sigma_{ir} = 1.28 \cdot 10^{-3} Re^{0.35} \alpha^{1.29}$	1.6	16	6.8
This report	**1.6**	**16**	**2.7**

Table 4.5 Comparing σ_{ir} with values from previous research on hydrofoils.

4.4.2 Ducted tip propeller

The video recordings of the ducted tip propeller speak for themselves: the ducted tips substantially delay inception of tip vortex cavitation on marine propellers. An inception point can not be determined for the ducted tip propeller, although we know for sure that tip cavitation did not occur for any shaft rotations up to, and including, N = 404 rpm, which corresponds to a 47% cavitation improvement relative to the shaft rotation rate at inception on the conventional propeller. The delay, or absence of tip vortex cavitation also confirms the encouraging results of the efficiency measurements. In addition to this most important observation, there are additional observations that warrant mention.

At N between 400 and 450 rpm a vapor cloud emerges from the exit of the ducts. Exactly what happens can not be deduced from the video owing to limitations of underwater filming. Due to poor light conditions, in spite of two 650 watt underwater lamps, it was not possible to film at shutter speeds higher than 1/1000 seconds. In addition, the diver could not film too close to the propeller, and using a zoom lens underwater is not recommended due to its very short depth of field. The vapor clouds are most likely the tip vortices that at this point are starting to cavitate, but are being diffused by the flow exiting through the ducts. However, the clouds could also be surface cavitation from the inside edge of the ducts, or a combination of both. To determine what the flow looks like at the exit of the ducts will require a flow visualization experiment set up in a cavitation tunnel.

Cavitation from the leading edge of the ducts can not be observed until a shaft rotation close to 400 rpm is obtained. At advance ratios higher than those during bollard pulls, the ducts will have lower angles of attack relative to the incoming flow, and chances are therefore that duct leading edge cavitation will not occur at all as soon as the boat is given a forward velocity. These observations suggest that the orientation of the ducts, aligned with the chord of the blade where the tips were cut, is correct. The video does, however, not offer much information about the effect of the duct geometry. The near absence of duct leading edge cavitation may be a result of our efforts to round off the leading edges, or it could be a result of the receding duct leading edge as it extends from the suction surface to the pressure surface. The design of this 1 inch lip was based on the intuition that it will "capture" more of the tip vortices in their incipient phase, and therefore better retard the rest of the roll-up process, than does the straight duct leading edge. The tapered lip it could also have reduced the duct leading edge separation.

At all shaft rotation rates there was substantially less radial spread of the race aft of the ducted tip propeller, which is in accordance with the observations of the boat owner, who commented on how the wake of the boat was different after the ducts had been installed.

Chapter 5 - CONCLUSION AND RECOMMENDATIONS

5.1 Conclusion

The sea trials of the ducted tip propeller culminated in the following results:

1. The ducted tips substantially delayed tip vortex cavitation inception on a propeller that is representative of a large number of propellers installed on smaller commercial vessels, such as tug boats and fishing boats. For this particular propeller, cavitation was delayed by a minimum of 47%, based on the shaft rotation rate at inception.
2. The ducted tip propeller did not suffer from efficiency losses due to the extra wetted surface of the ducts. On the contrary, the measurements indicate that up to a 10% improvement in the efficiency is possible.

The success of the sea trials can largely be attributed to the size and geometry of the ducted tips: the partial chord duct length offers a limited drag penalty, but remains very effective as a tip vortex suppressing device, both by obstructing the roll-up process itself, and further retarding it as the internal and external flow mix at the exit of the ducts.

Obviously, the ducted tip propeller has a large commercial potential as it offers both an increased efficiency and improved cavitation performance. For most applications one of these factors, alone, would be sufficient to substantiate installation of ducted tips, provided the installation costs can be kept at a reasonable level. For the propeller described in this report, the installation costs amounted to approximately $300, which is very modest. It still remains to be determined if the results of the current research can be transferred to commercial application.

5.2 Recommendations for future work

Assuming that an optimum duct design can be found, and extraordinary propeller geometries and extreme tip speeds are avoided, the effectiveness of the ducted tips is essentially a function of the propeller characteristics, such as pitch, diameter and blade area, as well as the incoming flow. In order to develop the ducted tip propeller into a commercial product, the following research should be carried out:

1. Optimization of the ducted tip design, including flow visualization to determine which type of cavitation appears at the exit of the ducts at high shaft rotations. This work should involve studies to determine the best combination of duct length and duct diameter relative to the average chord and propeller radius, respectively.
2. Systematic experiments with ducted tips installed on model propellers with different P/D and A_E/A_0 ratios. This information should be compiled and expressed as a *ducted tip efficiency improvement* as a function of K_Q or K_T of the conventional propeller. From such diagrams the feasibility of installation of ducted tips can readily be assessed without having to know the details of the inflow.
3. It would be of interest to study the effects of the ducted tips installed on *controllable pitch* propellers and propellers with highly skewed leading edge.
4. Strength considerations and studies of manufacturing procedures.

References

Abbott, I.H. and Doenhoff, A.E. von, 1959, "Theory of wing sections", Dover.

Arndt, R.E.A., Arakeri, V.H. and Higuchi, H., 1991, "Some observations of tip vortex cavitation", ASME Journal of Fluid Mechanics, vol.229, pp.269-289.

Arndt, R.E.A. and Keller, A.P., 1992, "Water quality effects on cavitation inception in a trailing vortex", ASME Journal of Fluids Engineering, vol.114, pp.430-438.

Arndt, R.E.A. and Maines, B.H., 1994, "Vortex cavitation: A progress report", ASME FED vol.190, pp.99-117.

Bevington, P.R., 1969, "Data reduction and error analysis for the physical sciences", chapter 4, McGraw-Hill.

Bjørheden, O., 1981, "Highly-skewed propellers - 4 years' experience", Canadian Shipping and Marine Engineering, September, pp.28-33.

Breslin, J.P. and Andersen, P., 1994, "Hydrodynamics of ship propellers", Cambridge Ocean Technology Series 3, Cambridge University Press.

Brophy, P., 1986, "That Grim (x-bladed) engine", Canadian Shipping and Marine Engineering, May, pp.7-8.

Brown, D.K., 1973, "Effect of number of blades on tip vortex cavitation", report no.2173, Admirality Experiment Work, Haslar.

Bystrøm, H., 1996, KaMeWa, Sweden, personal communication.

Chahine, G.L., Frederick, G.F. and Bateman, R.D., 1993, "Propeller tip vortex cavitation suppression using selective polymer injection", ASME Journal of Fluids Engineering, vol.115, pp.497-503.

Crump, S.F., 1948, "The effects of bulbous blade tips on the development of tip vortex cavitation on model marine propellers", report C-99, David Taylor Naval Ship Research and Development Center.

Duan, S.Z., 1995, Ph.D. thesis, Department of Mechanical Engineering, University of British Columbia, Canada.

Duan, S.Z., Green, S.I. and Acosta, A.J., 1992, "Lift/drag performance of conventional and ducted-tip wings", ASME Cavitation and Multiphase Flow Forum, Los Angeles.

English, J.W., 1992, "Observation and speculation on propeller cavitation induced vibration excitation", IMechE International Conference on Cavitation, paper C453/064, pp.231-238.

English, J.W., Suhrbier, K.R. and Stringer, P., 1992, "Propeller-hull vortex cavitation on a dynamically positioned support vessel. A comparative study with conventional and ducted propellers.", IMechE International Conference on Cavitation, paper C453/001, pp.223-230.

Engås, A., Misund, O.A., Soldal, A.V., Horvei, B. and Solstad, A., 1995, "Reactions of penned herring and cod to playback of original, frequency-filtered and time-smoothed vessel sound", Fisheries Research no.22, pp.243-254.

Falcao de Campos, J.A.C., George, M.F. and MacKay, M., 1989, "Experimental investigation of tip vortex cavitation for elliptical and rectangular wings", ASME FED vol.79, pp.25-30.

Fruman, D.H., 1988, "Tip vortex cavitation in polymer solutions", ASME FED vol.64, pp.81-83.

Fruman, D.H. and Aflalo, S.S., 1989, "Tip vortex cavitation inhibition by drag reducing polymer solutions", ASME Journal of Fluids Engineering, vol.111, pp.211-216.

Fruman, D.H., Cerrutti, P., Pichon, T. and Dupont, P., 1993, "Effect of hydrofoil planform on tip vortex rollup and cavitation", ASME FED vol.177, pp.113-124.

Gindroz, B., 1995, "Practical advantages of mastering cavitation nuclei", Le Magazine du Bassin D'Essais des Carenes, no.4.

Gindroz, B. and Billet, M.L., 1994, "Nuclei and propeller cavitation inception", ASME FED vol.190.

Goodman, T.R. and Breslin, J.P., 1980, "Feasibility study of the effectiveness of tip sails on propeller performance", report no. MA-RD-940-81006, Department of Ocean Engineering, Stevens Institute of Technology.

Glover, E.F., 1987, "Propulsive devices for improved propulsive efficiency", Transactions vol.99, pp.23-29, Institute of Marine Engineers, London.

Green, S.I., 1991, "Correlating single phase flow measurements with observations of trailing vortex cavitation", ASME Journal of Fluids Engineering, vol.113, pp.125-129.

Green, S.I., 1995, "Wing tip vortices", Fluid Vortices, chapter 10, Kluwer.

Green, S.I., Acosta, A.J. and Akbar, R., 1988, "The influence on tip geometry on trailing vortex rollup and cavitation", ASME, Cavitation and Multiphase Flow Forum, pp.76-80.

Green, S.I. and Duan, S.Z., 1995, "The ducted tip - a hydrofoil with superior cavitation performance", ASME Journal of Fluids Engineering, vol.117, pp. 1-8.

Haggarty, B., 1994, Ulstein Maritime Ltd., Canada, personal communications.

Henriksen, H.L., 1988, "The new Liaaen SPEED-Z propulsion system", Canadian Shipping and Marine Engineering, Oct./Nov., pp.11-12.

Higuchi, H., Arakeri, V.H. and Arndt, R.E.A., 1986, "Further studies of tip vortex cavitation", ASME FED vol.36, pp.19-22.

Isin, Y.A., 1987, "Practical Bollard-Pull Estimation", Marine Technology, Vol.24, No.3, pp.220-225.

Itoh, S., 1987, "Study of the propeller with small blades on the blade tips (2nd report: cavitation characteristics)", Journal of the Society of Naval Architects of Japan, vol.161, pp.82-91. Published in Japanese with English abstract.

Itoh, S., Ishii, N., Tagori, T., and Ide, T., 1987, "Study of the propeller with small blades on the blade tips (1st report)", Journal of the Society of Naval architects of Japan, vol.159, pp.82-90. Published in Japanese with English abstract.

Jessup, S.D., Remmers, K.D and Berberich, W.G, 1993, "Comparative cavitation performance evaluation of a naval surface ship propeller", ASME FED-Vol.177, pp.51-62.

Johnsson, C.A. and Rutgersson, O.,1991, "Leading edge roughness - a way to improve propeller tip vortex cavitation", Propellers and shafting symposium, paper no.12.

Katz, J. and Bueno Galdo, J., 1989, "Effect of roughness on rollup of tip vortices on a rectangular hydrofoil", Journal of Aircraft, vol.26, no.3, pp.247-253.

Kuiper, G., 1978, "Scale effects on propeller cavitation inception", 12th Symposium on Naval Hydrodynamics, vol.12.

Lammeren, W.P.A. van, Manen, J.D. van and Oosterveld, M.W.C., 1969, "The Wageningen B-screw series", SNAME Transactions, Vol.77.

Lodha, R.K. and Arakeri, V.H., 1984, "Observations of tip vortex cavitation inception from a model marine propeller", Journal of the Indian Institute of Science, 65(a), pp.11-20.

Manen, J.D. van and Oossanen, P. van, 1988, "Propulsion", SNAME Principles of Naval Architecture, vol.2, chapter 6.

Maines, B.H. and Arndt, R.E.A., 1993, "Viscous effects on tip vortex cavitation", ASME FED vol.177, pp.125-129.

Mani, K., Sharma, S.D. and Arakeri, V.H., 1988, "Effect on propeller blade modification on cavitation induced noise", ASME FED vol.64, pp.64-67.

McCormick, B.W., 1962, "On cavitation produced by a vortex trailing from a lifting surface", Journal of Basic Engineering, pp.369-379.

McGreer, D., 1994, Kvaerner Masa Marine Inc., Canada, personal communication.

Millan, J., 1993, "Measurement of Strain due to Torque and Thrust Loads on Full Scale Propeller Shafts", report no. LM-1993-03, NRC/IMD.

Olsen, K., Angell, J., Pettersen, F. and Løvik, A., 1983, "Observed fish reactions to a surveying vessel with special reference to herring, cod, capelin and polar cod", FAO Fisheries Report no.297, pp.131-136.

Oosterveld, M.W.C. and Oossanen, P. van, 1975, " Further computer-analyzed data of the Wageningen B-screw series", International Shipbuilding Progress, Vol.22.

Platzer, G.P. and Souders, W.G., 1979, "Tip vortex cavitation delay with application to marine lifting surfaces. A literature survey", report no.79/051, David Taylor Naval Ship Research and Development Center.

Savikurki, J., 1988, "Aquamaster with contra-rotating propellers", Canadian Shipping and Marine Engineering, Oct./Nov., pp.6-9.

Sharma, S.D., Mani, K. and Arakeri, V.H., 1990, "Cavitation noise studies on marine propellers", Journal of Sound and Vibration, 138(2), pp.255-283.

Smith, L., 1996, The Faeroe Fisheries Laboratories, personal communication.

Sponagle, N.C., 1989, "The sound from different types of propeller cavitation", Canadian Aeronautical Association.

Stinebring, D.R., Farrell, K.J. and Billet, M.L., 1991, "The structure of a three dimensional tip vortex at high Reynolds numbers", ASME Journal of Fluids Engineering, vol.113, pp.496-503.

Towland, W., 1994, BC Ferries, Canada, personal communication.

Troost, L., 1937, "Open water test series with modern propeller forms", Transactions vol.54, pp.321-326, North East Coast Institution of Engineers and Shipbuilders, Newcastle Upon Tyne.

Weitendorf, E.A., 1993, "On propeller vortex cavitation as a source of ship hull vibration", ASME FED vol.176, pp.1-2.

Appendix A - Calibration

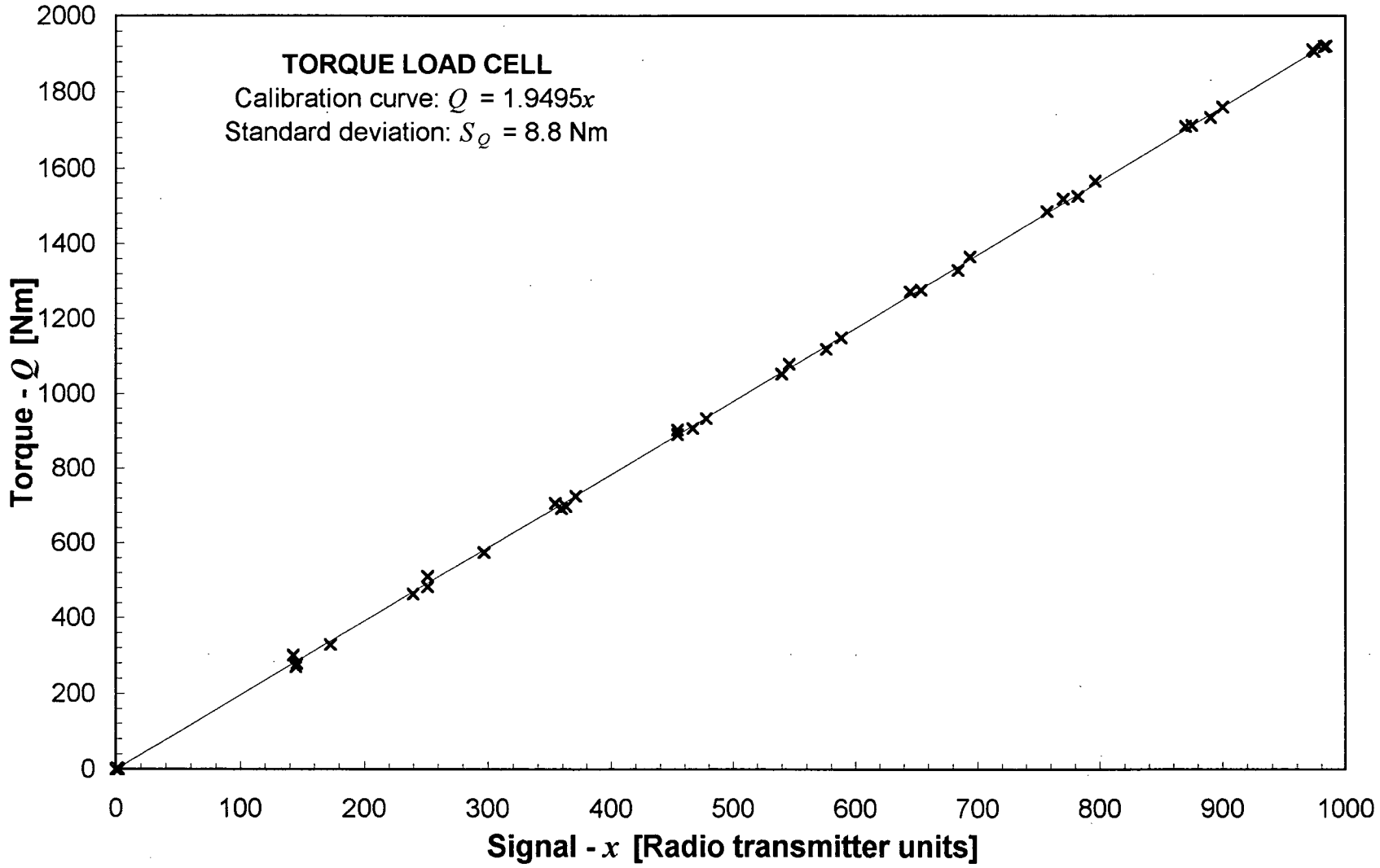

Figure A. 1 Calibration of the torque load cell.

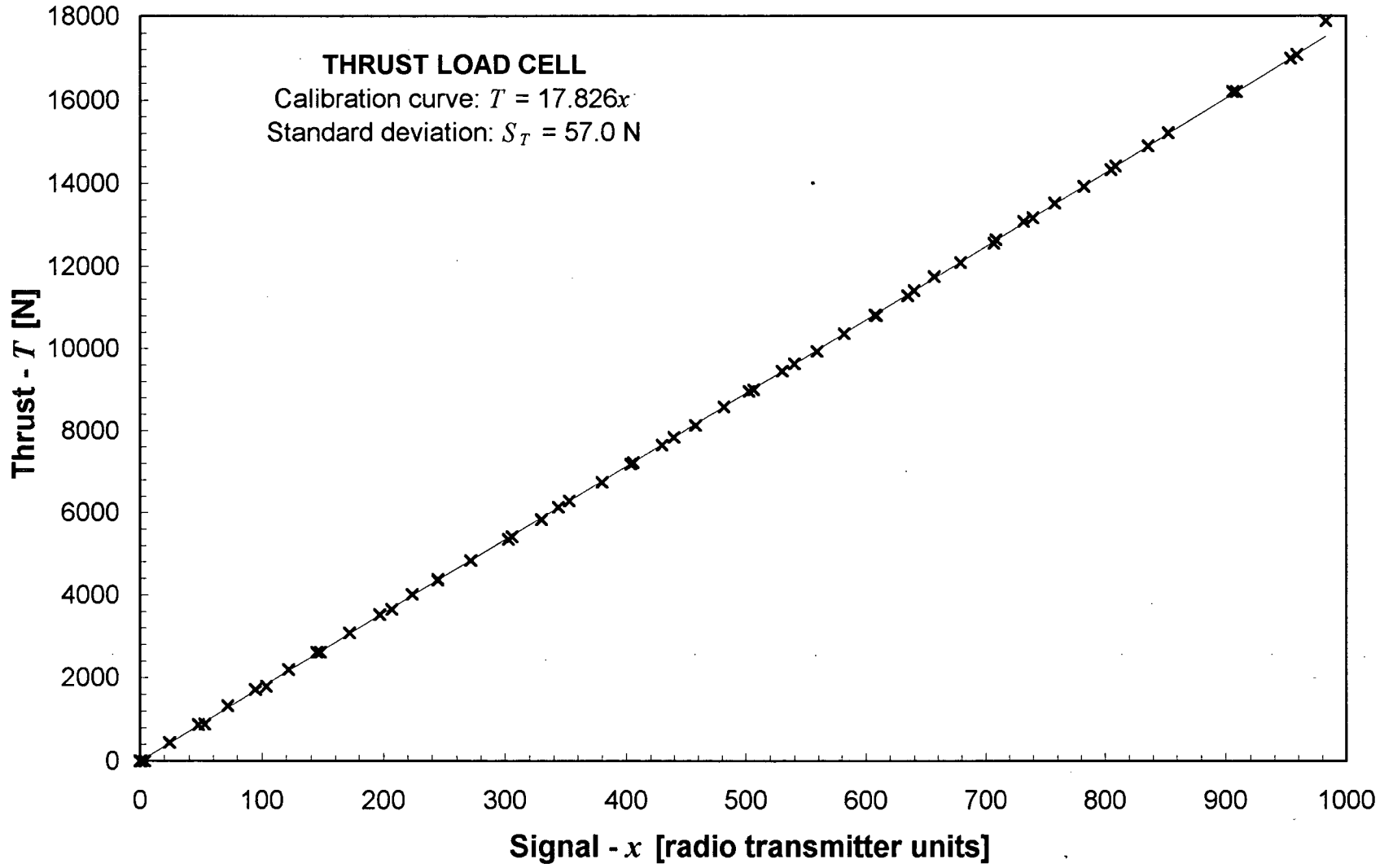

Figure A. 2 Calibration of the thrust load cell.

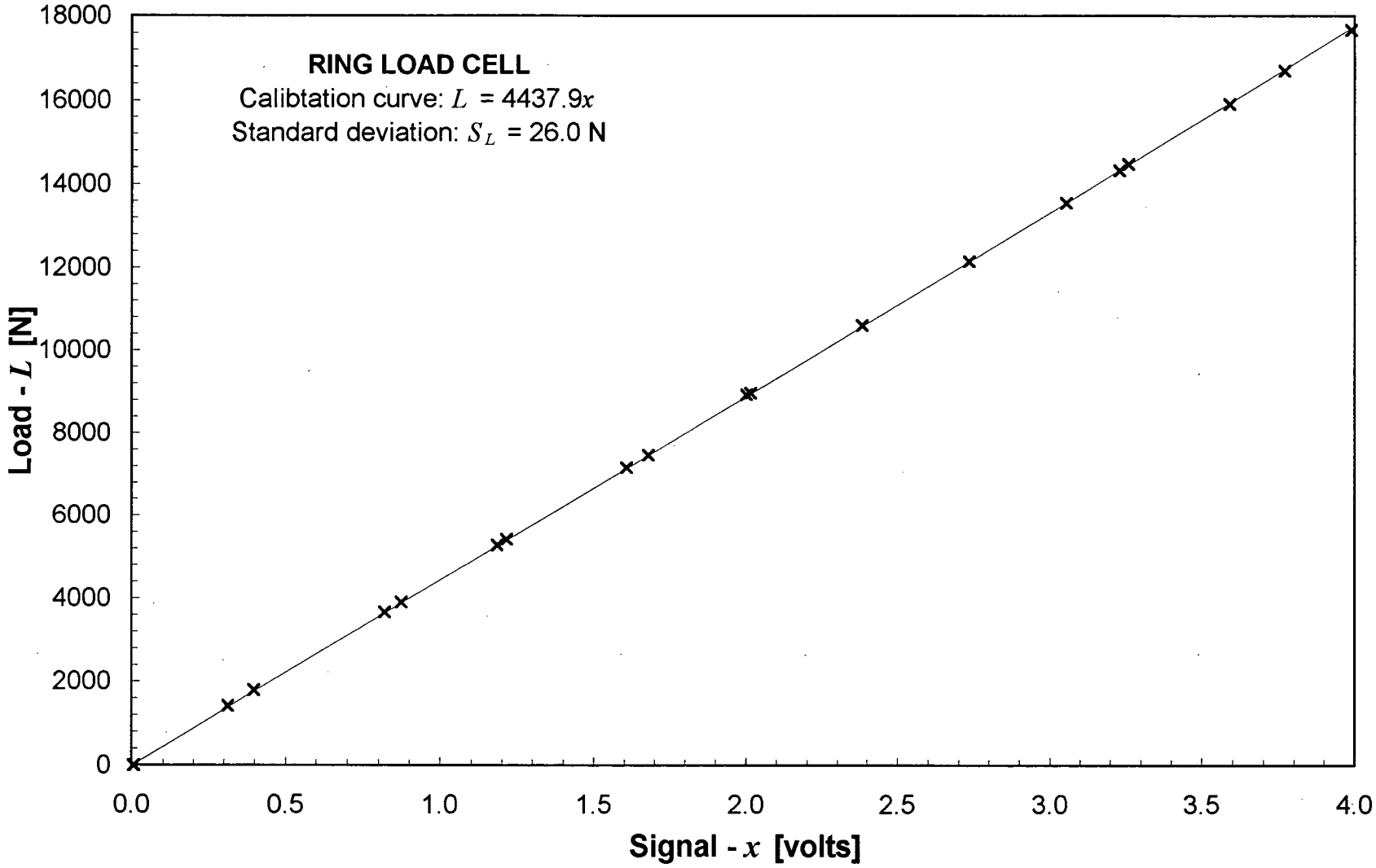

Figure A. 3 Calibration of the ring load cell.

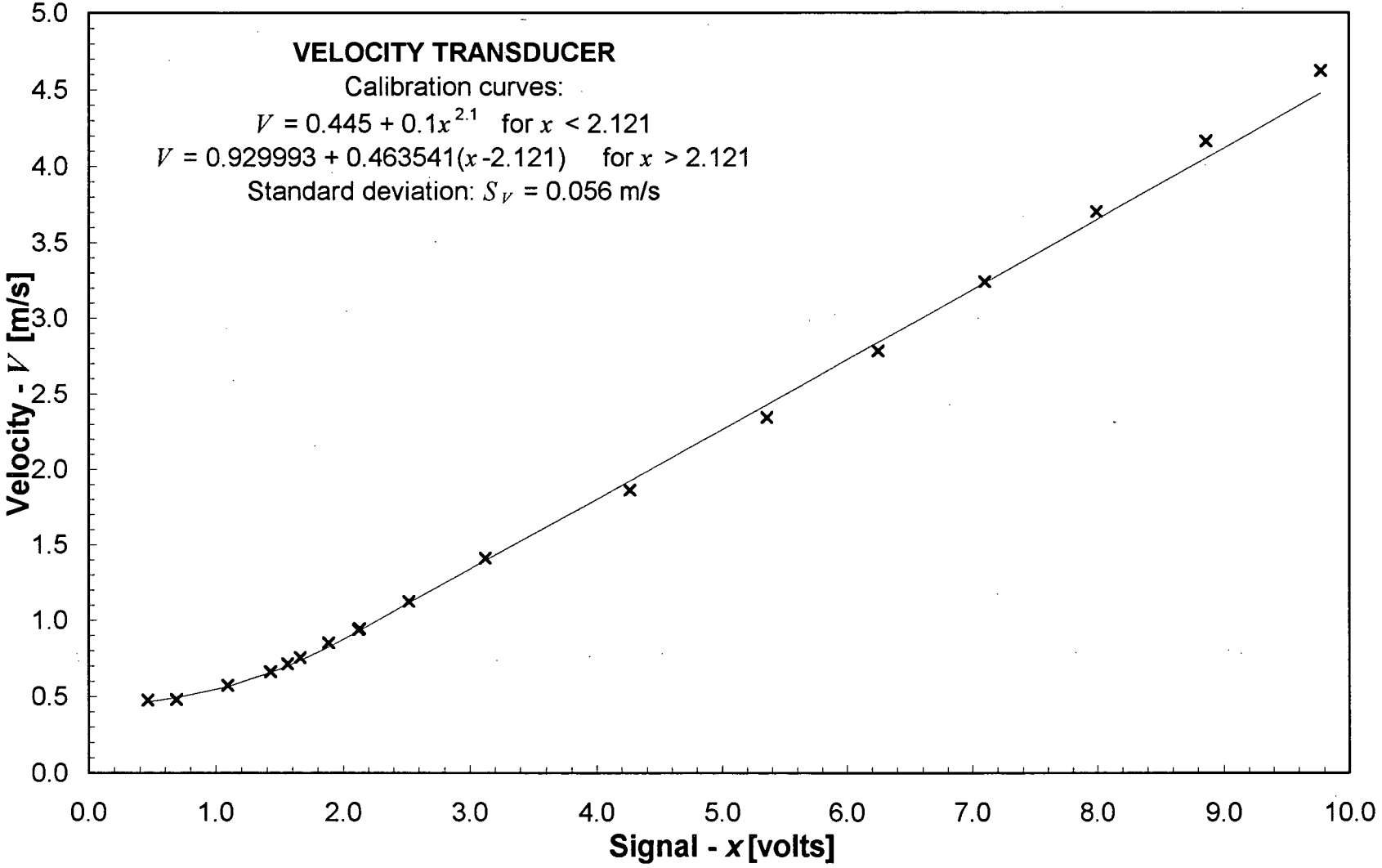

Figure A. 4 Calibration of the velocity transducer.

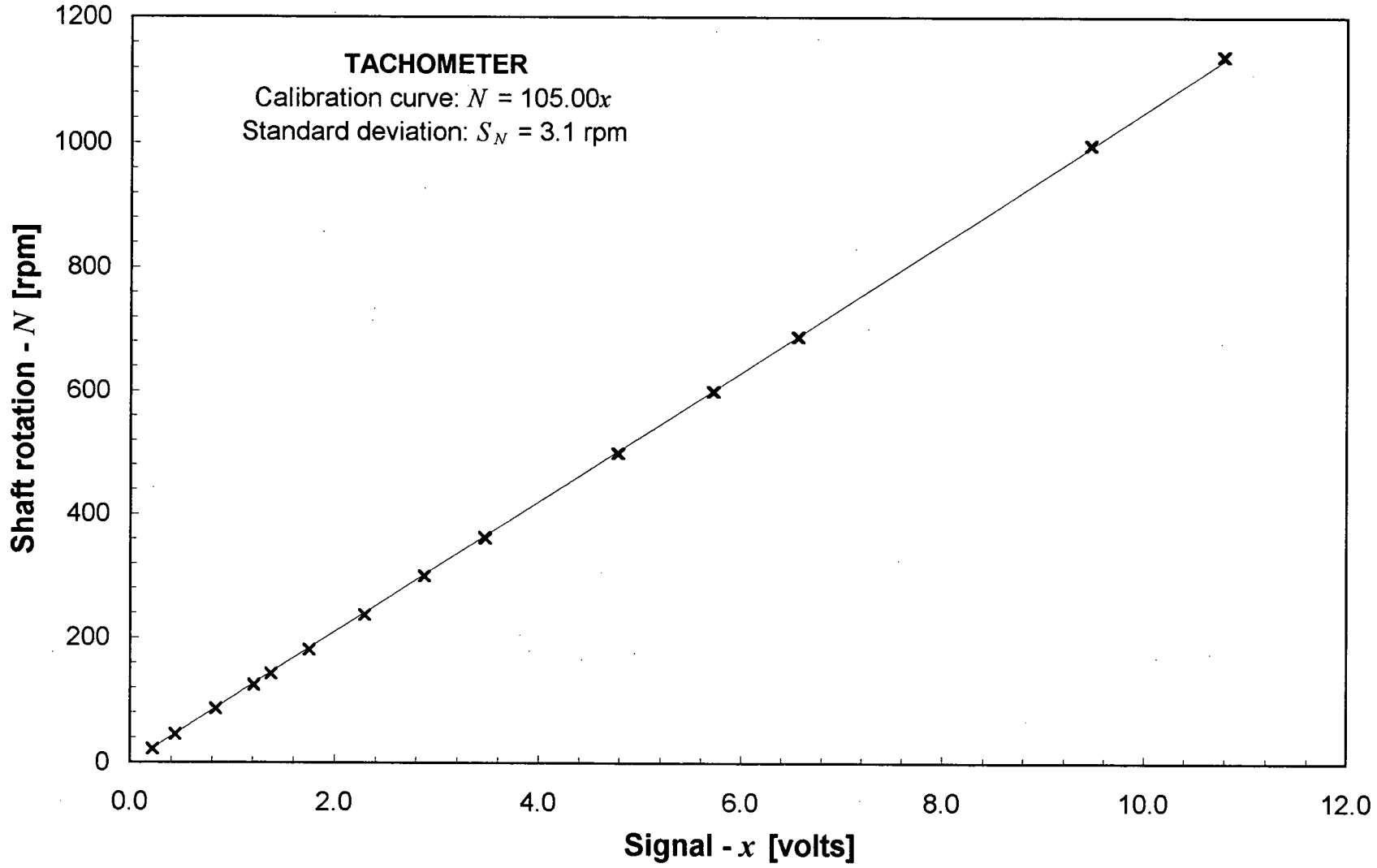

Figure A. 5 Calibration of the tachometer.

Appendix B - Schematic diagrams

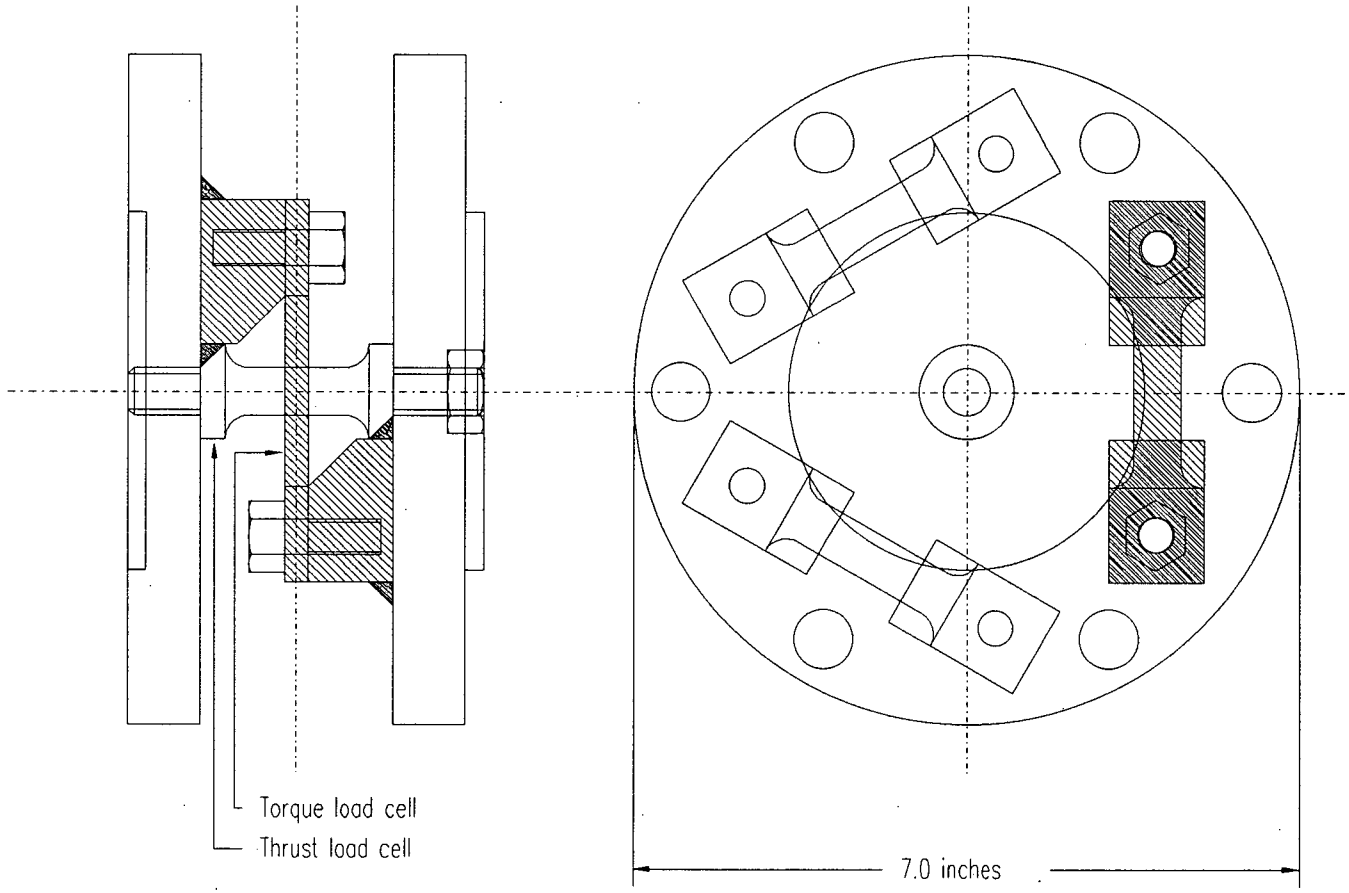

Figure B. 1 Torque and Thrust Transducer (TTT).

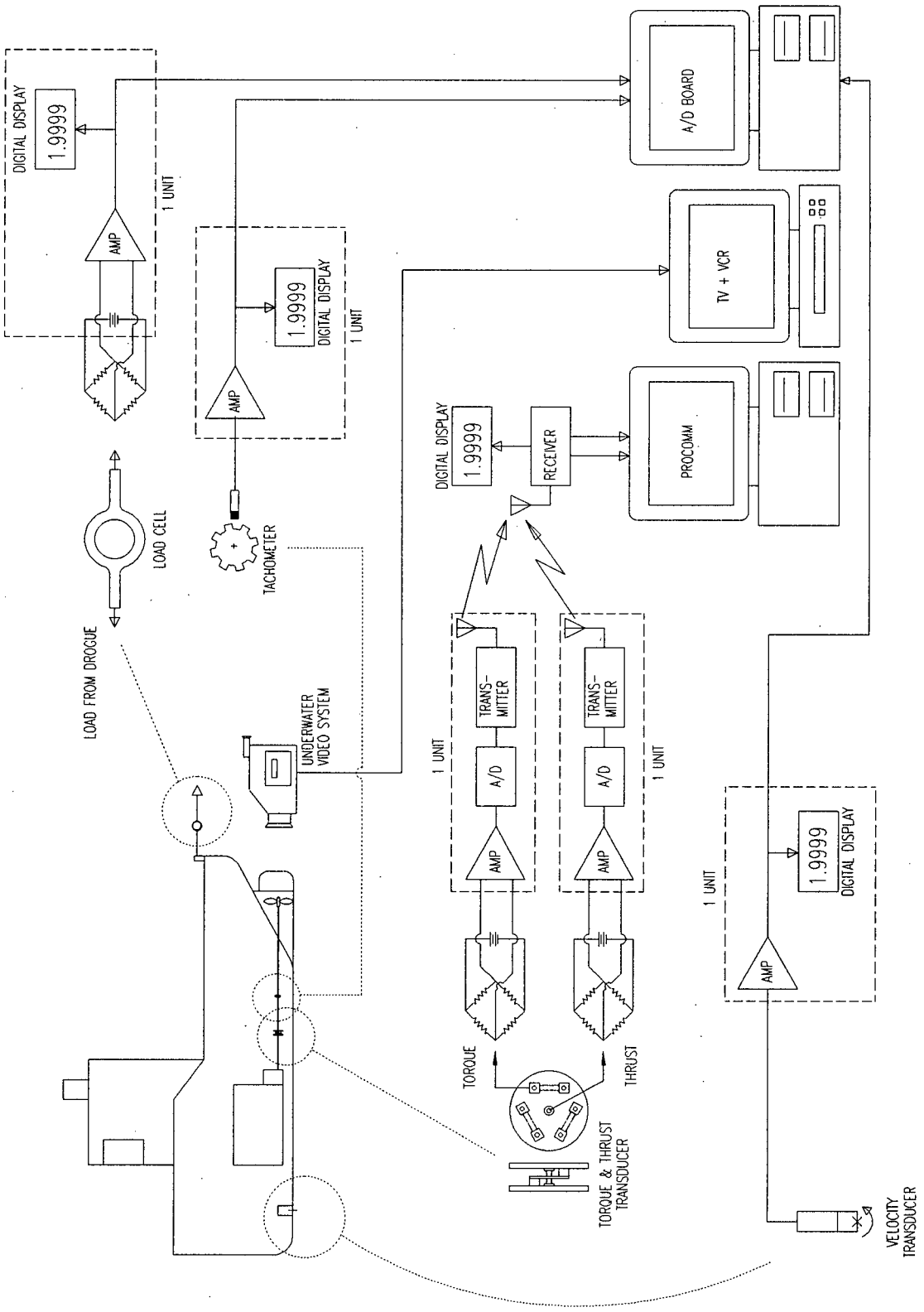

Figure B. 2 Data acquisition system.